(2)

NAVAL POSTGRADUATE SCHOOL
Monterey, California

THESIS

A STUDY OF NATURAL CONVECTION COOLING OF MULTIPLE DISCRETE HEAT SOURCES IN A VERTICAL CHANNEL

by

Thomas D. Willson

June 1988

Thesis Advisor: Yogendra Joshi

REPORT DOCUMENTATION PAGE

1a REPORT SECURITY CLASSIFICATION UNCLASSIFIED	1b RESTRICTIVE MARKINGS
2a SECURITY CLASSIFICATION AUTHORITY	3 DISTRIBUTION/AVAILABILITY OF REPORT Approved for public release; distribution is unlimited
2b DECLASSIFICATION/DOWNGRADING SCHEDULE	
4 PERFORMING ORGANIZATION REPORT NUMBER(S)	5 MONITORING ORGANIZATION REPORT NUMBER(S)
6a NAME OF PERFORMING ORGANIZATION Naval Postgraduate School 6b OFFICE SYMBOL (If applicable) Code 69	7a NAME OF MONITORING ORGANIZATION Naval Postgraduate School
6c ADDRESS (City, State, and ZIP Code) Monterey, California 93943-5000	7b ADDRESS (City, State, and ZIP Code) Monterey, California 93943-5000
8a NAME OF FUNDING/SPONSORING ORGANIZATION 8b OFFICE SYMBOL (If applicable)	9 PROCUREMENT INSTRUMENT IDENTIFICATION NUMBER
8c ADDRESS (City, State, and ZIP Code)	10 SOURCE OF FUNDING NUMBERS PROGRAM ELEMENT NO / PROJECT NO / TASK NO / WORK UNIT ACCESSION NO

11 TITLE (Include Security Classification)
A Study of Natural Convection Cooling of Multiple Discrete Heat Sources in a Vertical Channel

12 PERSONAL AUTHOR(S) Willson, Thomas D.

13a TYPE OF REPORT	13b TIME COVERED	14 DATE OF REPORT (Year, Month, Day)	15 PAGE COUNT
Masters Thesis	FROM ______ TO ______	1988, June	

16 SUPPLEMENTARY NOTATION
The views expressed in this thesis are those of the author and do not reflect the official policy or position of the Department of Defense or the U.S. Government.

17 COSATI CODES			18 SUBJECT TERMS (Continue on reverse if necessary and identify by block number)
FIELD	GROUP	SUB-GROUP	Natural Convection; Immersion Cooling; Protruding Heat Sources; Vertical Channel; Flow Visualization

19 ABSTRACT (Continue on reverse if necessary and identify by block number)

Natural convection liquid cooling of simulated electronic components in a vertical channel was investigated. The test surface contained a single column of eight rectangular, protruding heated elements, each simulating a 20 pin dual-in-line package. Temperature measurements and flow visualization were performed for a number of power dissipation levels and channel widths. Collectively, this information was used in interpreting the flow and transport characteristics. A correlation to predict the heat transfer rates was developed based on the component surface temperatures. Optimum channel widths were determined from these surface temperature measurements for the range of power levels investigated. Temperature distributions in the fluid were measured using a traversing thermocouple probe.

20 DISTRIBUTION/AVAILABILITY OF ABSTRACT ☒ UNCLASSIFIED/UNLIMITED ☐ SAME AS RPT ☐ DTIC USERS	21 ABSTRACT SECURITY CLASSIFICATION UNCLASSIFIED
22a NAME OF RESPONSIBLE INDIVIDUAL Yogendra Joshi	22b TELEPHONE (Include Area Code) (408) 646-3400 22c OFFICE SYMBOL Code 69 Ji

DD FORM 1473, 84 MAR — 83 APR edition may be used until exhausted. All other editions are obsolete

SECURITY CLASSIFICATION OF THIS PAGE

☆ U.S. Government Printing Office 1986—606-243

UNCLASSIFIED

A Study of Natural Convection Cooling of Multiple Discrete Heat Sources in a Vertical Channel

by

Thomas D. Willson
Lieutenant Commander, United States Navy
B.S., Pennsylvania State University, 1975

Submitted in partial fulfillment of the requirements for the degree of

MASTER OF SCIENCE IN MECHANICAL ENGINEERING

from the

NAVAL POSTGRADUATE SCHOOL
June 1988

Author: Thomas D Willson
Thomas D. Willson

Approved by: Yogendra Joshi
Yogendra Joshi, Thesis Advisor

Anthony J. Healey, Chairman,
Department of Mechanical Engineering

Gordon E. Schacher, Dean of
Science and Engineering

ABSTRACT

Natural convection liquid cooling of simulated electronic components in a vertical channel was investigated. The test surface contained a single column of eight rectangular, protruding heated elements, each simulating a 20-pin dual-in-line package. Temperature measurements and flow visualization were performed for a number of power dissipation levels and channel widths. Collectively, this information was used in interpreting the flow and transport characteristics. A correlation to predict the heat transfer rates was developed based on the component surface temperatures. Optimum channel widths were determined from these surface temperature measurements for the range of power levels investigated. Temperature distributions in the fluid were measured using a traversing thermocouple probe.

TABLE OF CONTENTS

LIST OF FIGURES

LIST OF SYMBOLS

Symbol	Description	Units
A_T	Area	m^2
A_1	Area of component front face	m^2
A_2	Combined area of component top and bottom faces	m^2
A_3	Combined area of component side faces	m^2
A_{TOTAL}	Total surface area of component	m^2
D	Component breadth	m
DTB	Temperature difference between component bottom face and ambient	°C
DTF	Temperature difference between component front face and ambient	°C
DTH	Temperature difference between component heater temperature and ambient	°C
DTR	Temperature difference between component right side face and ambient	°C
DTT	Temperature difference between component top face and ambient	°C

g	Acceleration due to gravity	$\frac{m}{s^2}$
Gr^*	Modified Grashof number	Dimensionless
h	Heat transfer coefficient	$\frac{W}{m^2K}$
k	Fluid thermal conductivity	$\frac{W}{mK}$
L	Test surface length	m
$\bar{L}$	Characteristic length	m
Nu	Nusselt number	Dimensionless
Nu^*	Modified Nusselt number	Dimensionless
P	Combined perimeters of the five component faces exposed to the fluid	m
Pr	Prandtl number	Dimensionless
Q_{COND}	Energy loss via conduction through the back of the test surface per component	W
Q_{CONV}	Energy convected into the fluid per component	W
q''	Energy flux convected into the fluid per component	$\frac{W}{m^2}$
T	Temperature	°C
T_{FILM}	Temperature at which fluid properties are evaluated	K
T_{inf}	Ambient temperature	°C

T_s	Surface temperature	°C
T^*	Temperature scaling factor	°C
v	Specific volume	$\frac{m^3}{Kg}$

Greek Symbol	Description	Units
β	Expansion coefficient	$\frac{1}{K}$
ν	Kinematic viscosity	$\frac{M^2}{s}$
μ	Dynamic viscosity	$\frac{N}{sm^2}$
θ_F	Temperature difference between component front face and ambient	K
θ_0	Temperature scaling factor	K

ACKNOWLEDGMENTS

The author would like to express his sincere gratitude to Assistant Professor Y. Joshi, his thesis advisor, for his superb guidance, patience, and concern during the endeavor.

He also wishes to express appreciation to the technicians of the Mechanical Engineering Department, especially Mr. Mardo Blanco, for their timely and superior efforts in providing construction assistance.

The author would further like to thank Ms. Dale Ward of the Educational Media Department and Ms. Jane Kretzmann of the Computer Center for their assistance in solving graphics problems.

Finally, and most assuredly, the greatest thanks go to my wife, [redacted] whose love, understanding, and support stand behind this work.

I. INTRODUCTION

A. STATEMENT OF PROBLEM

The continuing trend toward microminiaturization of electronic components has made thermal design critical to achieving higher packaging densities. The ever-increasing heat fluxes must be removed while keeping the device junction temperatures typically below 100°C [Ref. 1]. The failure of microelectronic chips increases exponentially as the junction temperatures increase [Ref. 2].

Microchips act as discrete sources of thermal energy. Effective removal of the generated energy is of major import in determining how they might be used without overheating the elements themselves or the surrounding package. Thermal control is one of the critical considerations in the design of any electronic cooling system. The thermal designer's task is further complicated by the presence of arrays of electronic components placed in proximity to each other, requiring detailed considerations of transport interactions between neighboring elements.

The design of packaged electronic components must consider all anticipated modes of heat transfer. A complete thermal analysis will account for all three mechanisms of thermal energy transport:

- conduction
- convection
- radiation

The areas of concern include transferring heat, via conduction, from internal heat sources to the external surface of the package and the subsequent removal of heat from the external surface by a cooling medium. Also, the coolant temperature must be maintained at prescribed levels for a given environment.

The present work focuses on the heat removal from electronic packages through convective cooling. This convection may, in general, be forced or natural; the medium liquid or gas. Because of the higher density and thermal conductivity of liquids compared to air, heat transfer coefficients an order of magnitude or more larger than for air are attainable. Due to the significantly high heat transfer rates achievable, cooling of electronic components by direct liquid immersion has been identified as an extremely effective thermal control technique [Ref. 2].

Convection heat transfer rate from a surface at temperature T_S of area A to surrounding fluid environment T_{INF} is given by Newton's law of cooling:

$$q^{\cdot} = Ah(T_s - T_{INF})$$

This is a definition of h, the convective heat transfer coefficient, more than a phenomenological law. Evaluation of h depends upon heat source geometry, orientation, fluid properties, and fluid velocity.

Natural convection results when fluid density gradients exist in the presence of a body force field such as gravity. Density gradients in the fluid commonly occur due to temperature gradients. Advantages of

employing natural convection in electronic cooling include high reliability, low cost, reduced noise, and a simpler design. Despite these potential benefits, only a limited number of studies are available on liquid immersion natural convection cooling of electronic components.

Most existing natural convection studies, both experimental and analytical, have considered heating surfaces that were semi-infinite. Electronic component cooling configurations typically employ arrays of small, discrete, flush, or protruding heat sources. The available heat transfer correlations are inadequate in predicting transport in these geometries. Convective heat transfer from an array of microchips is strongly dependent on package shape and array density. Indeed, in real systems, individual elements or modules often vary significantly in size, shape, and in the manner in which they are arranged on the substrate.

The geometric complexity is further compounded by the nonuniform nature of heat dissipation from the array. Individual component dissipation is a function of its utilization. Variation in power dissipation from component to component on the same board and from board to board within the system usually exists. The orientation of the boards on which the elements are mounted is yet another variable.

Often, these semi-regular arrays face the back of an adjacent board. The resulting vertical channel has one surface which is relatively smooth and the other one covered by an arrangement of large, heat-dissipating elements. Within the channel, local convective heat transfer is driven by two phenomena, a local buoyancy force due to the

heated components and a forced convection effect arising from the flow history, over the entire channel length, including both heated and unheated regions. A simultaneous consideration of these mechanisms is essential in obtaining predictive capability for transport rates in these systems.

The complexity of the problem described demands an approach which builds on the fundamental physical processes. Efficient cooling cannot be attained without understanding the heat transfer from each package by a determination of its flow and thermal fields. The overall goal is to develop a methodology based on sound physical principles which will allow the prediction of individual component temperatures, by superposition, in a nonuniformly heated array of components.

B. IMMERSION COOLING—ANALYTICAL AND EXPERIMENTAL STUDIES

Reference 3 provides an excellent literature review of previous work, both analytical and experimental, in the field of liquid immersion cooling of electronic equipment. Additionally, very relevant work has been performed by Ortega and Moffat [Refs. 4–6]. They have experimentally examined natural convection air cooling of simulated electronic components protruding from a vertical surface, with and without a shrouding wall. Heat transfer rates significantly higher than for a smooth vertical plate were found. They interpreted this as an indication of turbulent free convection. When a shroud was in place, they found plate-averaged heat transfer coefficients 40 to 50 percent higher than for a smooth, parallel plane channel.

Jaluria [Ref. 7] performed two-dimensional computations for natural convection air flow over a vertical surface with multiple wide, flush-mounted heaters. The study treated the flow as a boundary layer problem. Rajakumar and Johnson [Ref. 8] reported computations of free convection heat transfer using rectangular strip heating surfaces. Their finite element approach showed significant stagnant areas between the blocks.

C. OBJECTIVE

An experimental study was undertaken to to determine the hydrodynamic and thermal characteristics of buoyancy-induced flow over several heated protruding components mounted on a vertical surface.

A single column array was chosen because it provided the simplest geometry featuring discretized heat dissipation. The effects of a neighboring card were simulated by a movable vertical shroud plate. Specific objectives of this study were:

- to visualize the transient and steady-state, natural convection flow within an interrupted channel, for a range of component power dissipation levels and channel widths;
- to measure component temperatures for various power inputs and shroud spacings to develop an appropriate nondimensional correlation to predict the heat transfer rates for this geometry; and
- to measure temperature distributions in the adjacent fluid, using a traversing thermocouple probe to assist in evaluating the hydrodynamic and thermal nature of the flow.

This study was a follow-on to work described in Reference 3 and is part of a continuing effort to study natural convection liquid immersion cooling of electronic equipment.

II. EXPERIMENT

A. GENERAL DESIGN CONSIDERATIONS

Detailed descriptions of equipment design and construction are available in Reference 3. Only a brief overview is presented here.

As seen in Figure 1, the assembly consisted of a vertical test surface which contained a single column of eight rectangular protruding heated elements. Each protrusion simulated a 20-pin dual-in-line package. The elements were stainless steel blocks spaced one inch apart, center to center, on a plexiglass substrate. A 12.70 mm thick plexiglass shroud, when used, simulated the reverse side of a second printed circuit board.

The blocks (Figures 2 and 3) had imbedded thermocouples on each of the five surfaces in contact with the fluid to provide surface temperature measurements. A sixth thermocouple was placed in the center of each element mounting slot for measurements of heater temperature. A miniature thermocouple probe mounted on a three-dimensional traverse enabled measurements of temperature distributions within the fluid.

A foil heater mounted on the component side facing the substrate was powered using a regulated D.C. power supply. Each heater was run in series with a precision resistor and all eight heaters were in parallel with the power supply. The current to each heater was

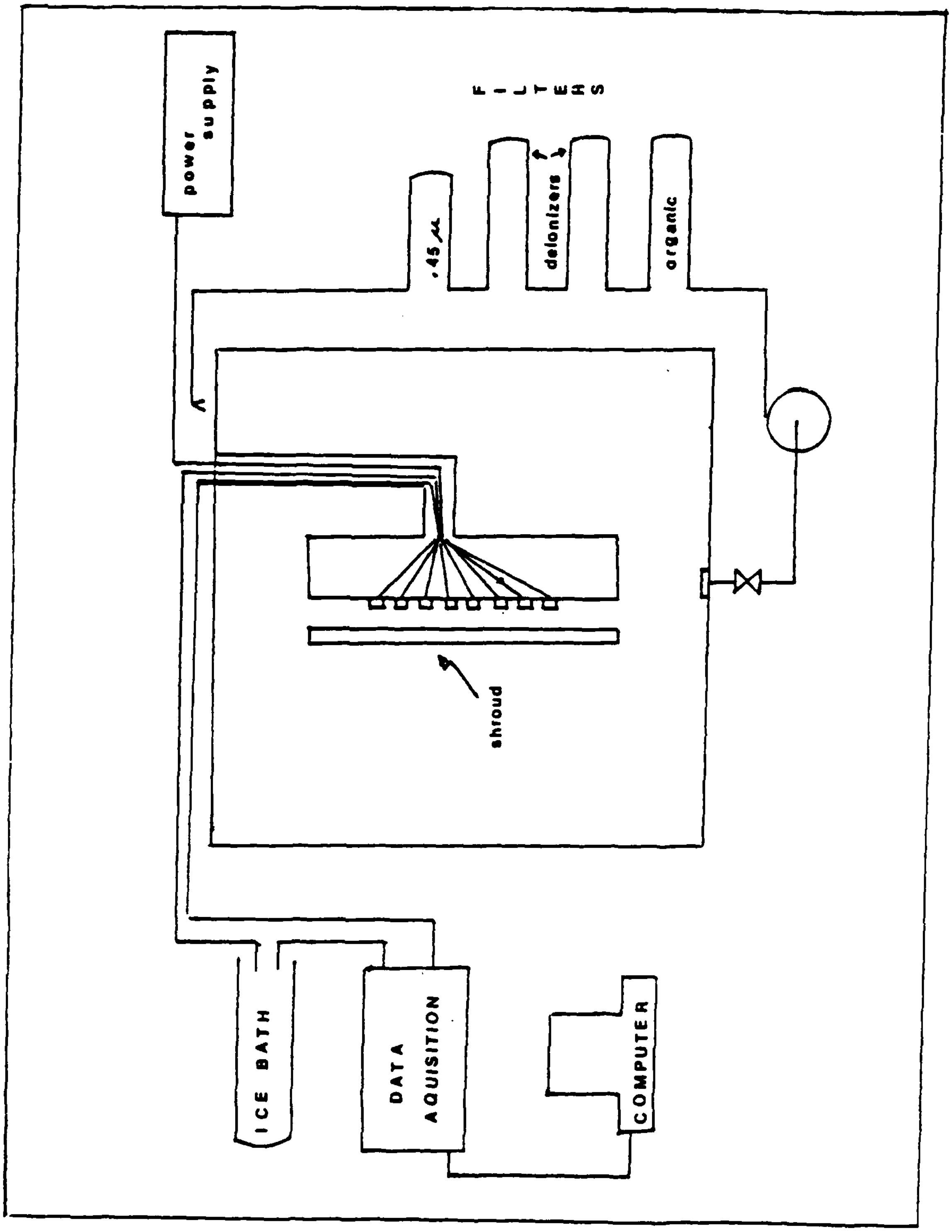

Figure 1. **System Configuration**

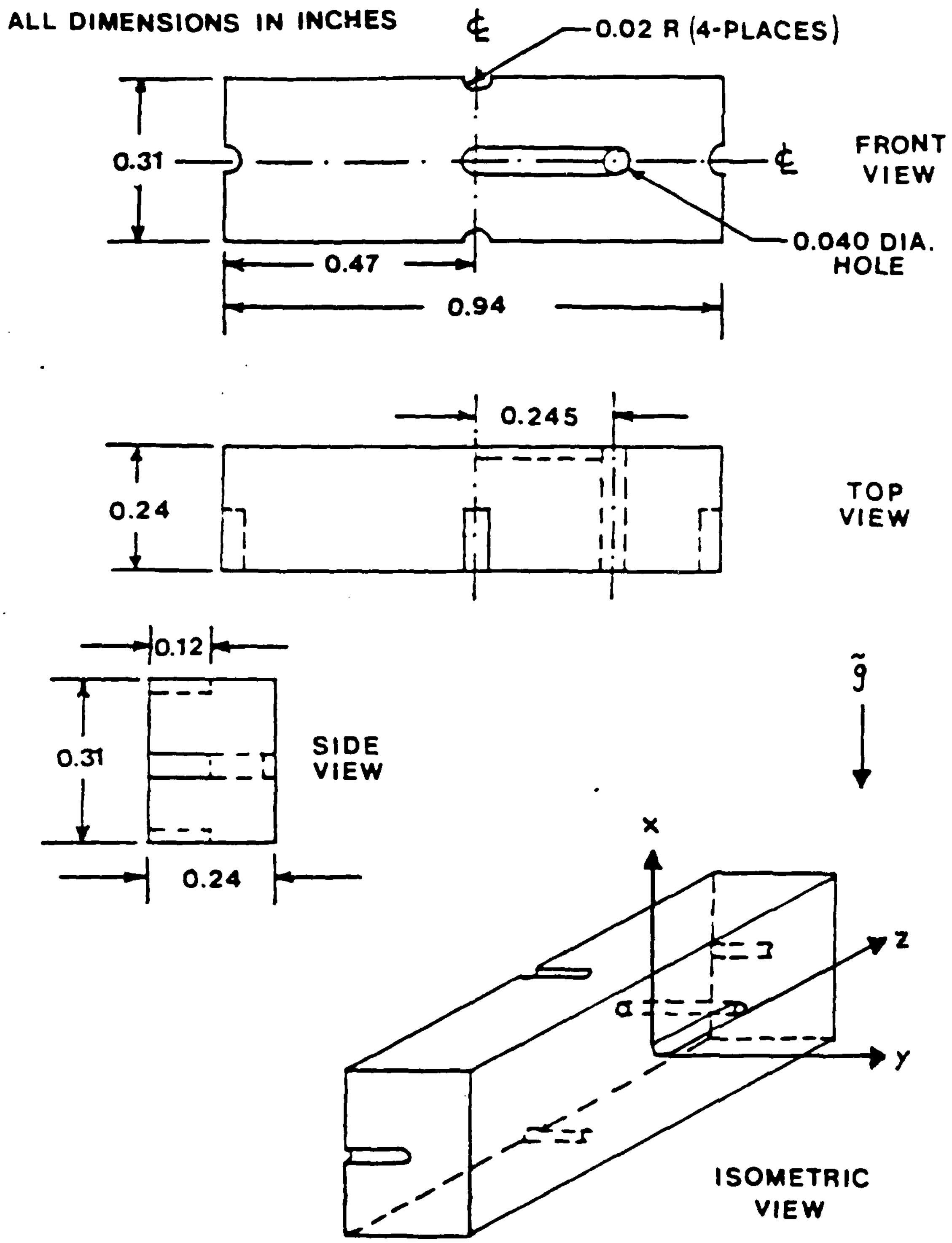

Figure 2. **Heater Block Schematic**
(after Hazard, Ref. 3)

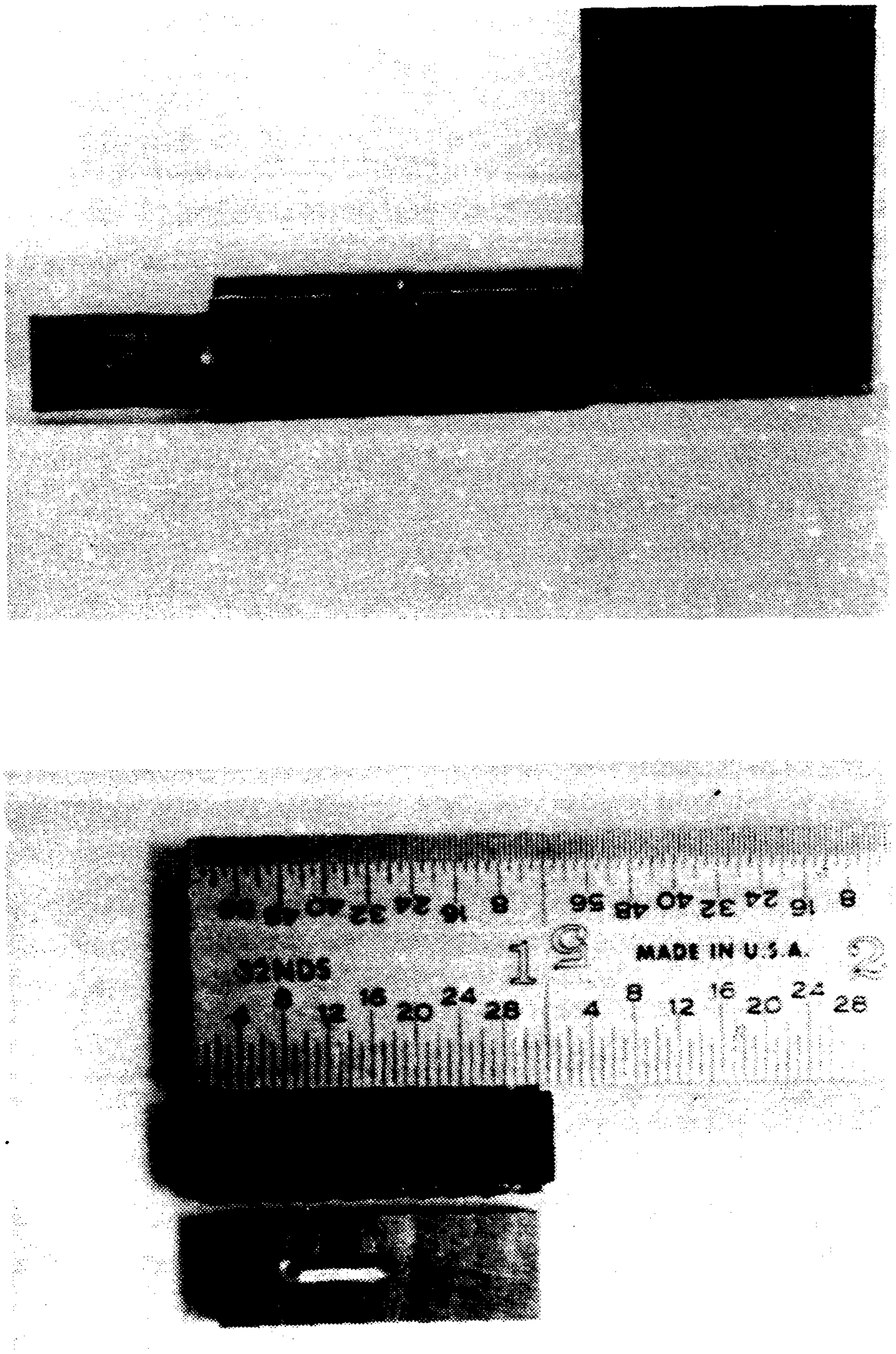

Figure 3. **Mounted Foil Heater, Two Perspectives**
(after Hazard, Ref. 3)

calculated by subtracting the heater voltage from the source voltage, then dividing by the resistance of the precision resistor. Power dissipation through each element was determined by calculating the product of heater voltage and heater current.

Figure 2 shows the orientation of the coordinate axes used in the discussion to follow. The front face of the component is that surface in the x-z plane in contact with the fluid. The side faces are the two x-y surfaces, right and left as determined by viewing the component from the front. The top and bottom faces are those in the y-z plane, downstream and upstream of buoyant fluid flow, respectively. Component height is in the x-direction, depth in y, and breadth in the z-direction.

The immersion fluid was purified water contained in a one cubic meter, plate glass tank. Suspended in the water were particles of Pliolite, an inert pigment with a specific gravity of 0.93. The particles were illuminated with an eight milliwatt helium neon laser split into a plane by use of a cylindrical lens. The plane of visualization was varied by realignment of the laser lens assembly and the camera.

B. EXPERIMENTAL PROCEDURE

1. Established Method

Details are again provided in Reference 3, hereafter referred to as the previous study. Noteworthy differences are noted here.

2. Instrument Settings

Power settings of 0.2, 0.5, 1.0, 1.2, and 1.5 watts were used for each channel width. Because of the inability to de-aerate the

immersion fluid, 1.5 watts was the upper limit of power available. Settings above this generated bubbles on the block surfaces.

3. Instrument Readings

When measuring steady-state surface temperatures, successive temperature measurements at 10-minute intervals were compared. Only when all thermocouples varied less than 0.10° C were the final measurements taken. The temperature acquisition program of the previous study, modified to reflect the numbering of elements from bottom to top (flow direction) and to allow data storage (Appendix A), was then executed.

When using the traversing thermocouple probe, the data acquisition system was programmed to continuously monitor the voltage registered by a single channel. Observation of the on-screen printout allowed determination of temperature variation from point to point within the flow field, as well as at any point over time.

A program (Appendix A) which monitored from one to eight thermocouples over time was used when making a record of the transient temperature response of the surface thermocouples to power step up or step down. Typical data presented were for the front face temperatures of the various components.

4. Photographic Technique

Best results were obtained when using an f stop of 2.8 and exposure time of 20 to 40 seconds. Camera placement was approximately six inches from the tank wall at a height which allowed all eight blocks in the field of view. The camera was inclined at an angle

of about 5 degrees from the test surface when a shroud was present. This was helpful in minimizing reflected light. A shroud spacing of two times component height from the plexiglass substrate was determined to be the minimum at which useful pictures could be obtained.

C. DATA ANALYSIS

While Q_{COND} and Q_{CONV} were calculated exactly as recommended by the previous study, further data reduction differed significantly.

For each block, a surface-averaged temperature was generated by multiplying the temperature and area of each fluid-exposed face and dividing the summation over the block by the total exposed face area of the block. The average over the eight blocks of the surface-averaged temperatures was then averaged with the immersion fluid temperature to produce a film temperature. Fluid properties based on curve fits (Appendix B) of data from Incropera and Dewitt [Ref. 9] were then calculated for the film temperature.

A new characteristic length, $\bar{L}$, for determining a nondimensional temperature excess, $\frac{\theta}{\theta_0}$, a modified Grashof number, Gr^*, and Nusselt number, Nu, was chosen. The progression of its use for each block is as follows:

$$\bar{L} = \frac{\sum_{1}^{5} A_{EXPOSED\ FACES}}{\sum_{1}^{5} P_{EACH\ FACE}}$$

$$q'' = \frac{Q_{CONV}}{A_{HEATER}}$$

$$T^* = \frac{q''\bar{L}}{k_f}$$

$$h = \frac{q''}{\Delta T_{FACE}}$$

$$Gr^* = \frac{g\beta q''\bar{L}^4}{k_f \nu^2}$$

$$Nu = \frac{h\bar{L}}{k_f}$$

$$\theta_F = DTF = \Delta T_{FRONT\ FACE}$$

$$\theta_0 = T^*$$

$$\frac{\theta_F}{\theta_0} = DTFN = \frac{\Delta T_{FRONT\ FACE}}{T^*} = \frac{DTF}{T^*}$$

The various symbols used are defined in the List of Symbols section.

Other characteristic lengths, L to determine block spacing along the plexiglass substrate and D to represent the horizontal breadth of the element, were also chosen. Their use is as follows:

$\frac{x}{L}$ = nondimensional location of component centers along the test surface

$\frac{z}{D}$ = horizontal position along the element's front face

Quantitative development was best expressed as plots of:

- *Nu* vs. *Gr** relationships
- nondimensional block surface temperature excess vs. element position
- temperature distributions in the fluid adjacent to the test surface
- block surface temperatures vs. time

Pertinent trends in these variations are discussed next.

III. NO SHROUD—INFINITE CHANNEL WIDTH

A. ALL ELEMENTS POWERED, STEADY STATE

1. Flow Visualization

Photographs of the natural convection flow in a plane (x-y) geometrically centered through each component are shown in Figure 4. The visualizations represent all elements heated to power settings of 0.2, 0.5, and 1.0 watts, left to right, respectively. The exposure times were 40, 20, and 20 seconds, left to right. The photograph toning techniques required for mass printing of this work do not allow sufficient resolution for detailed study. Should the reader desire to see prints of much greater clarity, contact Y. Joshi at the address given in the distribution list of this study.

The flow appears to consist, in each case, of strong upward motion driven by the buoyant force near the test surface. The fluid tends to follow the contours of the protrusions. The particle traces are closer passing the element front face as compared to the interblock space. Dead zones are not obvious except perhaps for very small areas where the blocks' top faces intersects the substrate and for a slightly larger area above the top face of the last block in the array. There is no evidence of recirculation or formation of dead zones near the bottom face of any block.

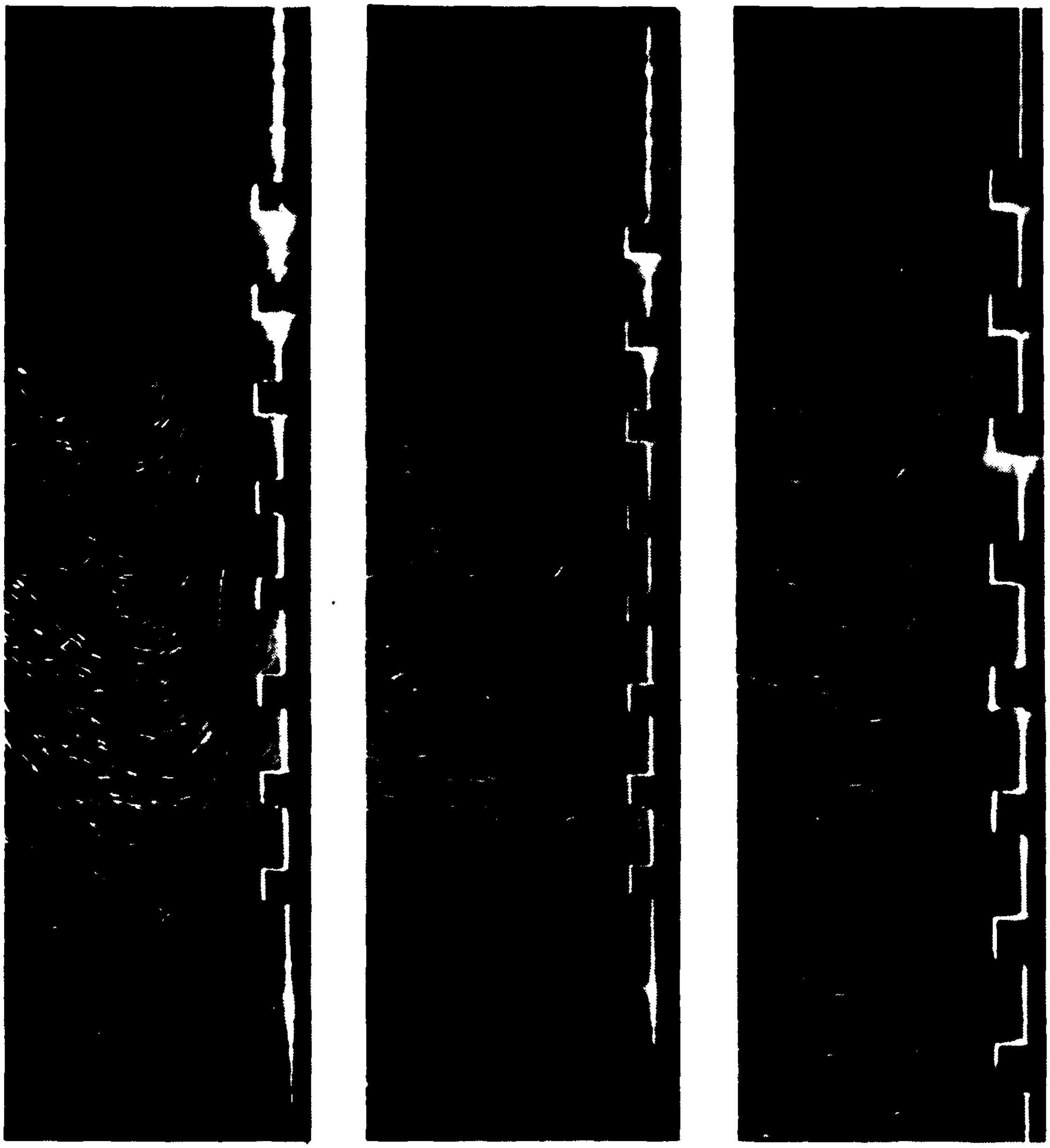

Figure 4. **Steady Flow in X-Y Plane at Power Levels of 0.2, 0.5, and 1.0 Watts. Powers Increase From Left to Right**

In all three photographs, a developing boundary layer characteristic is evident farther out from the protrusions. It attains a thickness of about 3.5 component depths for 0.2 watts and 2 for 1.0 watt. Its origin moves upstream with increased power, from about 1 component height at 0.2 watts to 3 component heights at 1.0 watt. The velocities appear greater and the boundary layer becomes thinner as power is increased. Ambient fluid is entrained over the entire length of the layer.

Figure 5 presents flow visualization in the plane (x-z) passing through the front faces of the elements. All elements were powered to 1.2 watts and exposure time was 40 seconds. The photograph shows an upward-moving buoyant layer near the components. Ambient fluid is entrained from each side into the flow, resulting in an increase in the horizontal extent of the upflow region downstream. The flow in the vicinity of the elements appears three-dimensional.

As with the side view, the flow appears to follow the contours of the projections to about the same degree (dipping in about 3-5 mm from the side faces). the flow also appears to wrap around the corners. The particle traces about 20 percent along the block (z direction) from the side edge appear to be largely in the x-y plane and those at the side face are in the x-z plane. The particle traces in between are 3-D, each progressively moving along the 90° arc.

Overall, the flow can best be described as following the contour of an hourglass split in the x-z plane. The elements are the upper

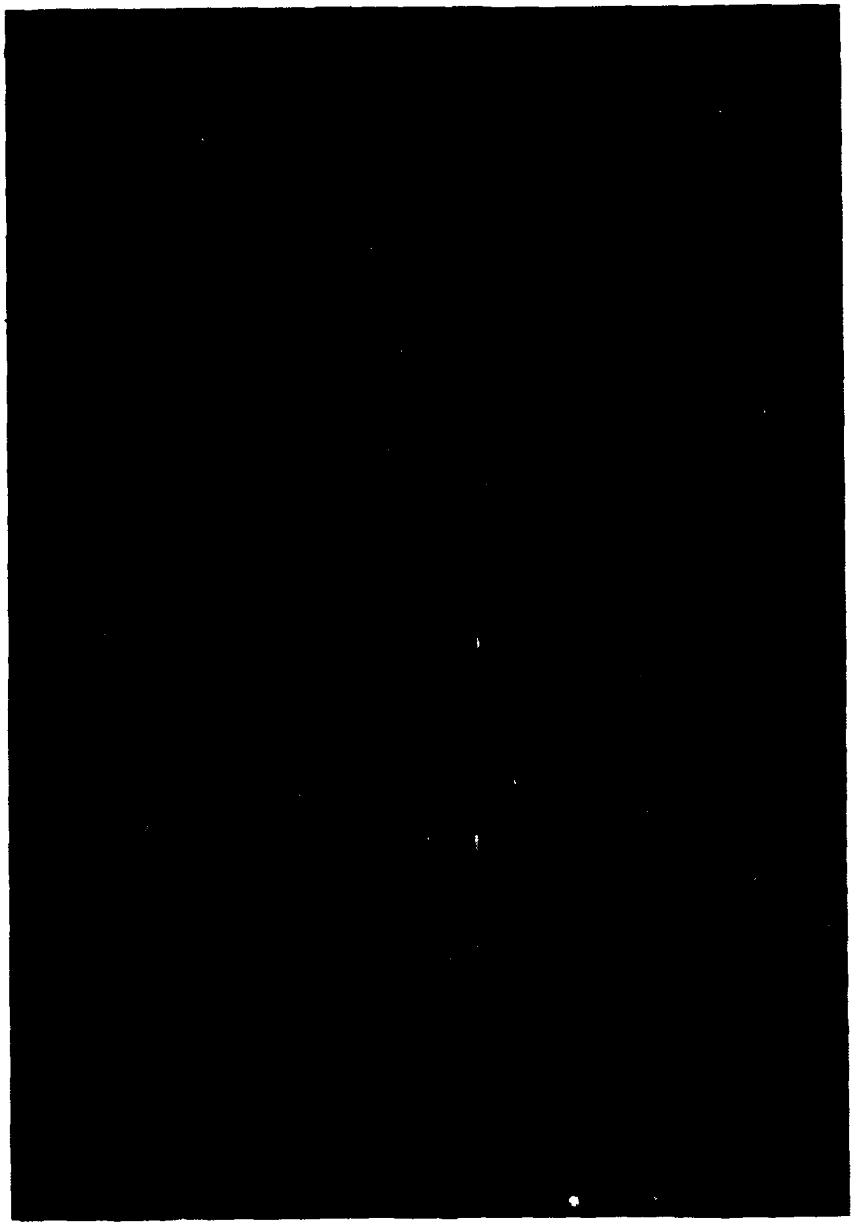

Figure 5. **Flow in X-Z Plane, 1.2 Watts**

and lower vessels. This configuration is repeated over the length of the array. It becomes more pronounced as the flow moves up the array and is eventually shed as a plume above the last element.

2. Quantitative

Figures 6 and 7 are nondimensional representations of temperature excess for 0.2 and 1.0 watts, measured on various component surfaces vs. block position. Also shown are the data for heater temperature measurements. The two plots follow the same patterns. The numbers for the 0.2 watts are, as expected, larger due to the inverse relationship with T^*, which is h dependent. Also as anticipated, the heater excesses are much greater. The drop in the heater temperature between blocks 6 and 7 could perhaps result from a slightly smaller (~4% less) power achieved by block 7. Unfortunately, the heater thermocouple for block 8 was inoperative. For both power settings, the imbedded surface thermocouples showed increasingly greater excesses along the array.

Of primary importance in thermal design is the availability of the appropriate heat transfer relationships. As discussed earlier, such correlations for discrete protruding heat sources in liquids have not been available in literature up to now. To this end, a logarithmic plot of Nu vs. Gr^* (Figure 8) was generated with eight curves representing element position. Each curve had five points for the power settings 0.2, 0.5, 1.0, 1.2, and 1.5 watts resulting in a range of Gr^*. Although a linear pattern with Gr^* was evident, the spread in data indicated an

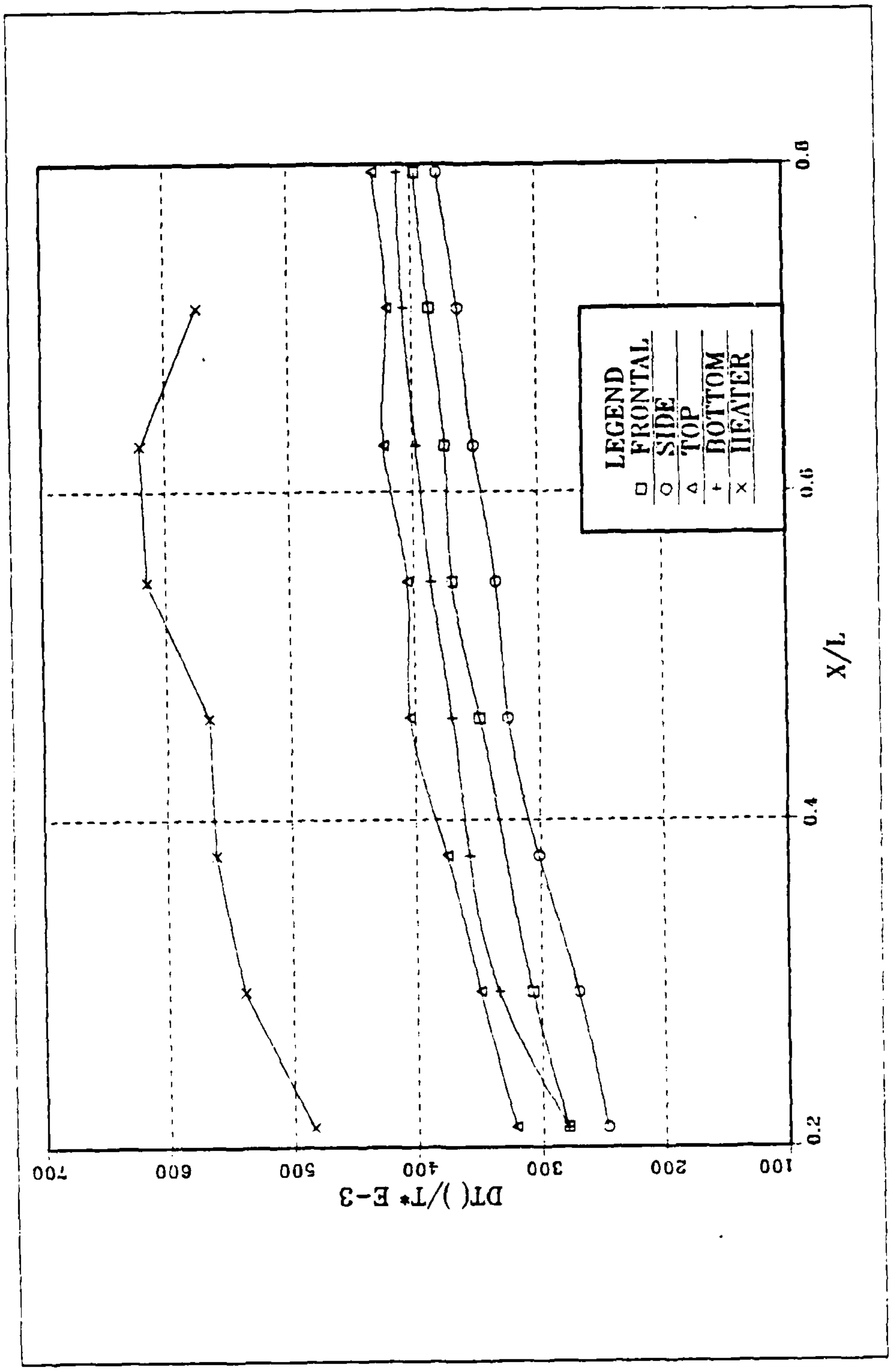

Figure 6. **Nondimensional Temperature Excess vs. Position, 0.2 Watts**

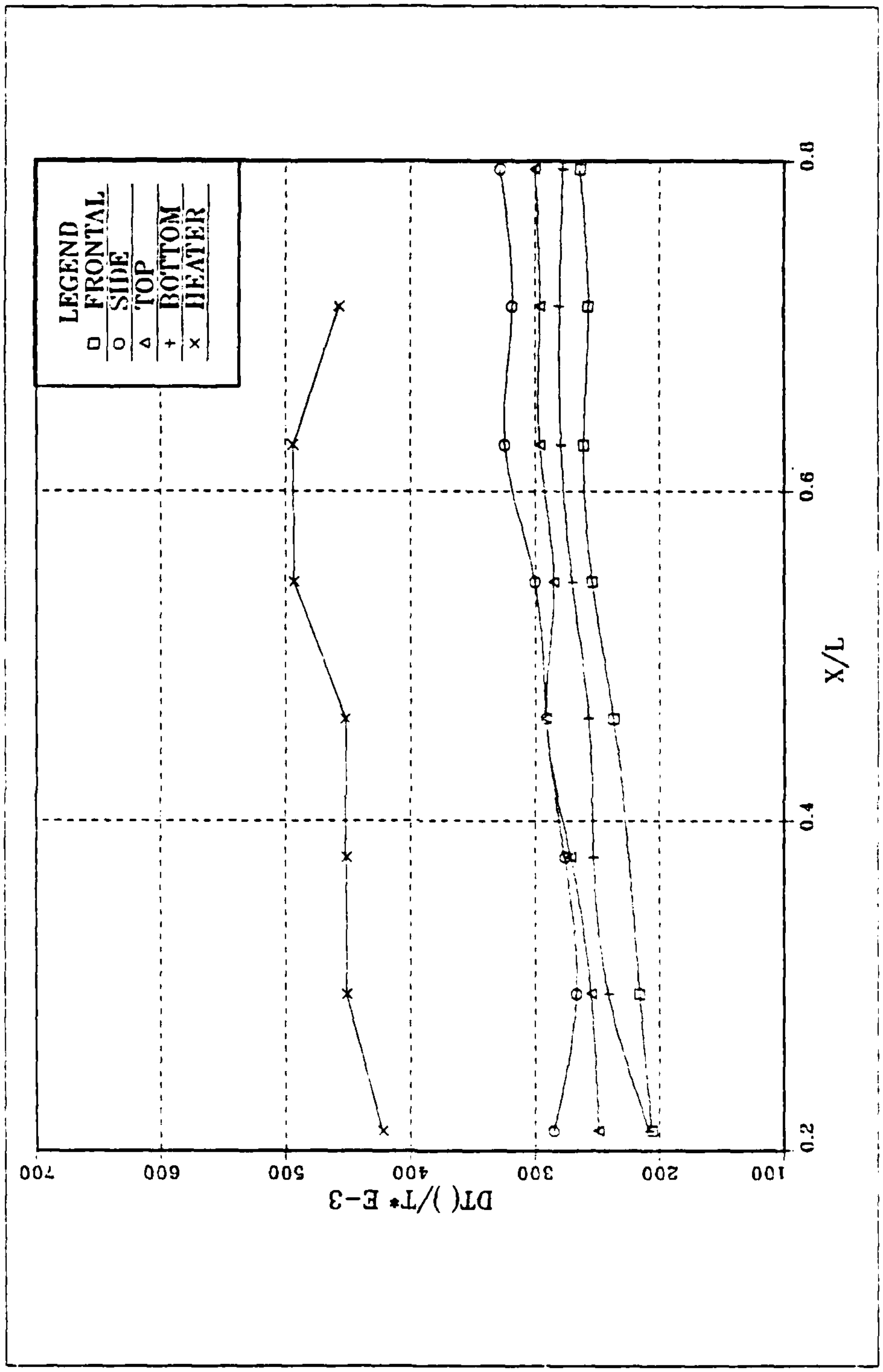

Figure 7. **Nondimensional Temperature Excess vs. Position, 1.0 Watt**

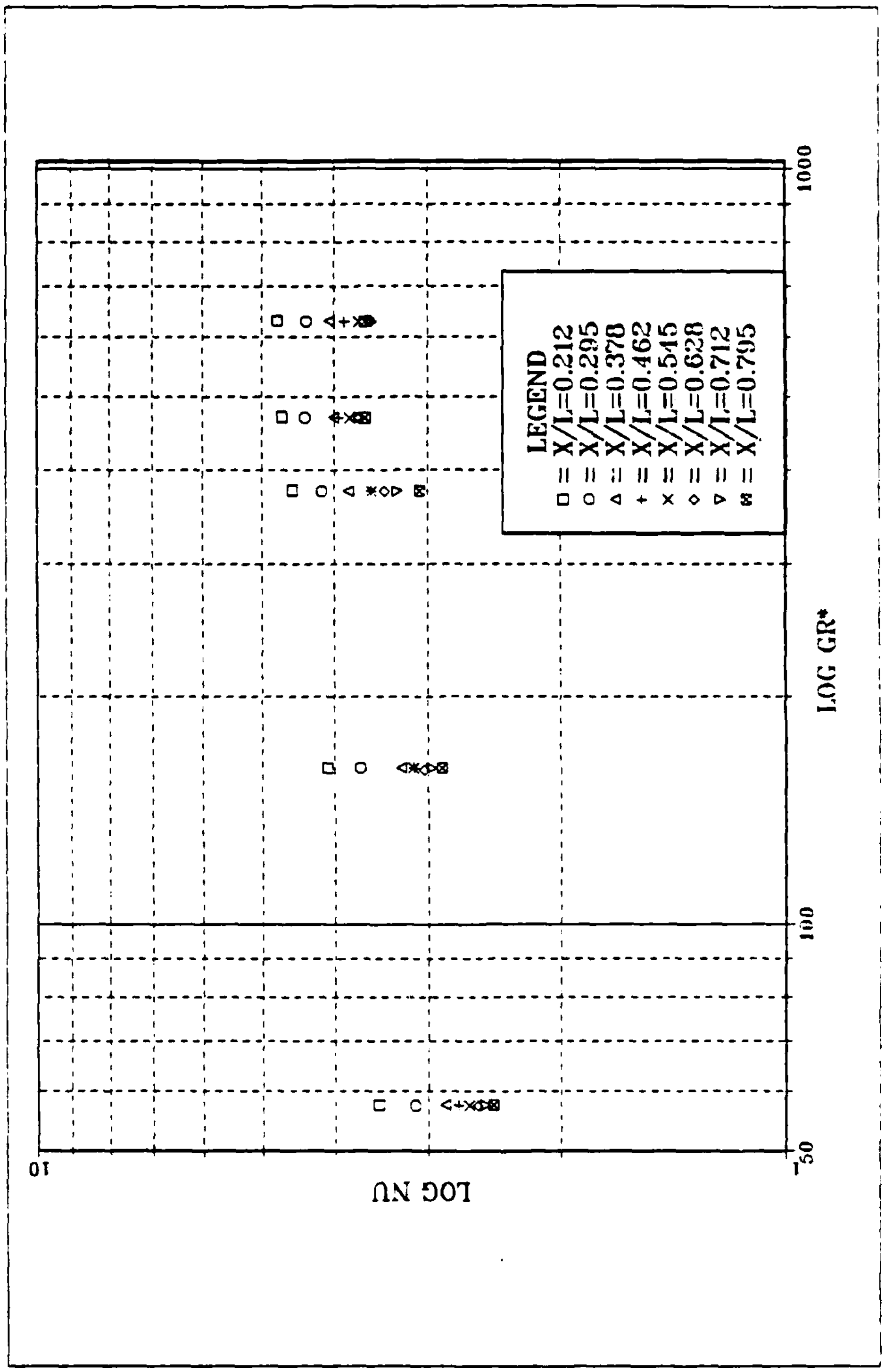

Figure 8. **Data for Nusselt Number vs. Flux-Based Grashof Number**

additional dependence on element location. A review of the data suggested a method by which it could be collapsed. A modified Nusselt number, Nu^*, was calculated by use of a scaling factor based on the net convected energy of the flow at a downstream location. Since each block dissipates approximately an equal amount of power, the net convected energy is proportional to the number of upstream components. The scaling factor was of the form Bn^a where Bn is the block number and $a > 0$. A value of $a = 1/6$ was found to provide the best correlation for the data. As expected, the strong three-dimensional effect on transport results in a weaker downstream dependence than the 1/5 exponent in the Fujii and Fujii correlation for a uniform flux, semi-infinite vertical surface. Therefore,

$$Nu^* = Nu \cdot Bn^{\frac{1}{6}}$$

for each element at each power setting. The modified data are plotted in Figure 9 along with the linear least squares fit. Based on this, the following correlating equation for the heat transfer rates is obtained:

$$Nu^* = 1.88(Gr^*)^{.15}$$

for 50 < Gr_x^* < 1000 and $Pr \sim 7$.

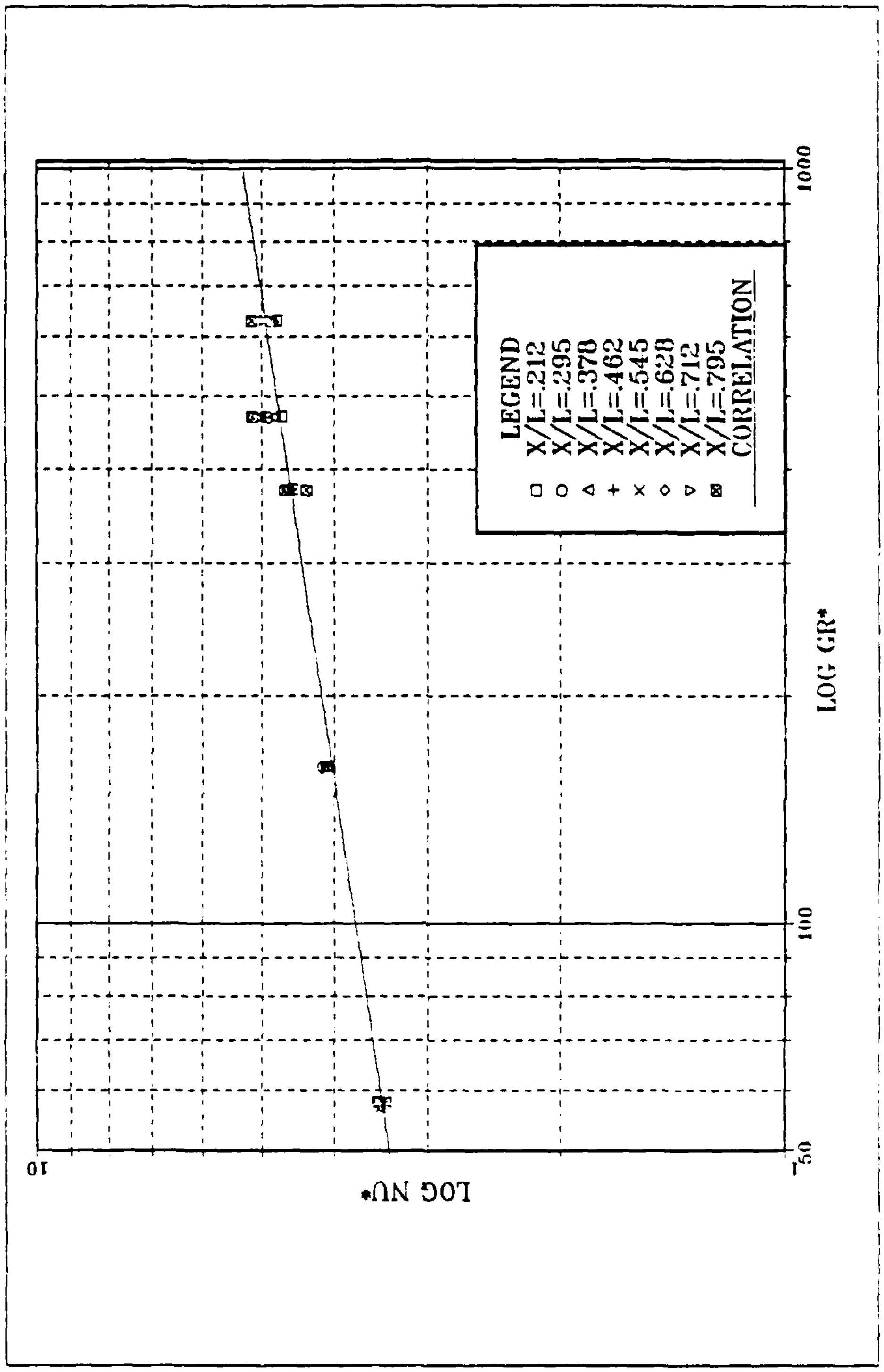

Figure 9. **Nusselt Number vs. Flux-Based Grashof Number With Least Squares Fit**

B. ALL ELEMENTS POWERED, TRANSIENT

1. Flow Visualization

Figure 10 is a series of photographs taken during the 0.2 watt step-up transient. For each picture, the exposure time was 20 seconds. Exposure of the first picture began with power application. The others were initiated at 20, 80, 120, and 200 seconds, respectively, following the start of heating. Clearly, the first two show predominantly parallel flow. The next pictures represent increasing development of the contour flow and boundary layer characteristic development. By 200 seconds, almost fully developed flow is recognized.

Figure 11 is a similar series, again of 20-second exposures, taken during the step-down transient from 1.0 watt. The first visualization at far left began at power down. The remaining photographs were initiated 80, 160, 240, and 440 seconds, respectively, following shutdown. The steady-state flow characteristics persist to an increasingly lesser degree for the entire period observed. The entrainment of ambient fluid lessens at large times. Additionally, flow origin moves slightly downstream over time.

2. Quantitative

The 1.0-watt step-up, step-down transient temperature responses for the component front surfaces are presented on the same graph (Figure 12). Steady state is achieved about 25 percent faster for the power up. The curves representing blocks 1 through 8

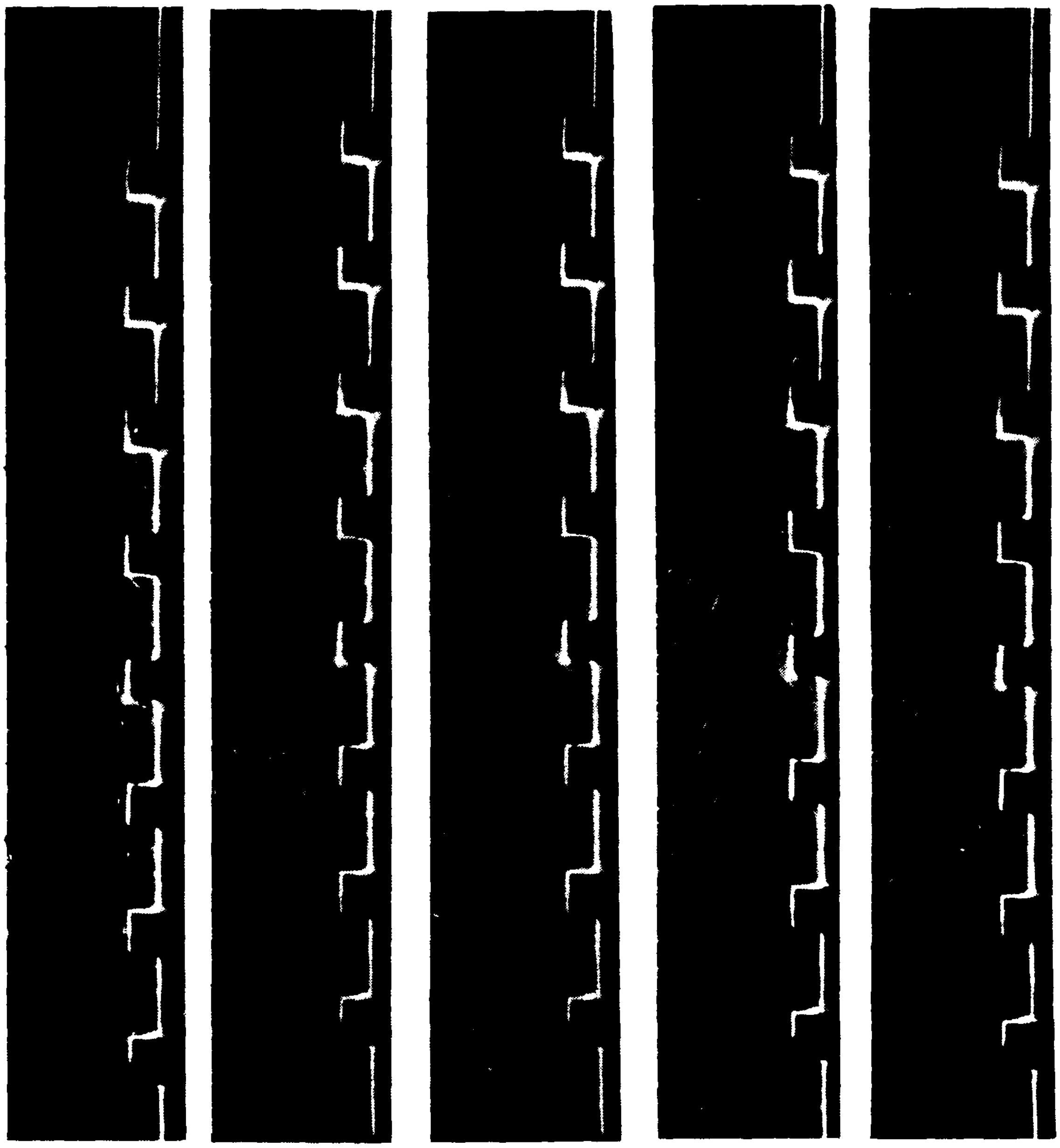

Figure 10. **0.2 Watt Step-Up Transient During Various Time Intervals**

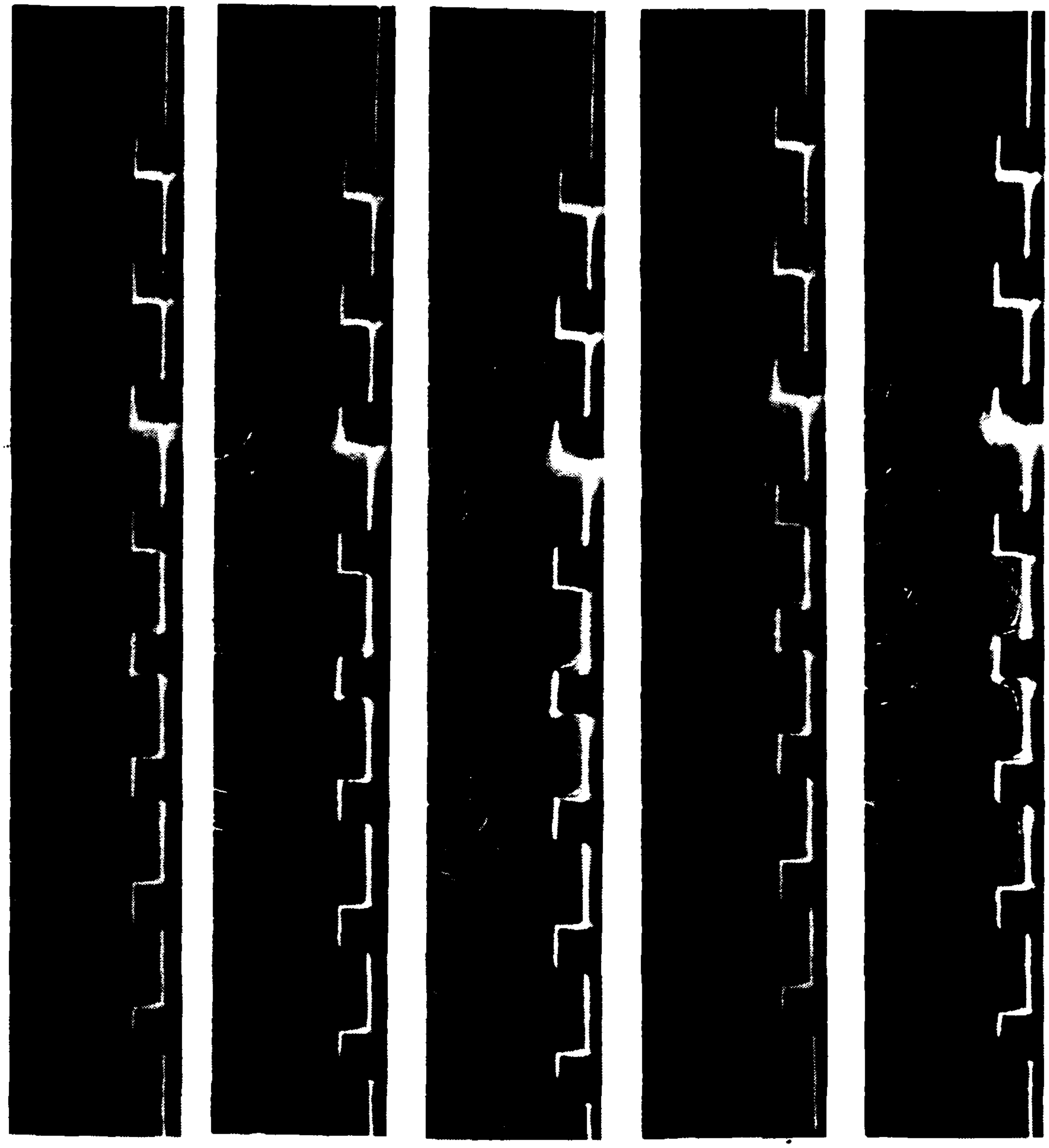

Figure 11. **1.0 Watt Step-Down Transient During Various Time Intervals**

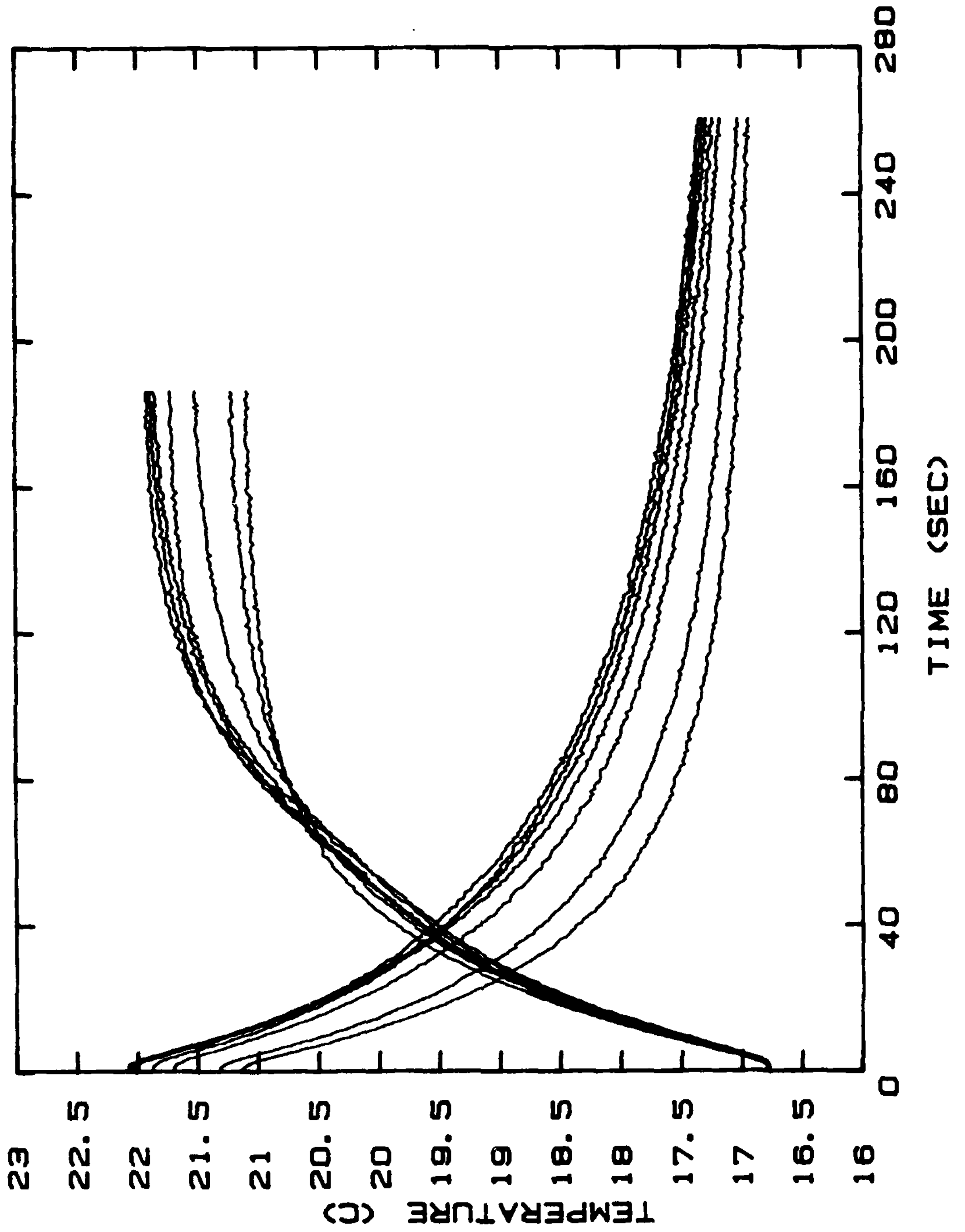

Figure 12. **Transient Temperature Response Following Initiation of Heating, 1.0 Watt**

excluding 3 travel closely together, especially in the first quarter of the response period for the step. The almost single line corresponds to the parallel flow pattern seen in the photographs. This indicates a purely diffusive transport response for a large part of the transient. Later, convective effects become appreciable as entrainment develops downstream. For the step down, steady state temperature is reached much more quickly than breakdown of the established flow. The persistence of flow is conducive to the rapid cooling of the blocks.

The plot for 0.2 watts (Figure 13) reaches steady state at about the same time for both step up and step down. This period is longer than for either 1.0-watt case and indicates that the stronger flow more readily establishes the final thermal pattern.

C. TEMPERATURE MEASUREMENTS IN THE FLUID

Characteristics of the thermal transport in the fluid were measured using a traversing thermocouple probe adjacent to all protruding elements and for points midway between the components (Figures 14 and 15). The fluid temperature responses near the blocks and interblock spaces follow the same pattern, with temperature levels in the vicinity of blocks 4 and 6 surprisingly greater than for the others. Indeed, both graphs can be seen to have four groupings. Block 1 by itself, the lowest curve, is followed by 2, 3, and 5; then 4, 7, and 8; and finally block 6 by itself. More detailed local measurements are needed to explain these variations.

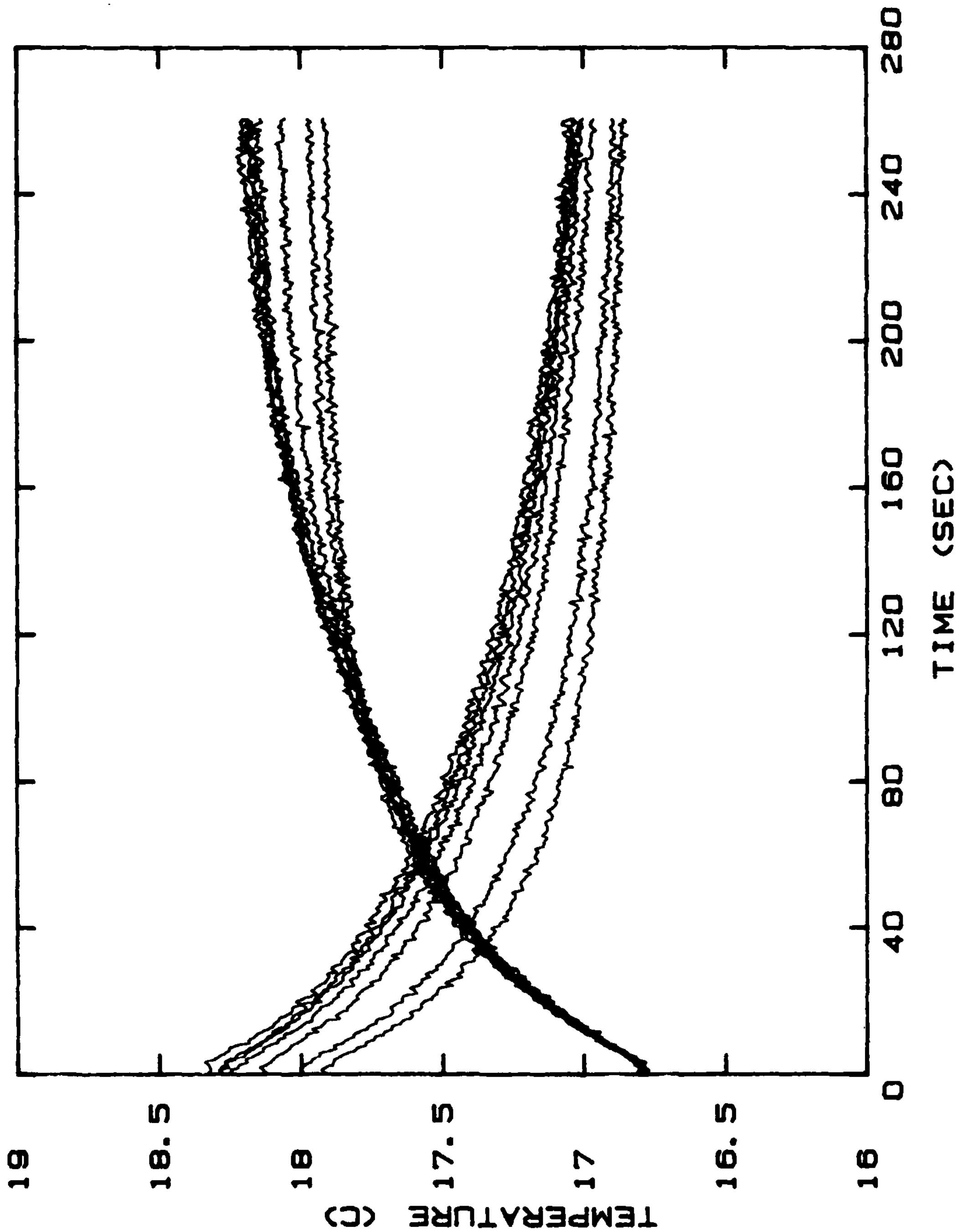

Figure 13. **Transient Temperature Response Following Termination of Power, 0.2 Watts**

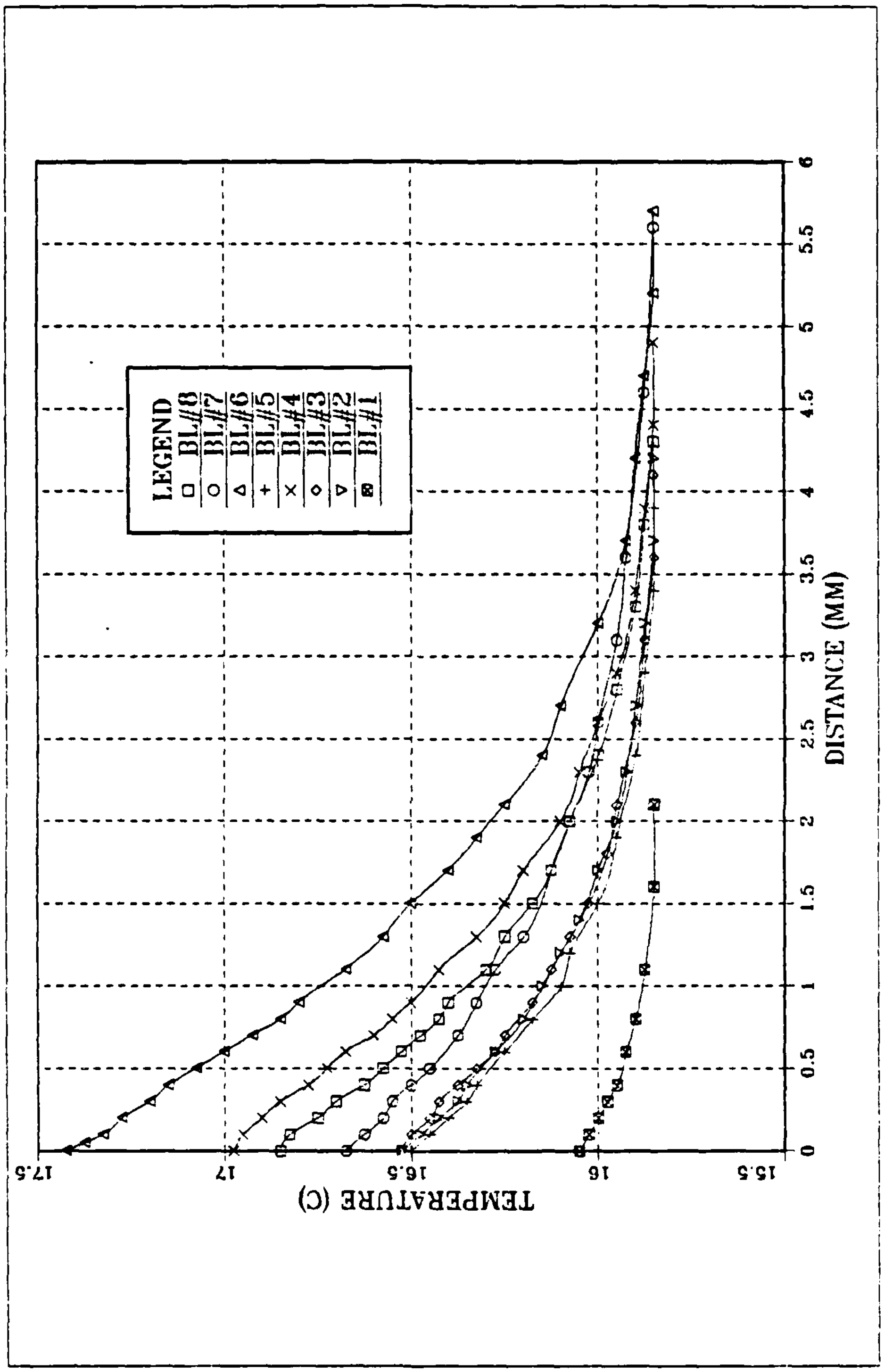

Figure 14. **Fluid Temperature Distribution in the Normal Direction, Away From Block Faces**

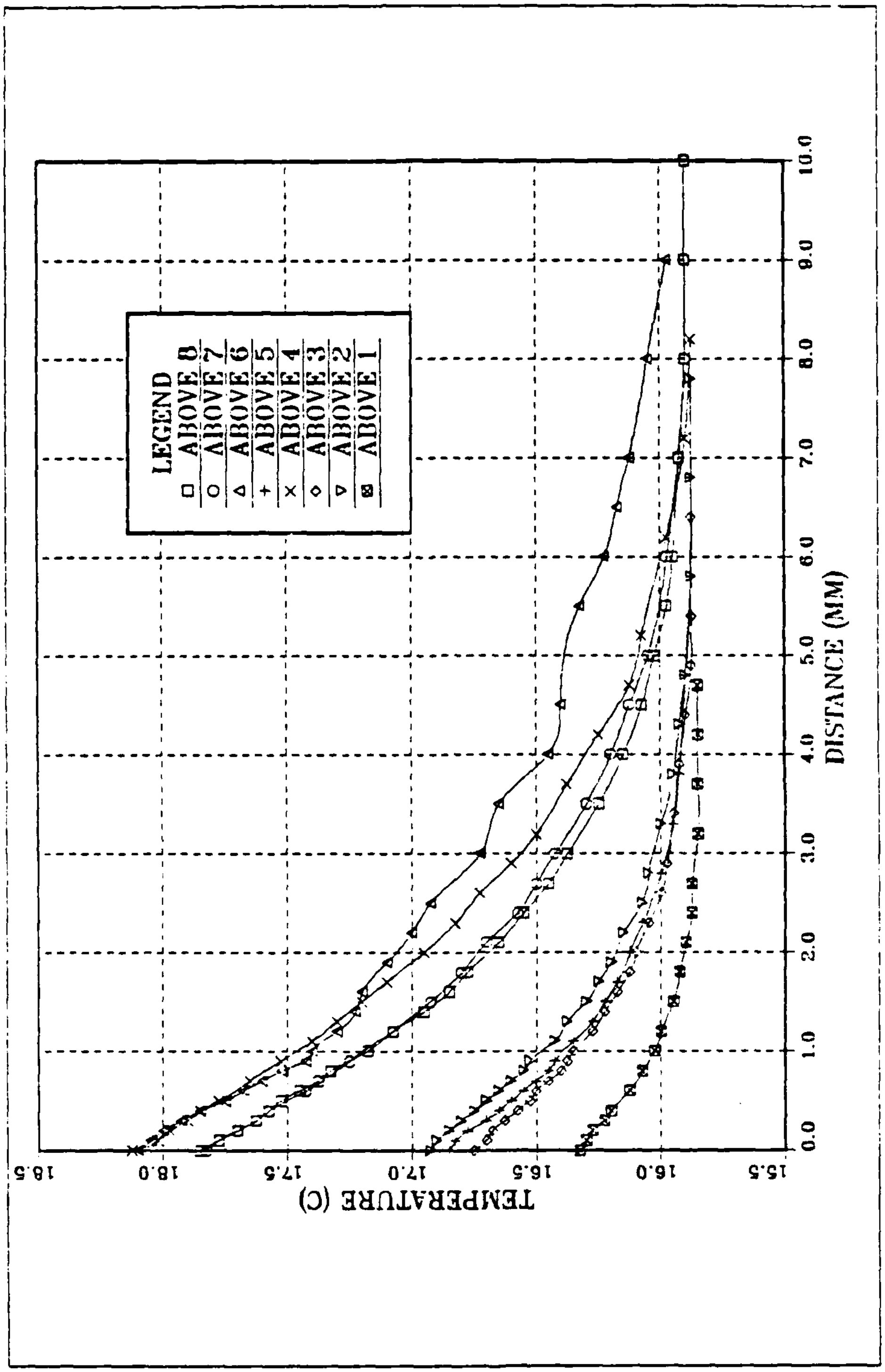

Figure 15. **Fluid Temperature Distribution in the Normal Direction, Away From Plexiglass Substrate**

The layer between the blocks is slightly thicker with respect to that at the block faces. This might be expected from the flow visualization (Figure 4) showing that the particle traces spread out between elements. In each case, the thermal layer is about one component height or less and is therefore deeply imbedded within the momentum exchange region. This is expected due to the relatively large $Pr \sim 7$ for water.

Next, the traversing probe was placed in the thermal layer, 1 mm from the surface, and moved in the x-z plane across the test surface face (Figures 16 and 17). The temperature variations, with position, reinforce the photographs in suggesting strongly three-dimensional transport. Ambient temperature is the lowest point shown. The peaks at about 15 percent from each edge (Figure 16) correlate with the regions in the visualization (Figure 5), where the flow begins to shift from x-y dominant to x-z and may indicate a common region through which those particles are flowing. The result is more, warmer fluid convected over that region. Likewise, the peaks of Figure 17 might represent a similar flow shift at locations between the components.

Finally, the probe was placed above the center of the top face of block 8, 2 mm out from the substrate to measure the downstream temperature decay (Figure 18). The extremely high temperature in the immediate vicinity of the top face suggests a dead zone, as did the

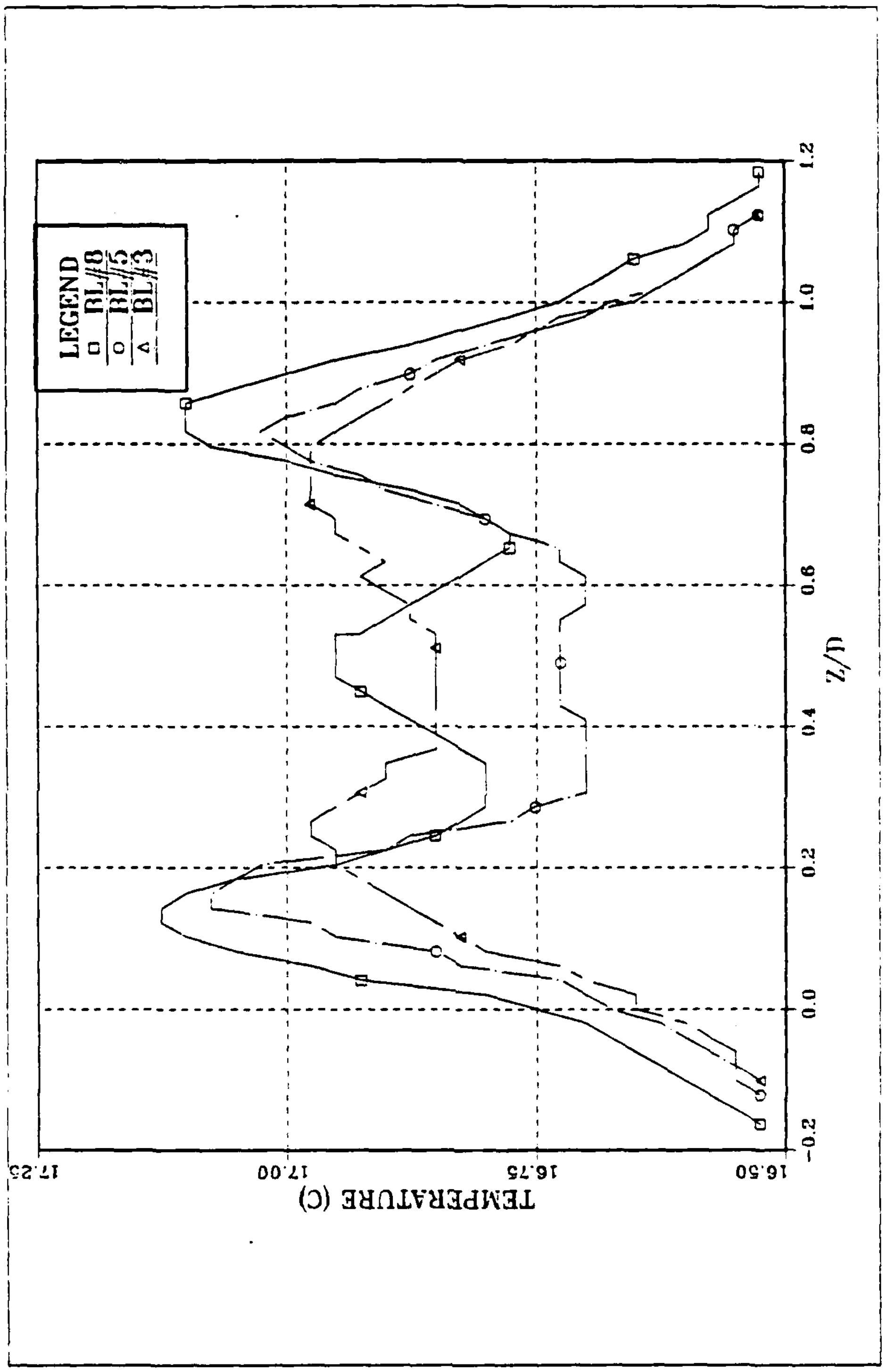

Figure 16. **Spanwise Fluid Temperature Distribution Across Components**

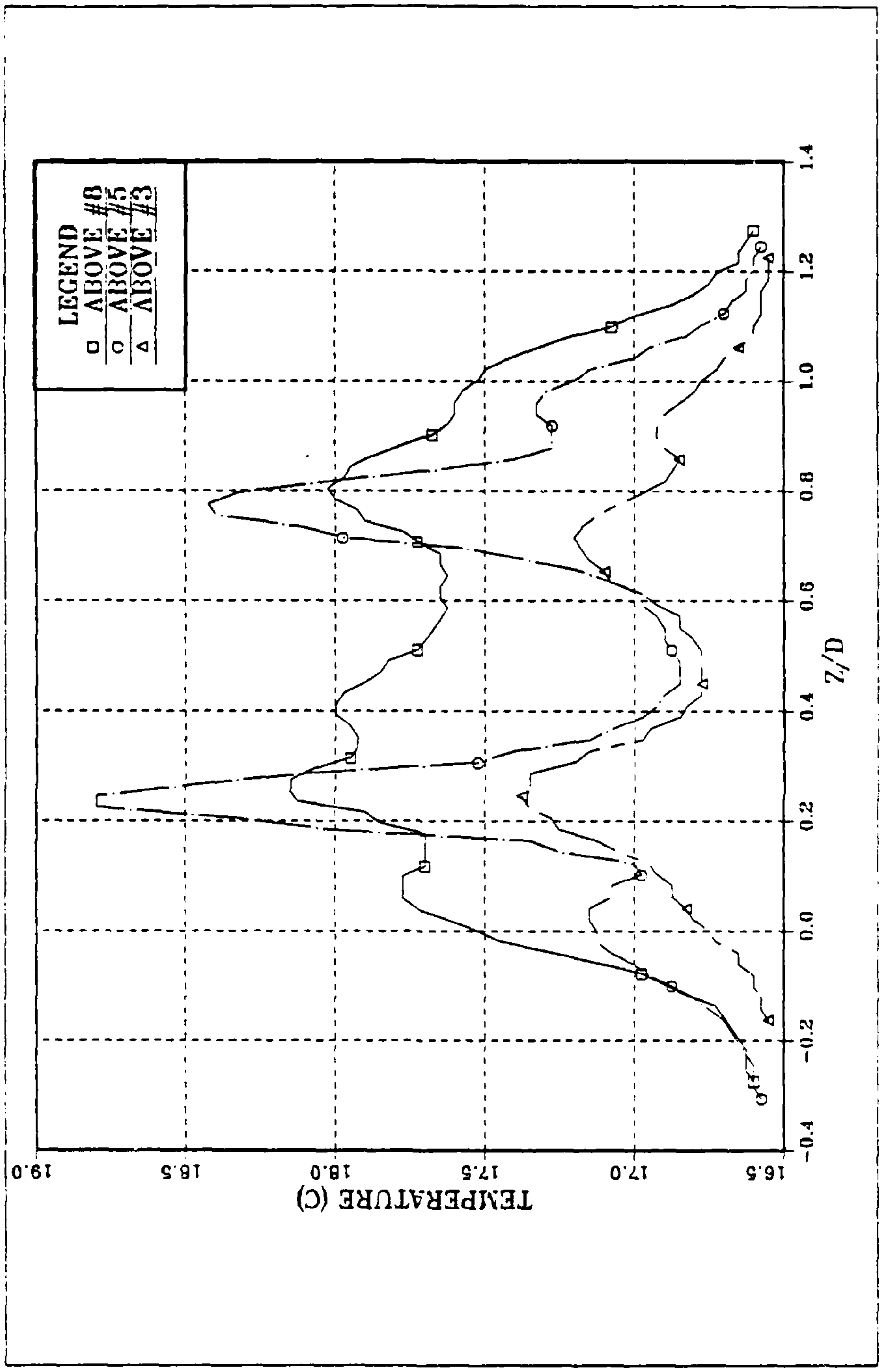

Figure 17. **Spanwise Fluid Temperature Distribution Across Intercomponent Spaces**

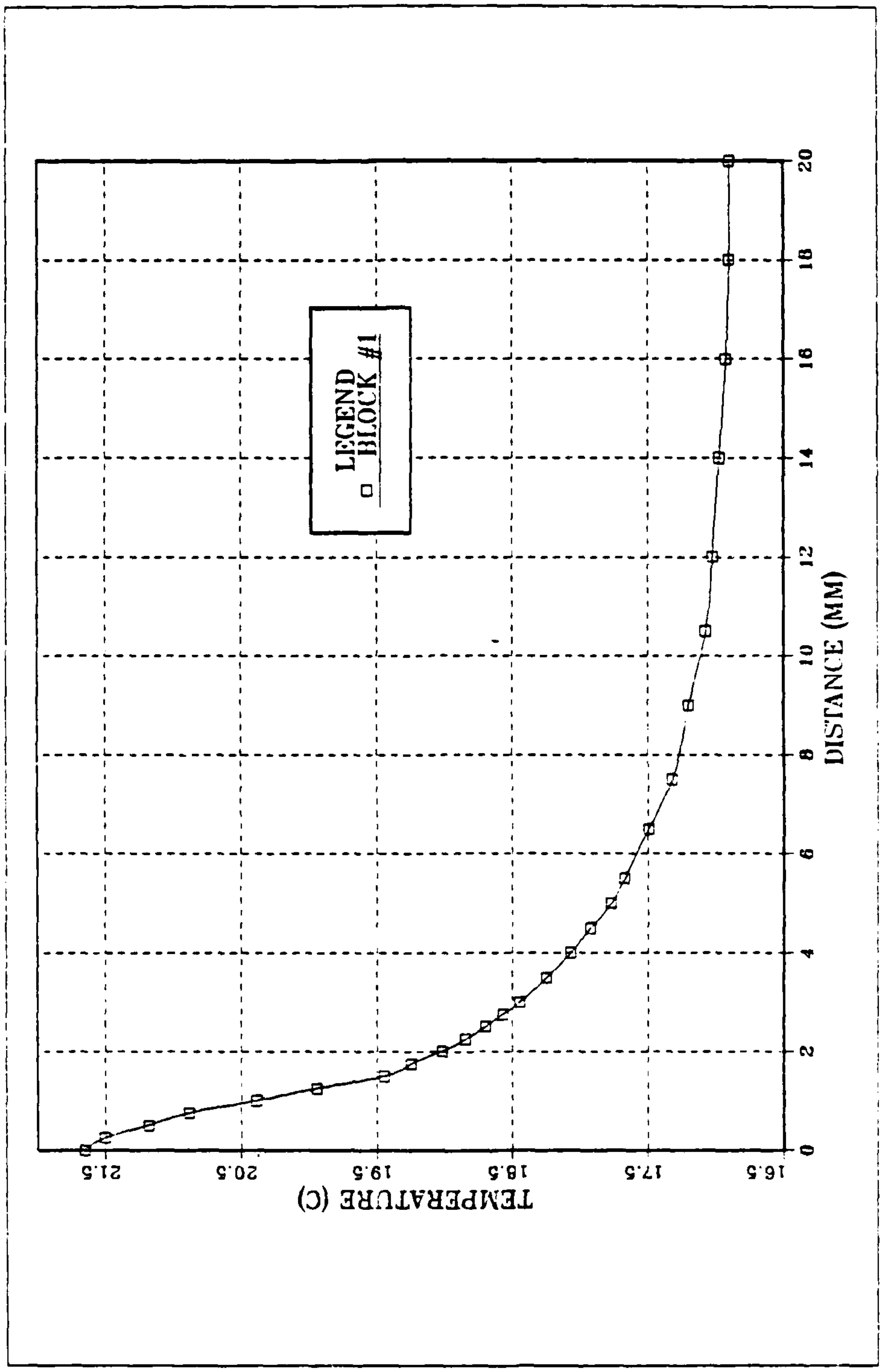

Figure 18. **Fluid Temperature Decay Downstream of Top Component**

visualizations, where a small pool of fluid is heated primarily by thermal conduction from the component upper surface. There was no sign of a vortex.

All measurements with the probe were remarkably consistent over time (±1 μv) at any position. No evidence by any measurement indicated the presence of turbulent flow for the power levels investigated.

D. INDIVIDUAL ELEMENTS POWERED

Individual blocks were powered to 1.0 watt, one at a time. The resulting steady-state array temperatures were monitored and the flow visualized. These are discussed next.

1. Flow Visualization

A series of photographs show single-element heating as that element changes from one block to the next up the array. The exposure times for all pictures presented were 40 seconds. Figure 19 presents left to right blocks 1, 3, and 4 heated and Figure 20 shows blocks 5, 6, and 7. The flow with only the lowest block heated resembles the all-components-heated case, indicating flow around block contours and a boundary layer characteristic over the entire length. As progressively higher blocks are heated, a quiescent area begins to develop adjacent to the lower part of the test surface. Typically, fluid entrainment results in vigorous flow around the first block upstream of the one heated. At two blocks upstream, a comparatively weaker flow is seen and at three the fluid is nearly quiescent.

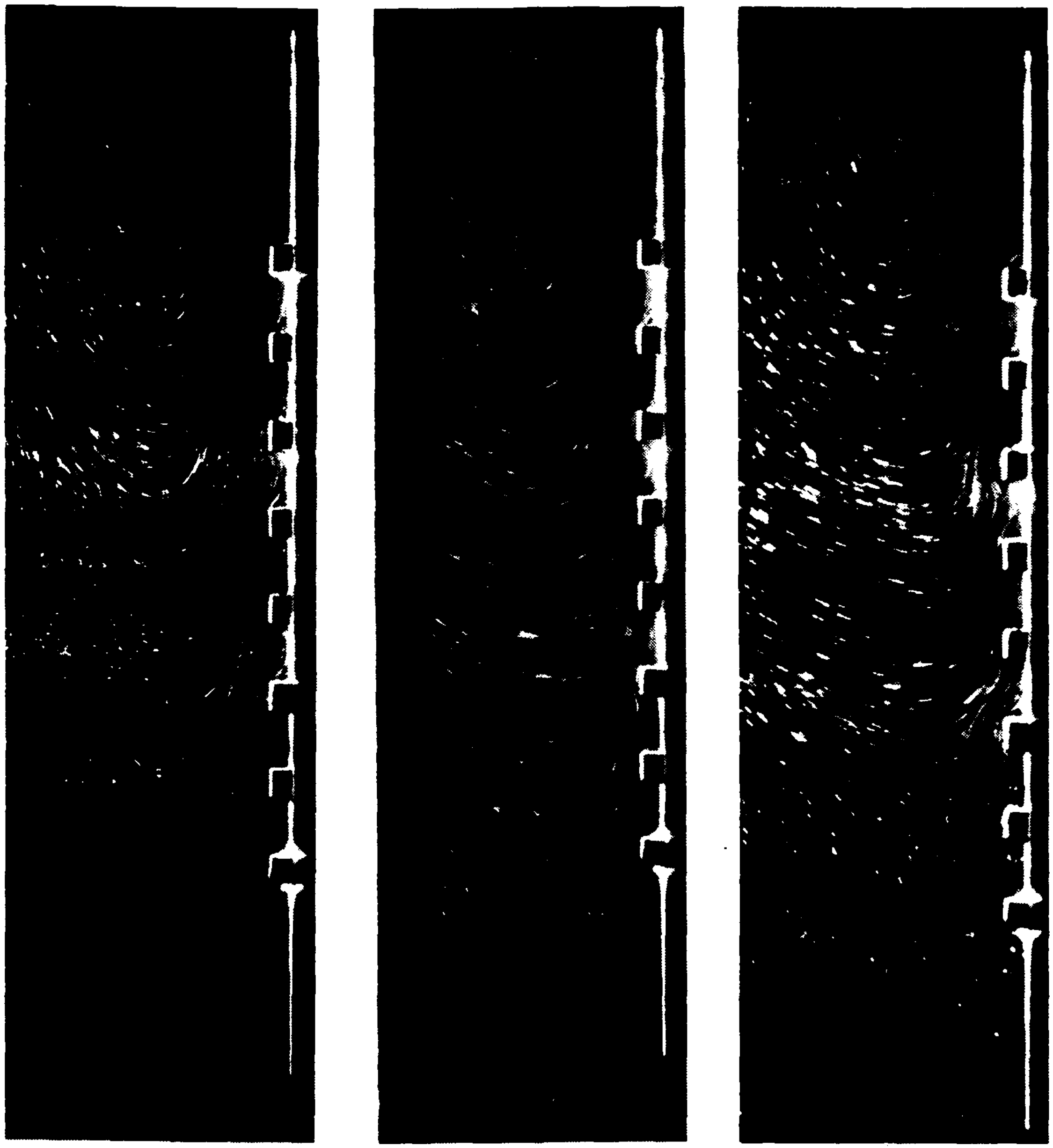

Figure 19. **Steady Flow Responses With Blocks 1, 3, and 4 Individually Heated**

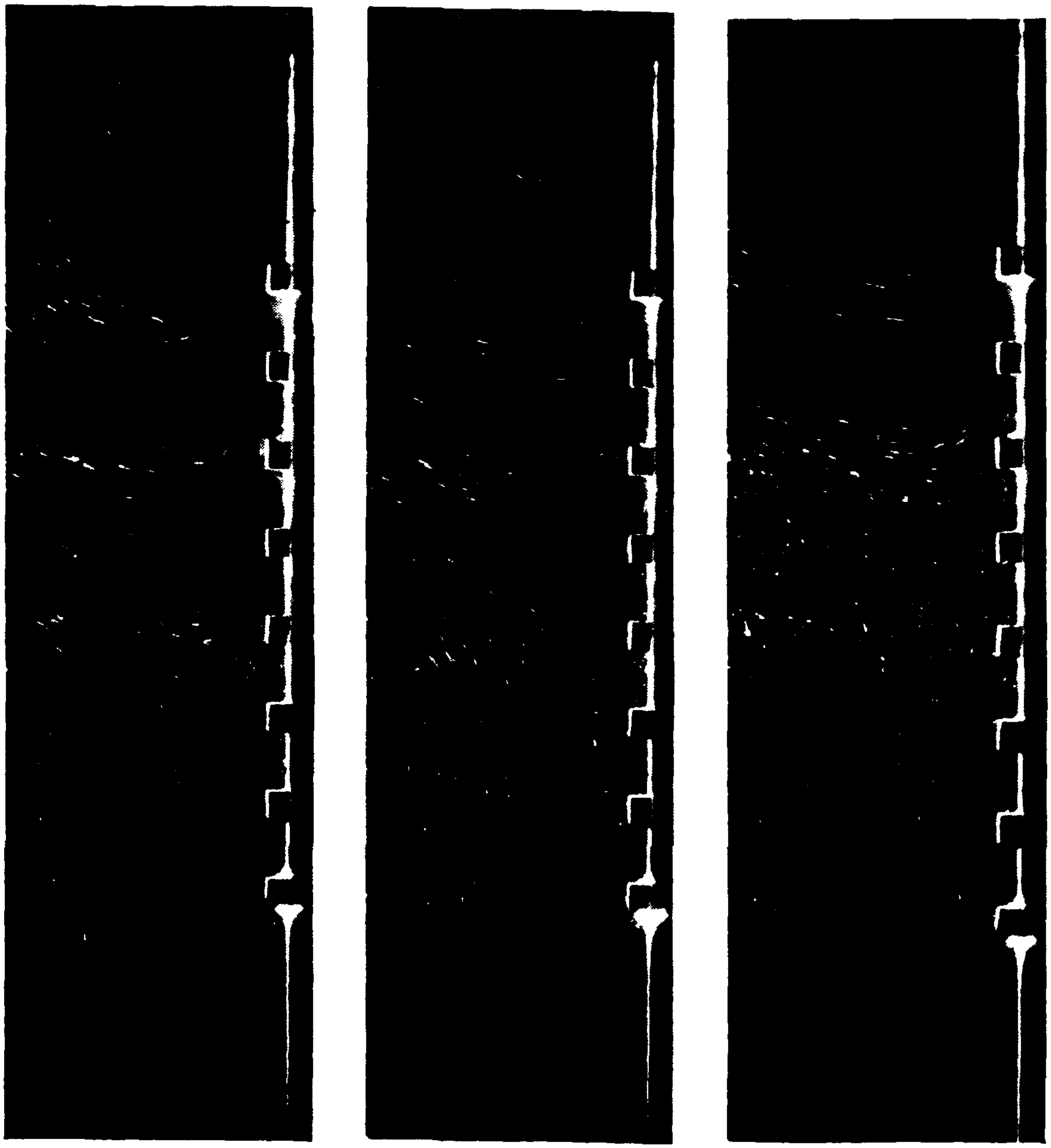

Figure 20. **Steady Flow Responses With Blocks 5, 6, and 7 Individually Heated**

2. Quantitative

Nondimensionalized temperature excesses for the faces and heater of each element are displayed (Figures 21 through 25). The plots show very similar temperature excess patterns around the heated element as the selected component progresses up the array. The protruding elements have minimal effect when they are part of the unheated starting length.

E. COMBINATIONS OF ELEMENTS HEATED

As in Section D, progression was made up the array, except that all upstream blocks remained heated. Figures 26 through 30 indicate very little effect of powering of downstream components on the temperature responses of already-powered upstream components. Also evident is a very sharp decay in temperature in the unheated blocks.

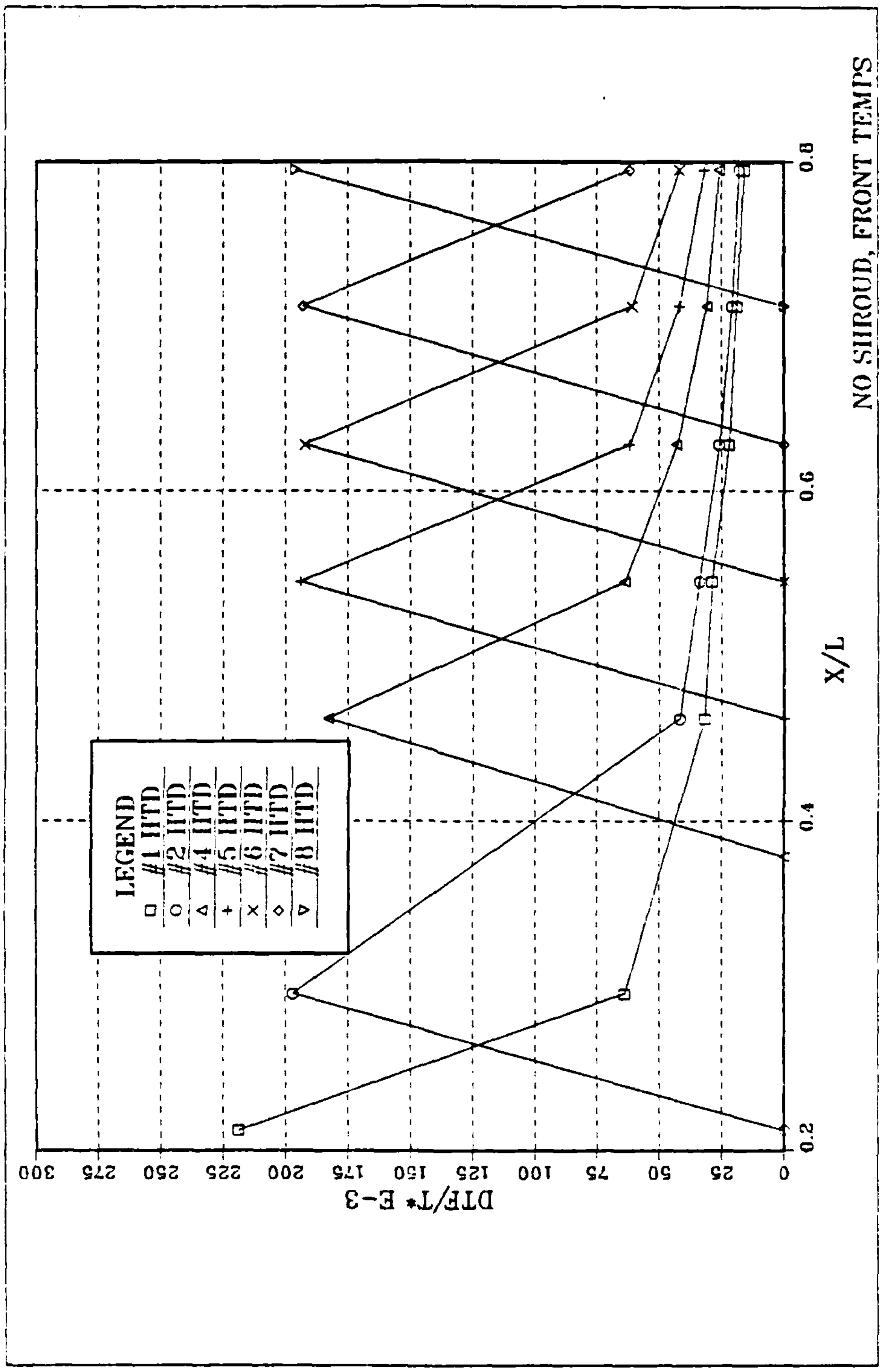

Figure 21. **Nondimensional Temperature Excess Levels at Front Faces of Individually Heated Components**

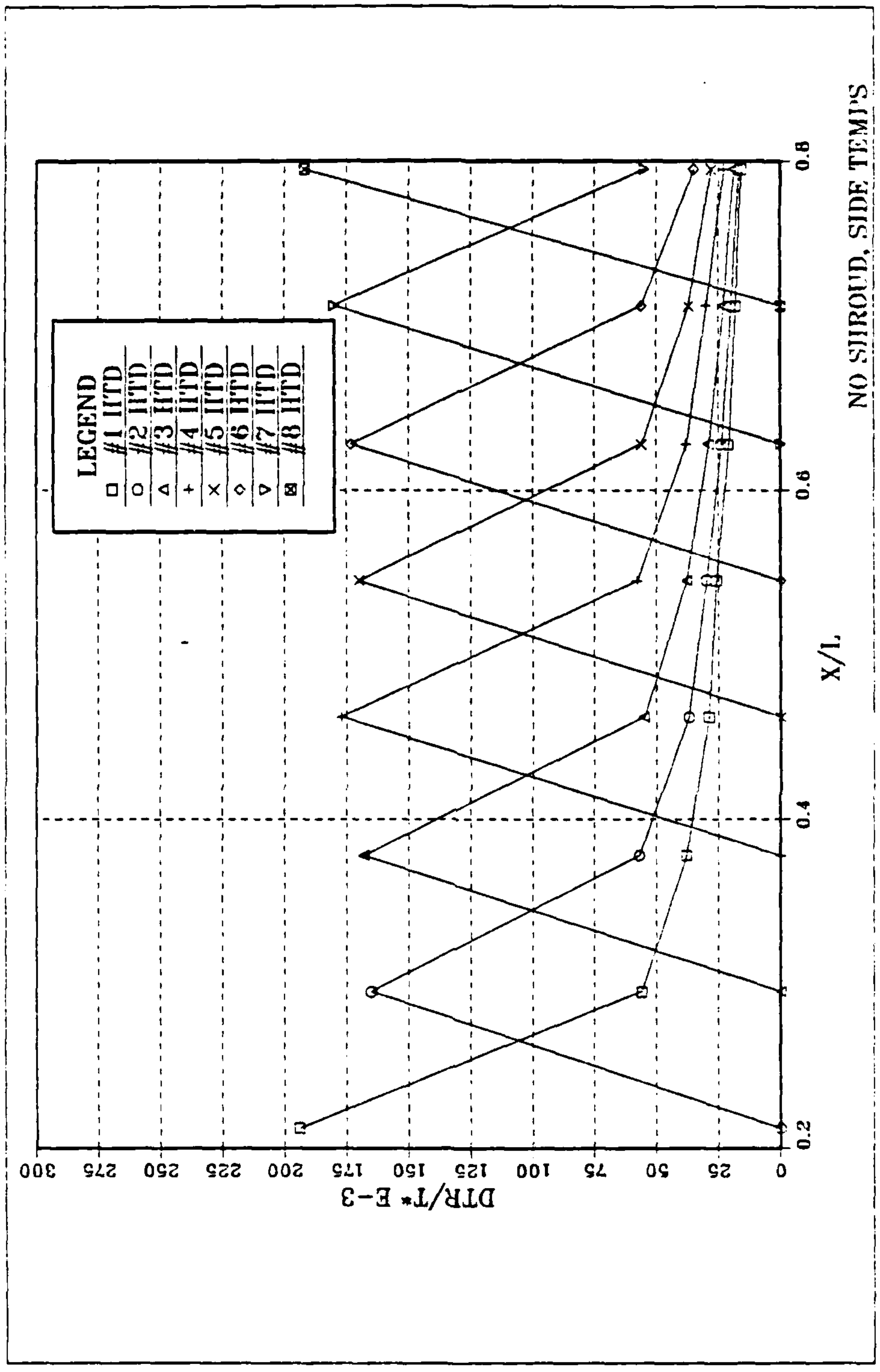

Figure 22. **Nondimensional Temperature Excess Levels at Right Faces of Individually Heated Components**

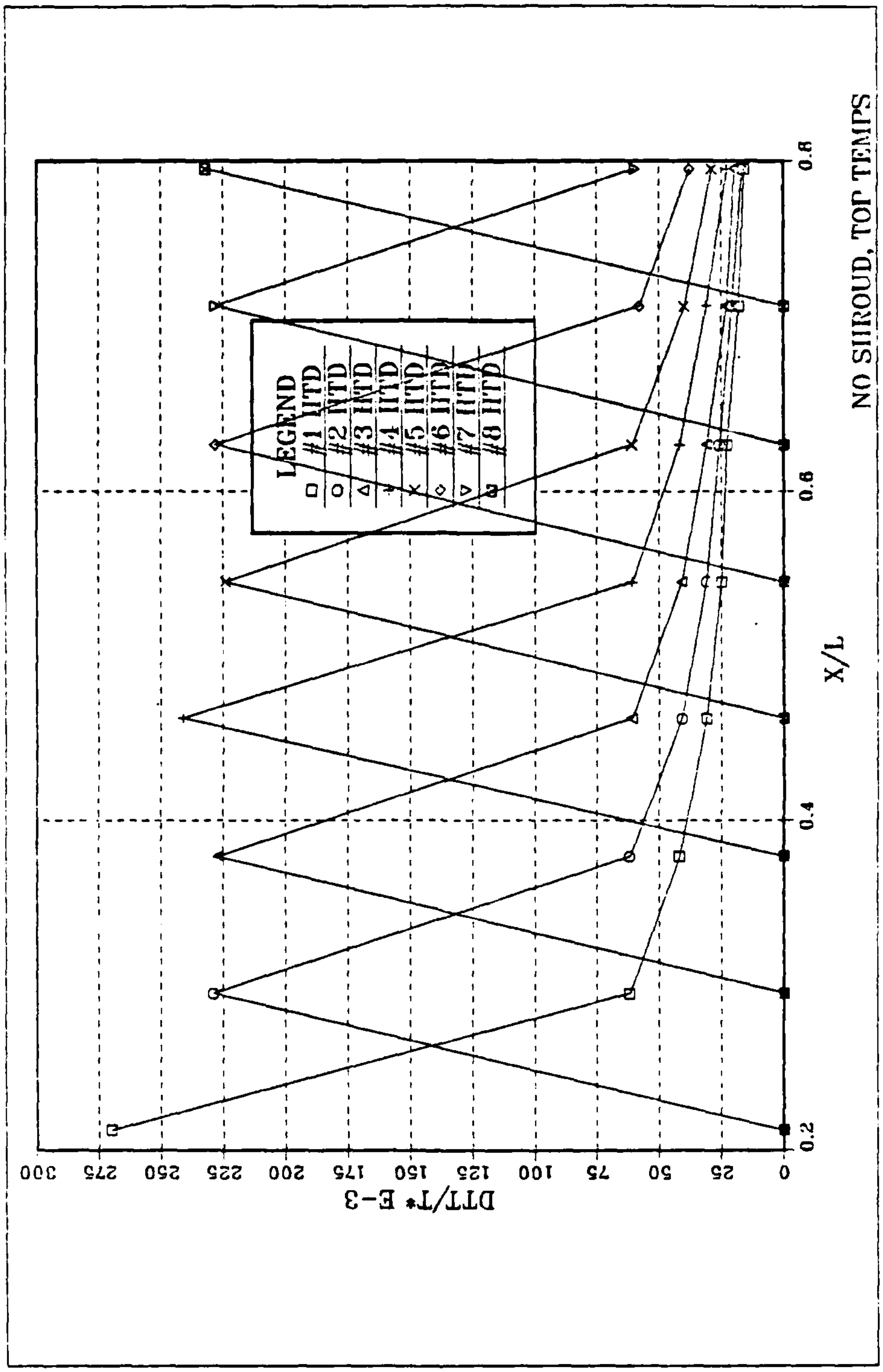

Figure 23. **Nondimensional Temperature Excess Levels at Top Faces of Individually Heated Components**

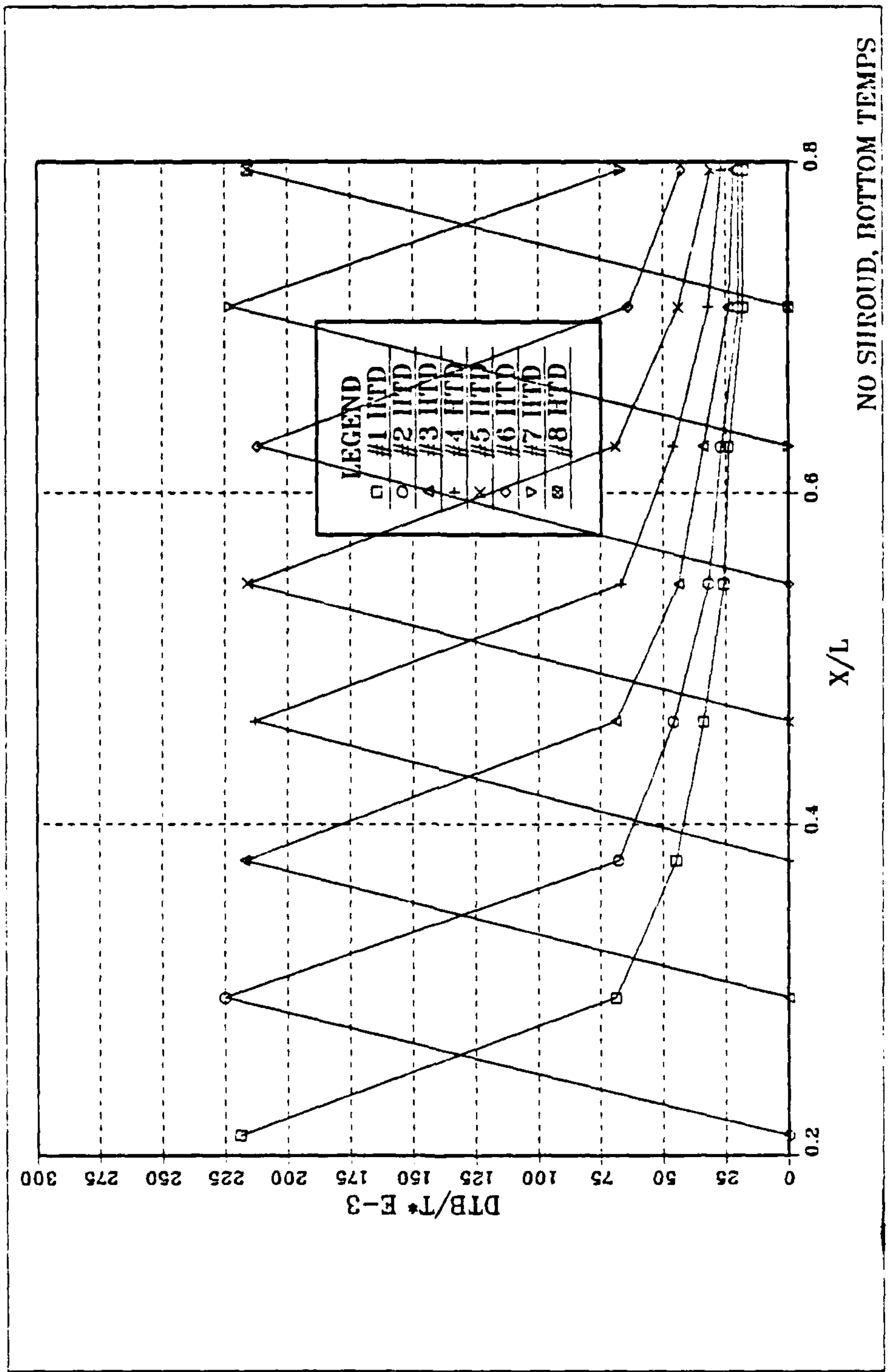

Figure 24. **Nondimensional Temperature Excess Levels at Bottom Faces of Individually Heated Components**

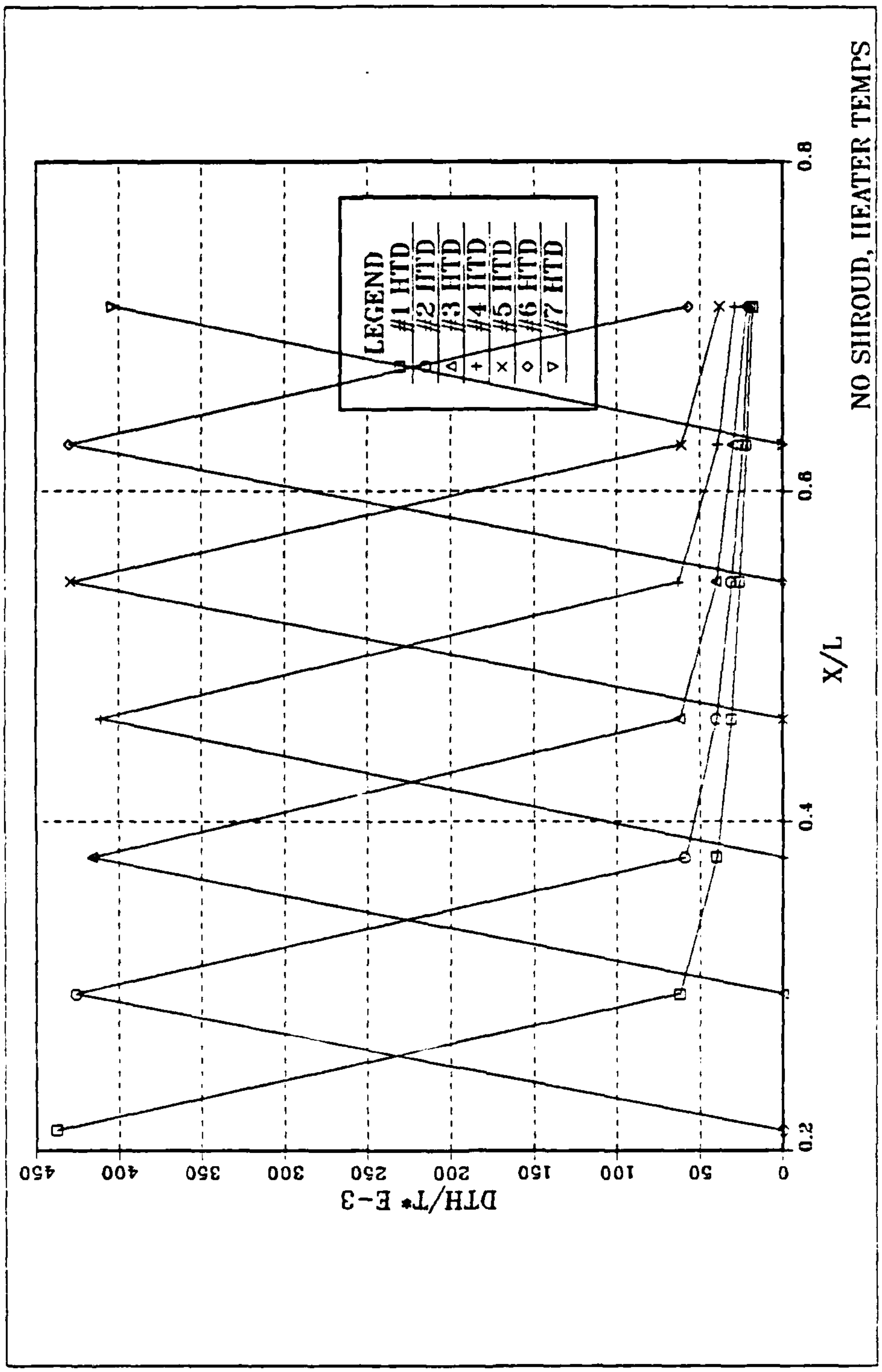

Figure 25. **Nondimensional Temperature Excess Levels at Heaters of Individually Heated Components**

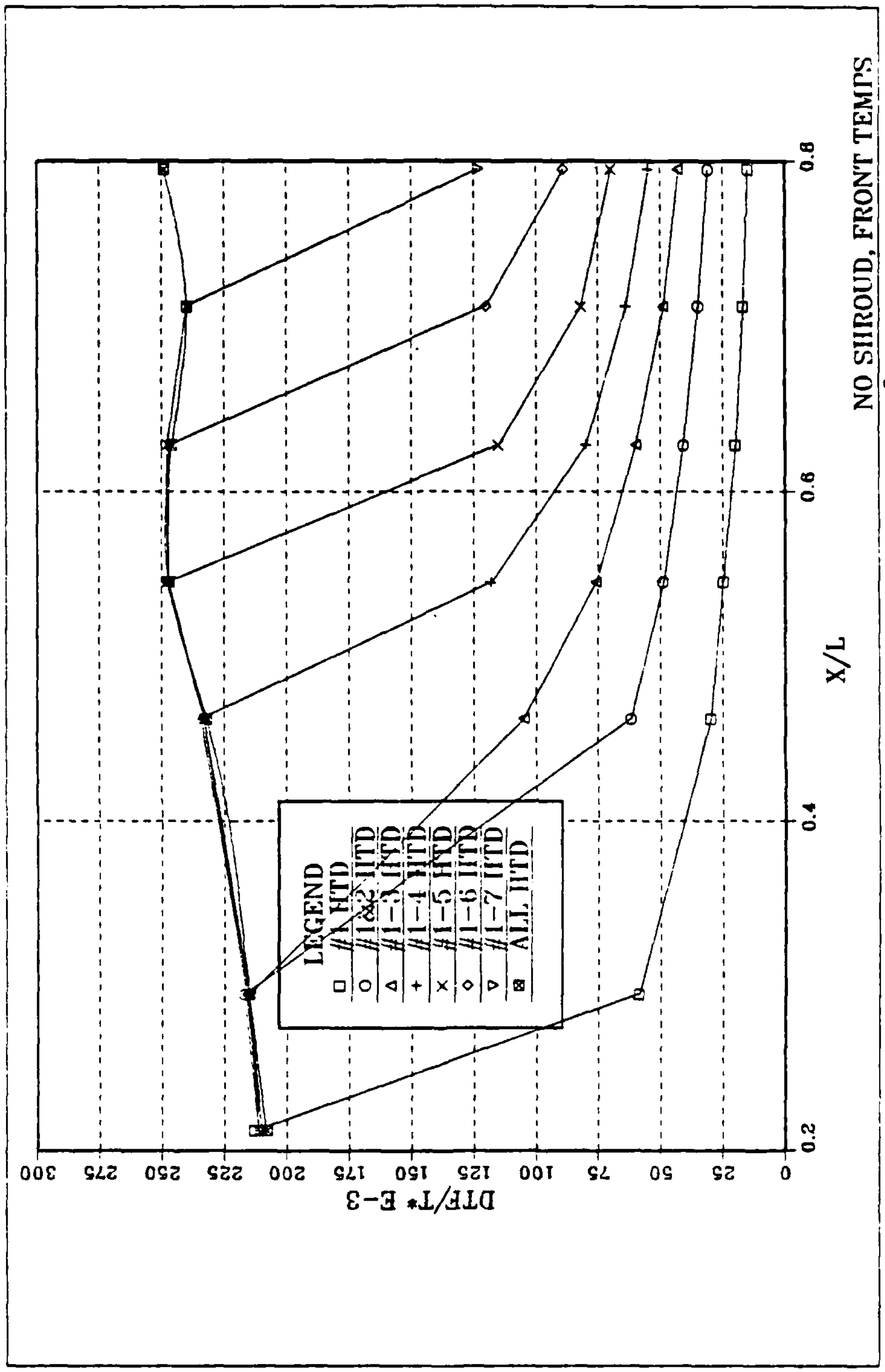

Figure 26. **Nondimensional Temperature Excess Levels at Front Faces of Multiple Heated Components**

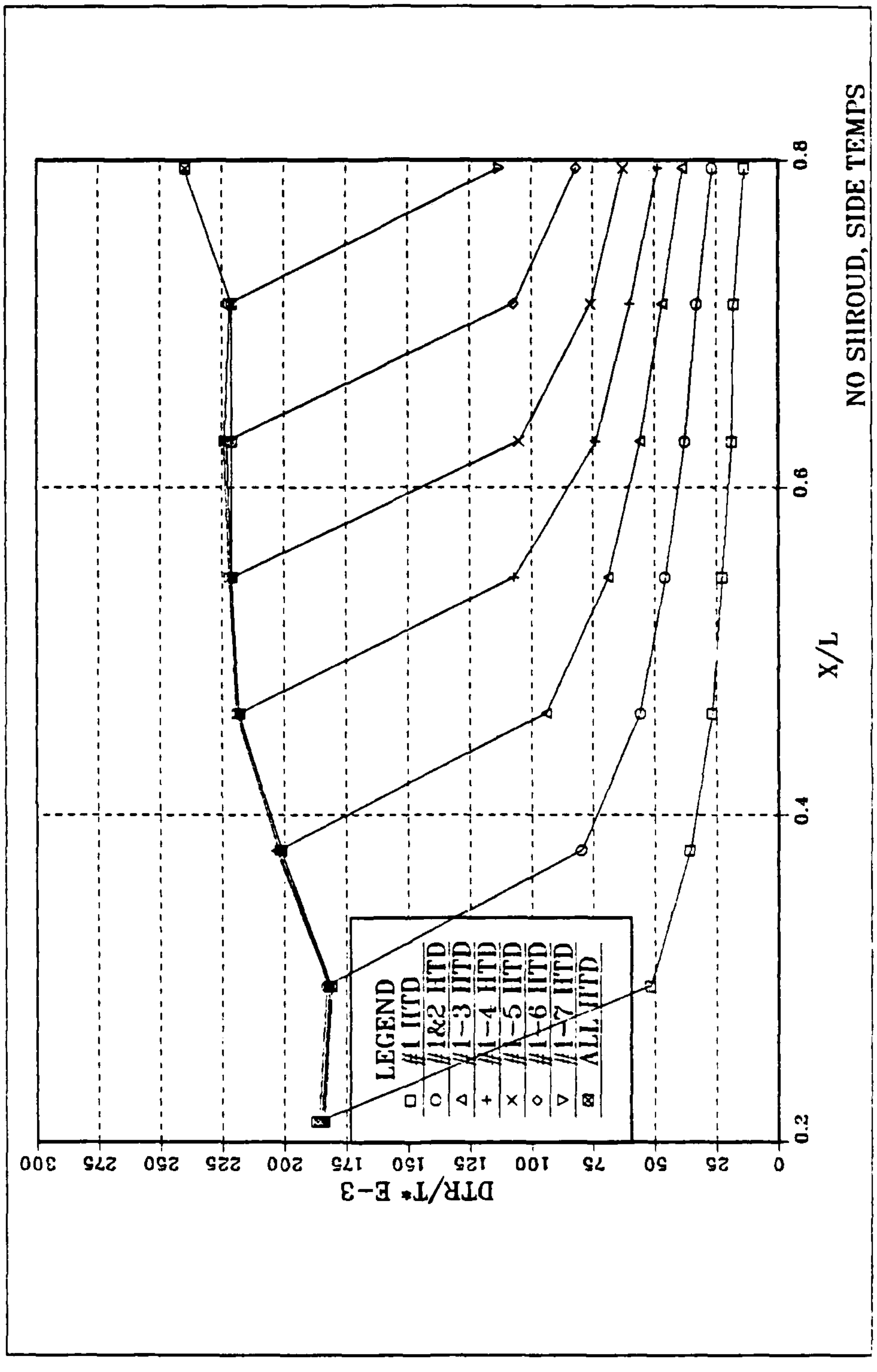

Figure 27. **Nondimensional Temperature Excess Levels at Right Faces of Multiple Heated Components**

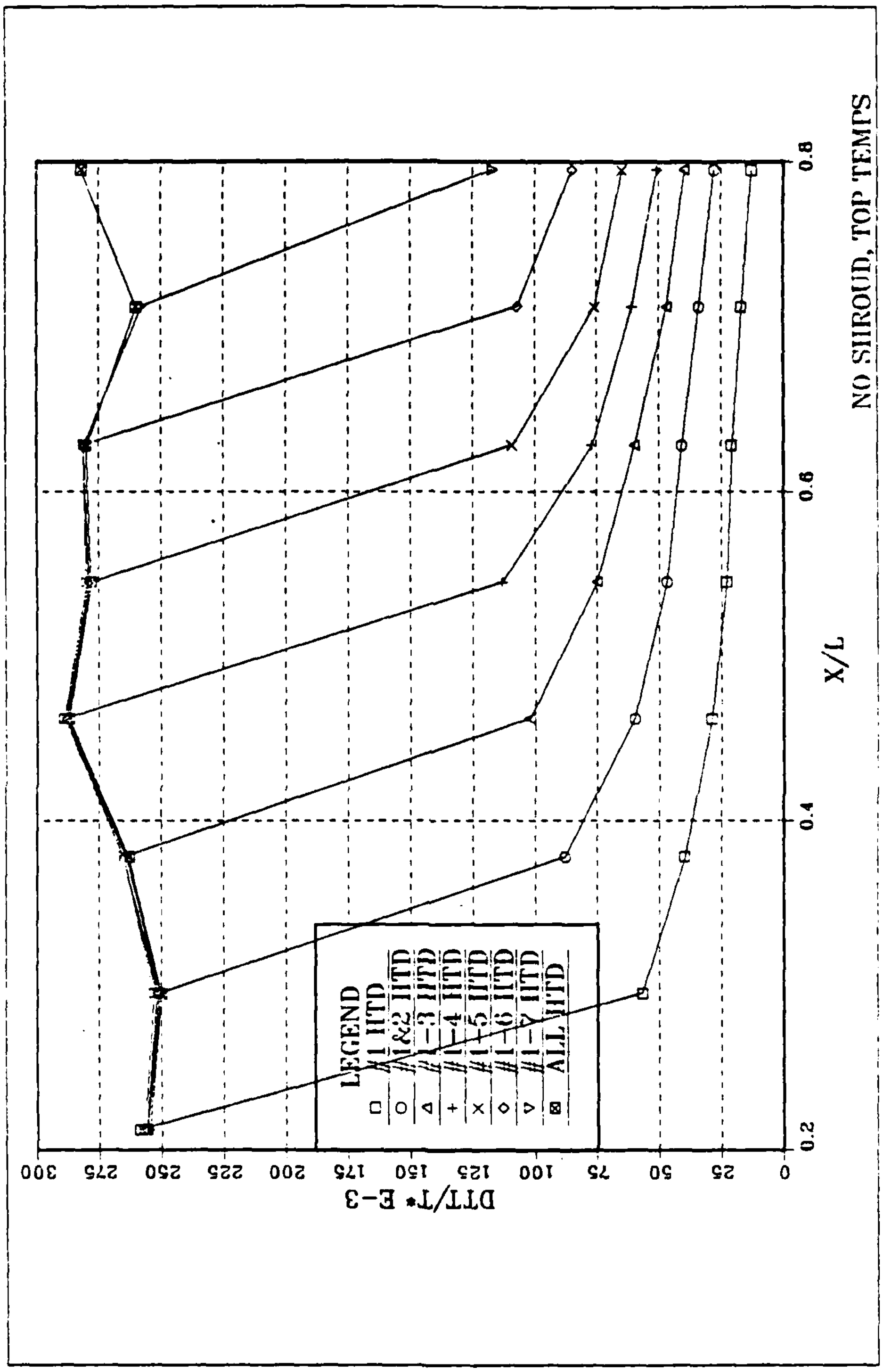

Figure 28. **Nondimensional Temperature Excess Levels at Top Faces of Multiple Heated Components**

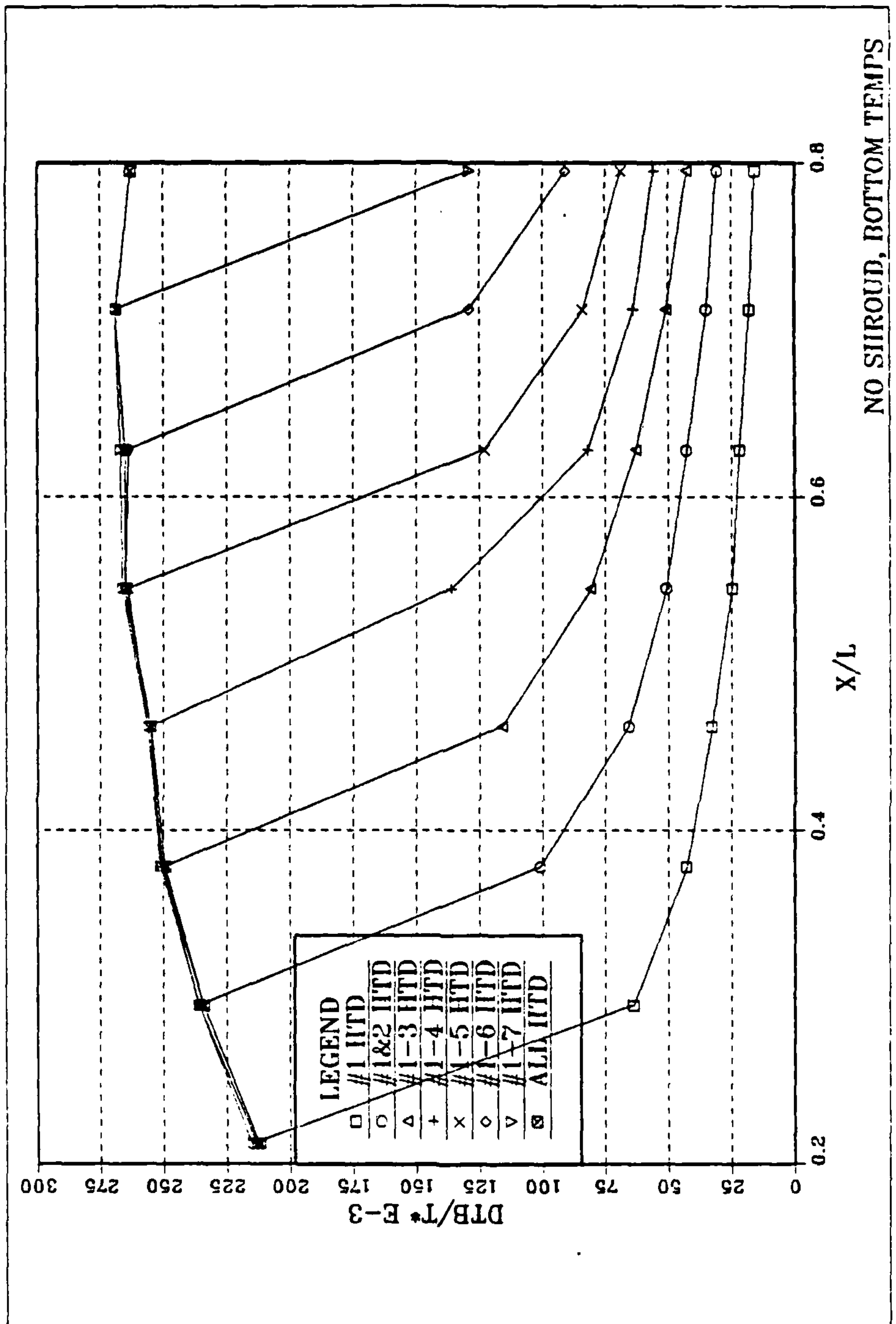

Figure 29. **Nondimensional Temperature Excess Levels at Bottom Faces of Multiple Heated Components**

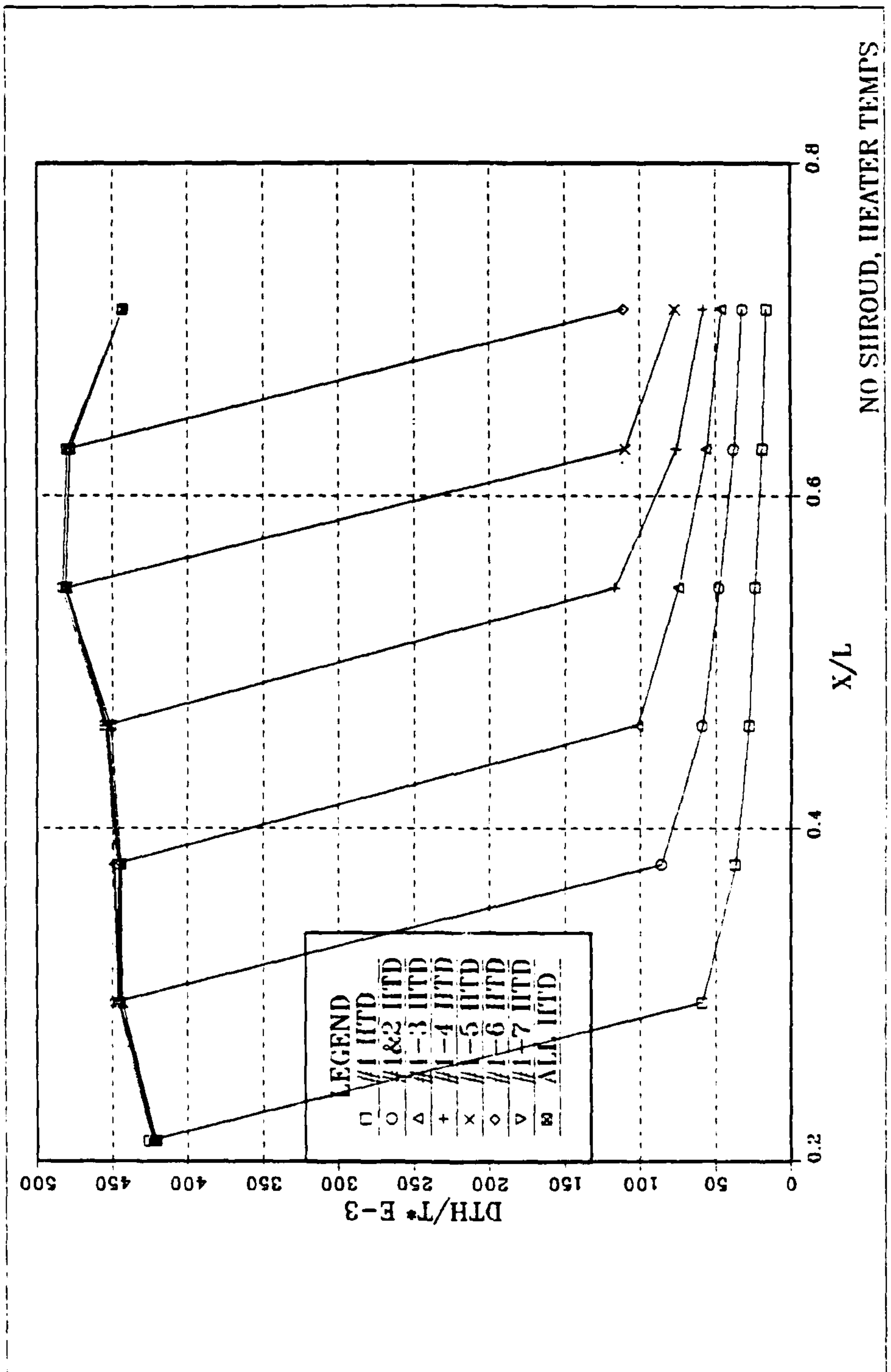

Figure 30. **Nondimensional Temperature Excess Levels at Heaters of Multiple Heated Components**

IV. SHROUD IN POSITION—FINITE CHANNEL WIDTHS

A plexiglass plate (shroud) was used (Figure 1) to simulate the channel formed by two adjacent parallel printed circuit boards. The test surface as before has protruding heated elements. The shroud simulates the reverse side of the second board in an array.

A. ALL ELEMENTS POWERED, STEADY STATE

1. Flow Visualization

Photographs presenting natural convection flow in the x-y plane, geometrically centered through each component (Figure 31), were evaluated. The visualizations are for all elements heated to 0.5, 1.0, 1.2, and 1.5 watts. The exposure times were 20 seconds. The shroud distance was 18 mm from the substrate or approximately three component depths. The first six blocks are clearly visible in each picture. Figure 32 shows the top portion of the test surface for 0.5 watts. The other power settings do not differ significantly and are not shown.

The flow near the elements appears similar to that observed in the absence of the shroud. However, the shrouding wall prevents ambient fluid from entrainment into the buoyant up-flow in this plane. As power is increased, the paths described by the particle traces are more closely spaced, indicative of increased velocity and increased fluid flow.

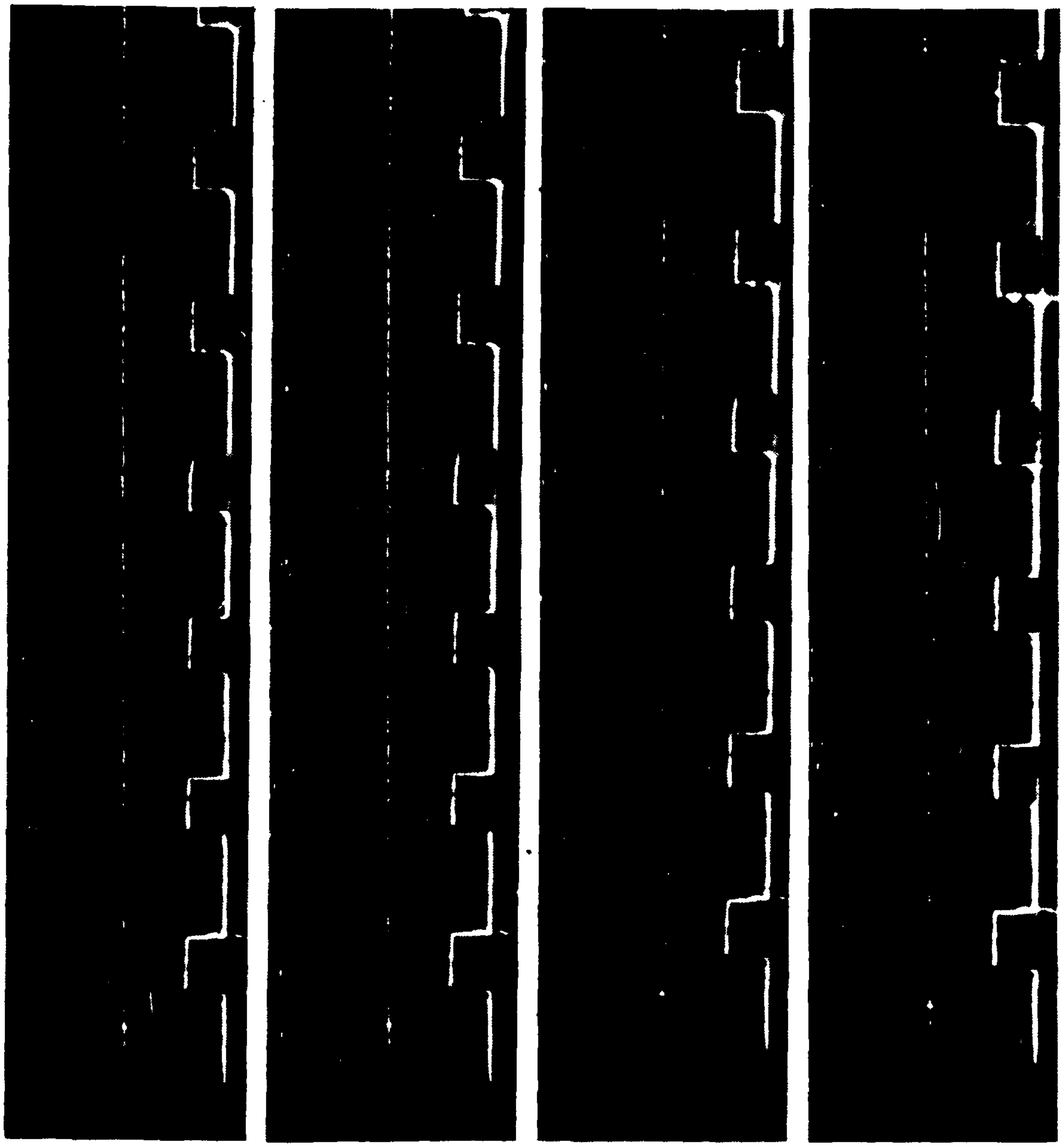

Figure 31. **Steady Flow in X-Y Plane, 0.5, 1.0, 1.2, and 1.5 Watts, 18 mm Channel Spacing, Bottom Blocks**

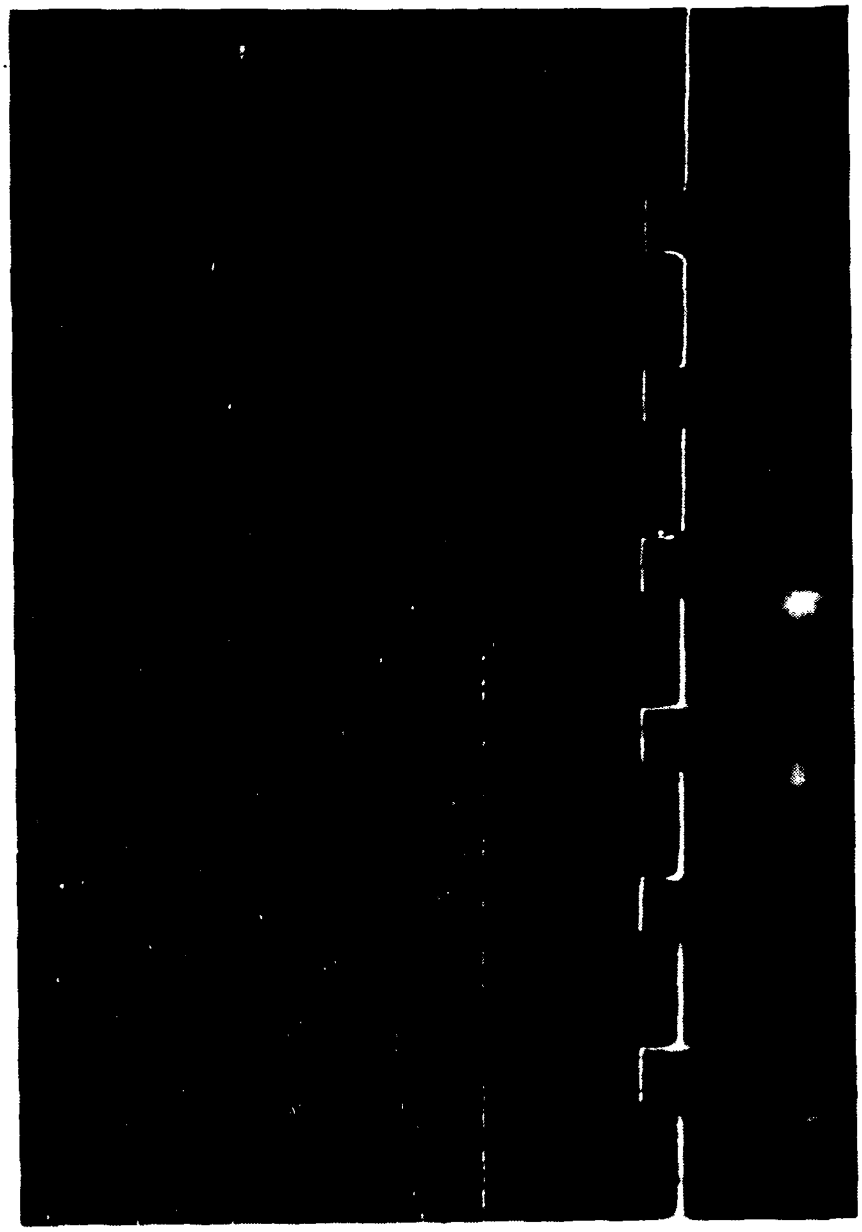

Figure 32. **Steady Flow in X-Y Plane, 0.5 Watts, 18 mm Channel Spacing, Top Blocks**

Figure 33 is the front view of flow in the x-z plane through the front surface of the elements. It is for 1.0 watt, 18 mm shroud spacing, and exposure time of 40 seconds. Unlike the no-shroud condition, flow is more restricted to the sides of the protruding blocks. The characteristic hourglass flow seen for infinite channel width is weak in the vicinity of the middle two blocks and absent elsewhere. The entrained fluid turns very sharply into the flow direction. Because the flow is restricted to the channel width and is predominant on the block sides, its velocity is much greater here. Consequently, there is more forceful entrainment of fluid in the x-z plane.

2. Quantitative

Due to the large amount of data collected, temperature excesses for power settings of 1.2 and 0.2 watts only are presented in graphical form. These settings are representative of the upper and lower ends of the power range available. Channel widths presented are 6.2, 8, 14, 18, and 23 mm measured from the substrate.

The first width was just barely greater than component height. This spacing is representative of pure conduction dominated transport. The nondimensionalized temperature excess vs. element position graphs for 0.2 watts (Figures 34–38) and 1.2 watts (Figures 39–43) show significant difference between the smallest spacing and all others. With that spacing excluded, Figures 44 through 53 present the relevant data in a manner better suited for analysis. The plots for 0.2 watts show the next closest spacing, 8 mm from the substrate, to

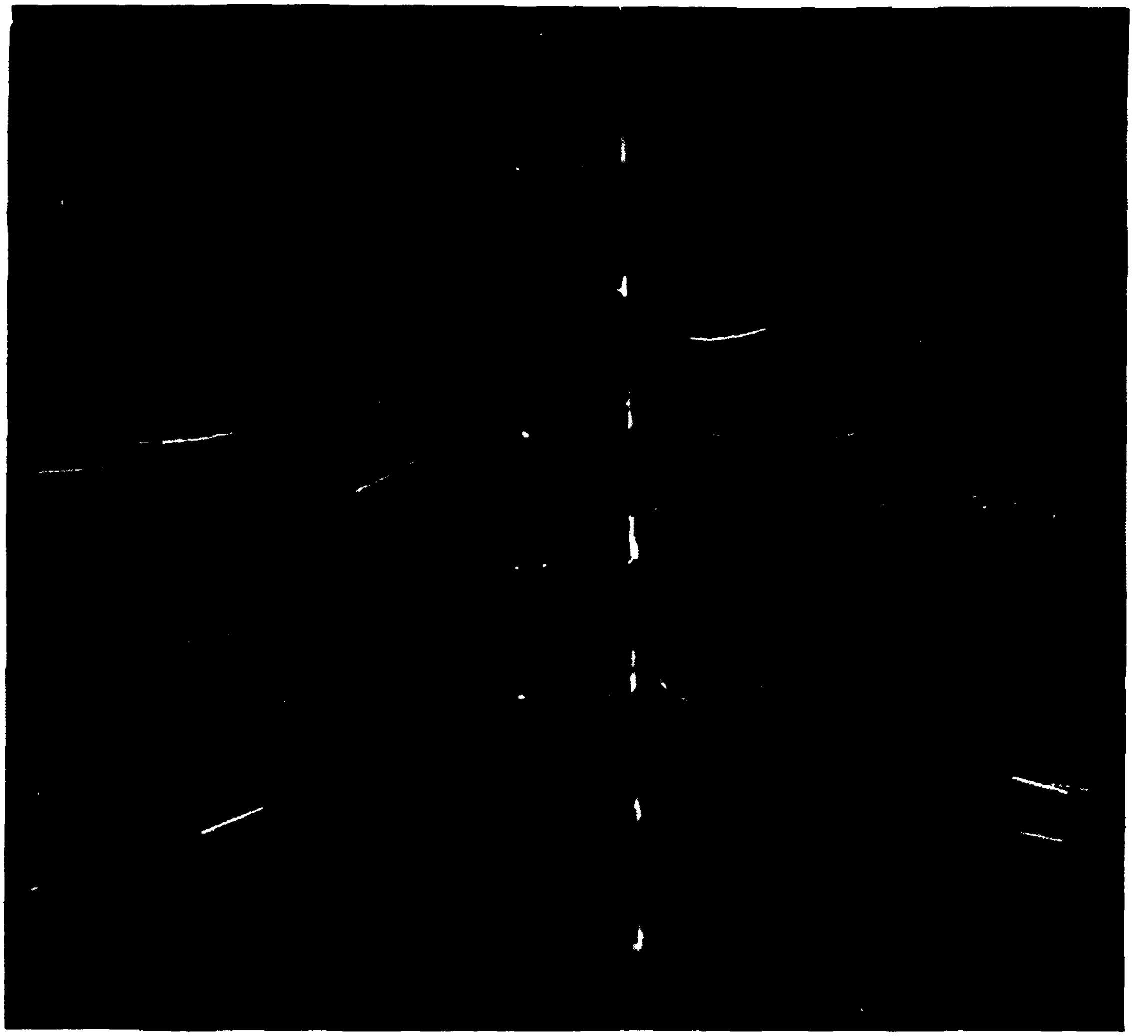

Figure 33. **<u>Flow in X-Z Plane, 1.0 Watt, 18 mm Channel Spacing</u>**

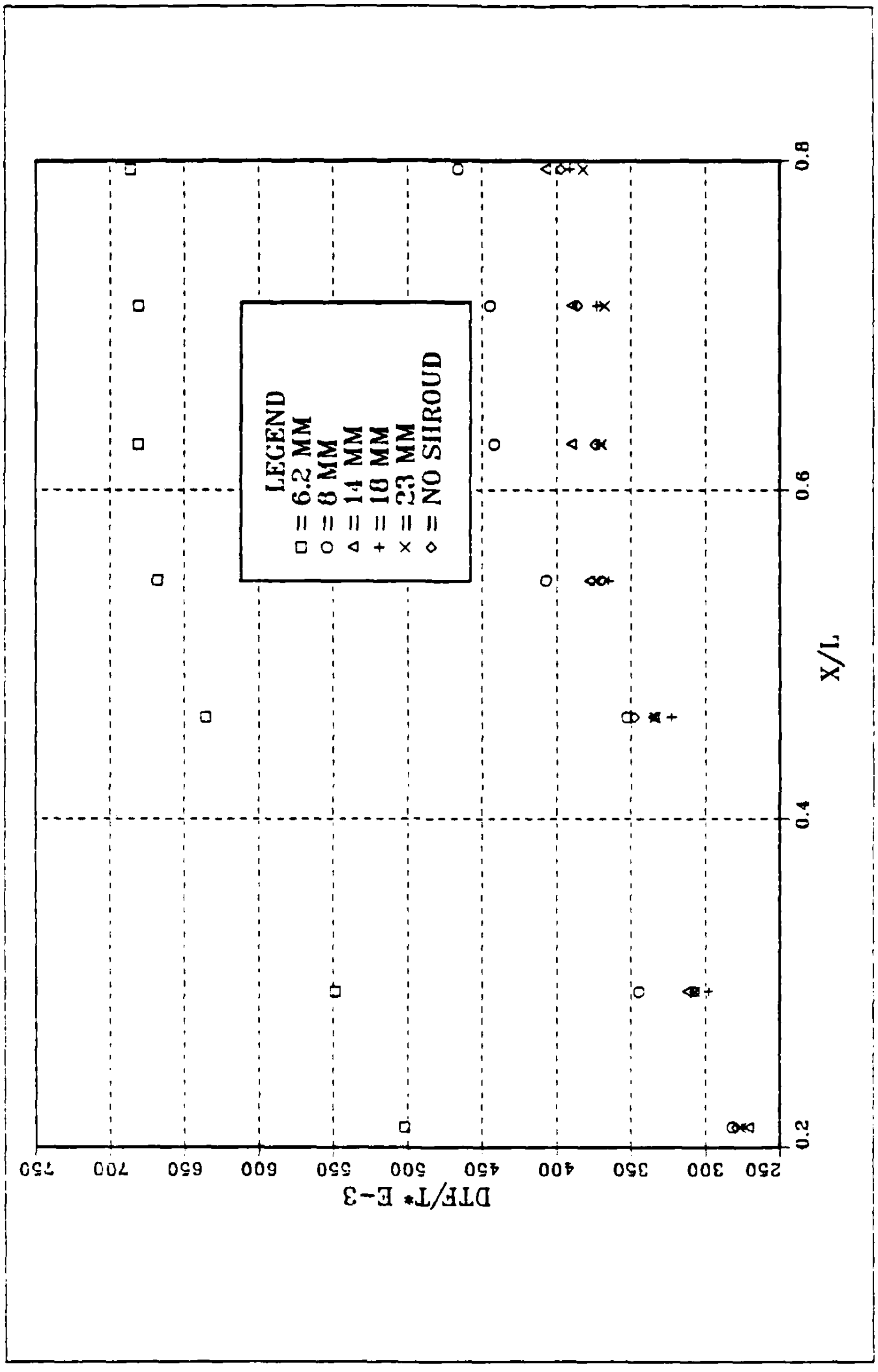

Figure 34. **Nondimensional Temperature Excess, 0.2 Watts, Various Spacings, Front Faces**

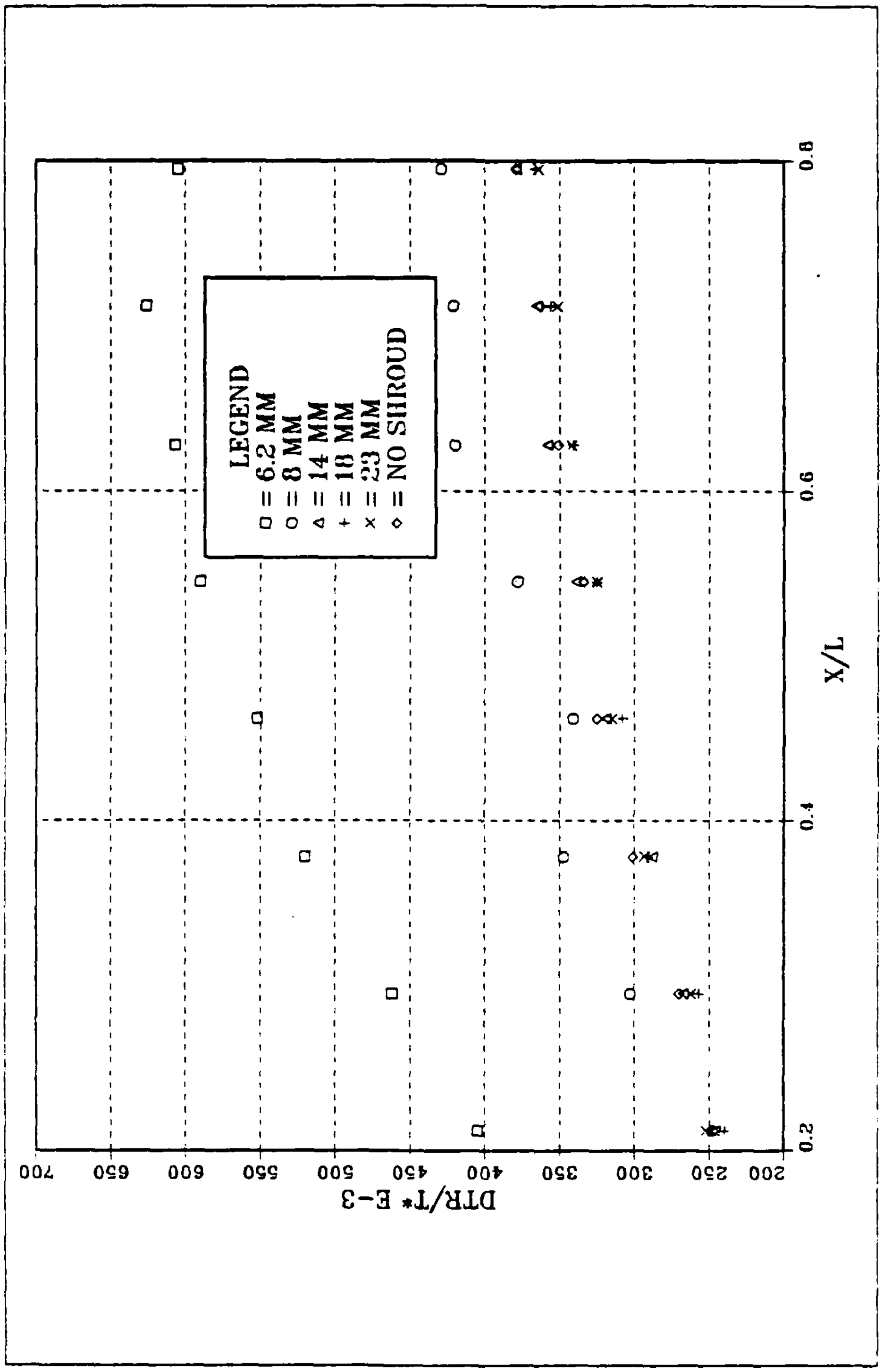

Figure 35. **Nondimensional Temperature Excess, 0.2 Watts, Various Spacings, Right Faces**

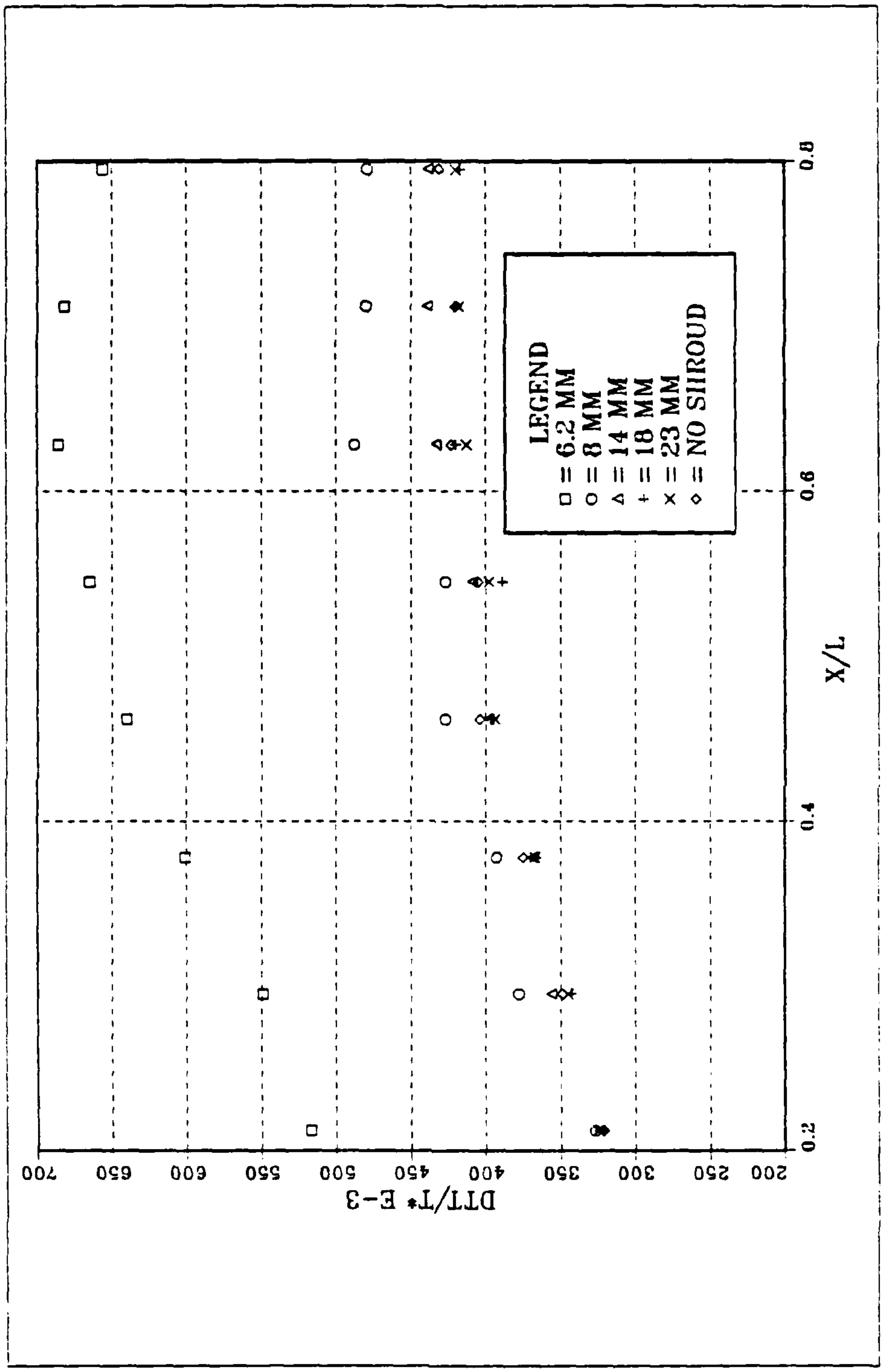

Figure 36. **Nondimensional Temperature Excess, 0.2 Watts, Various Spacings, Top Faces**

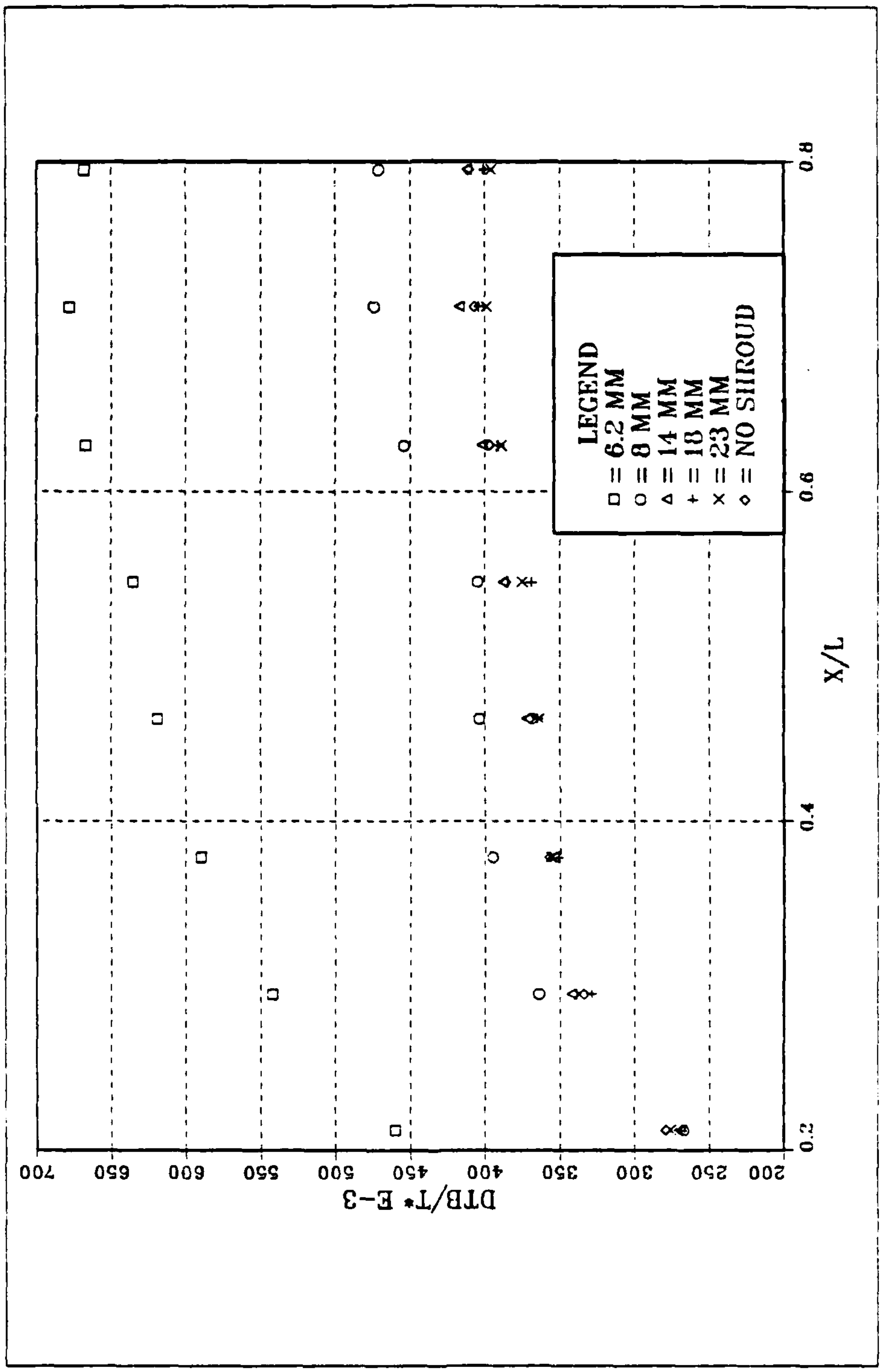

Figure 37. **Nondimensional Temperature Excess, 0.2 Watts, Various Spacings, Bottom Faces**

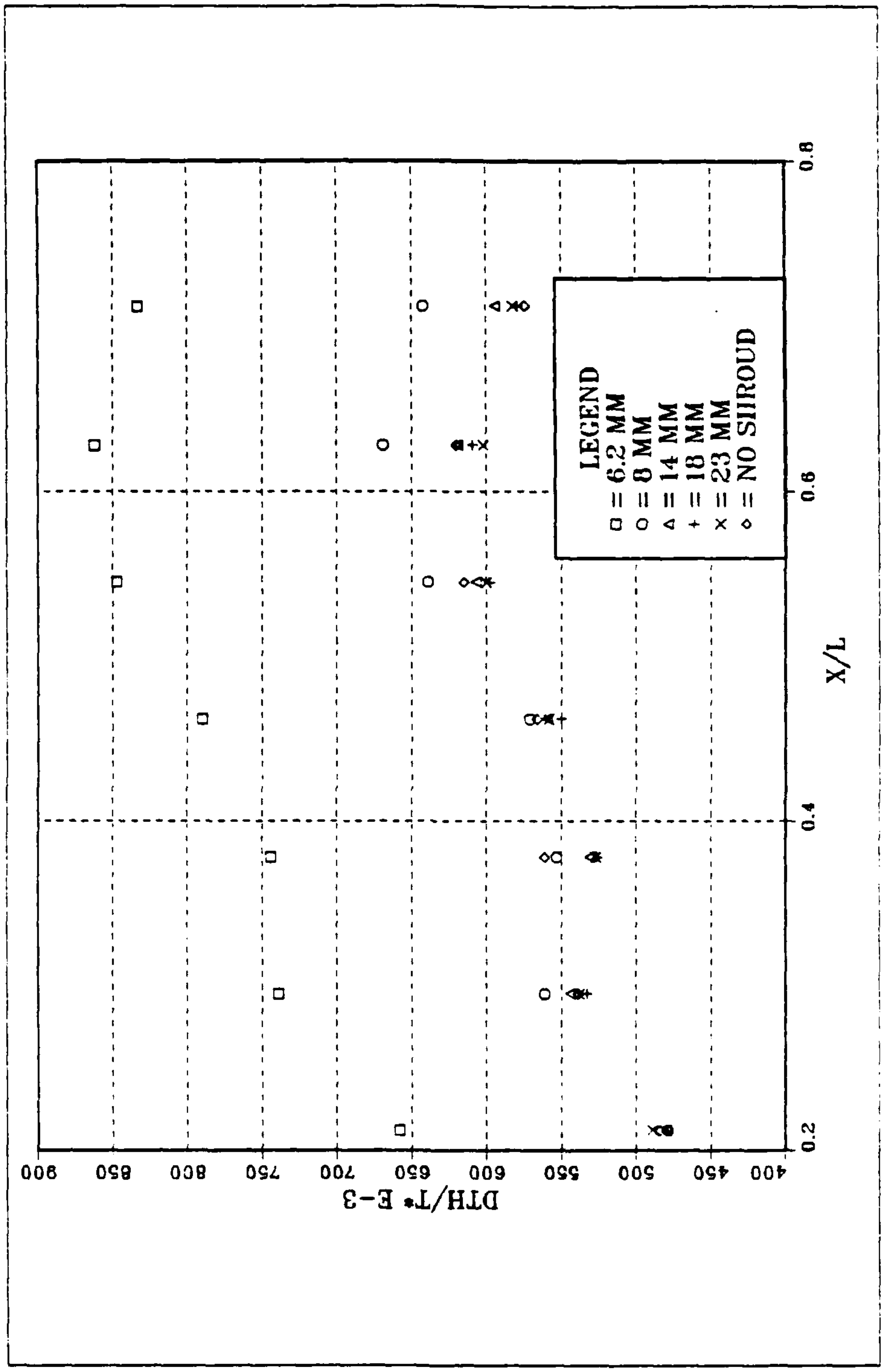

Figure 38. **Nondimensional Temperature Excess, 0.2 Watts, Various Spacings, Heaters**

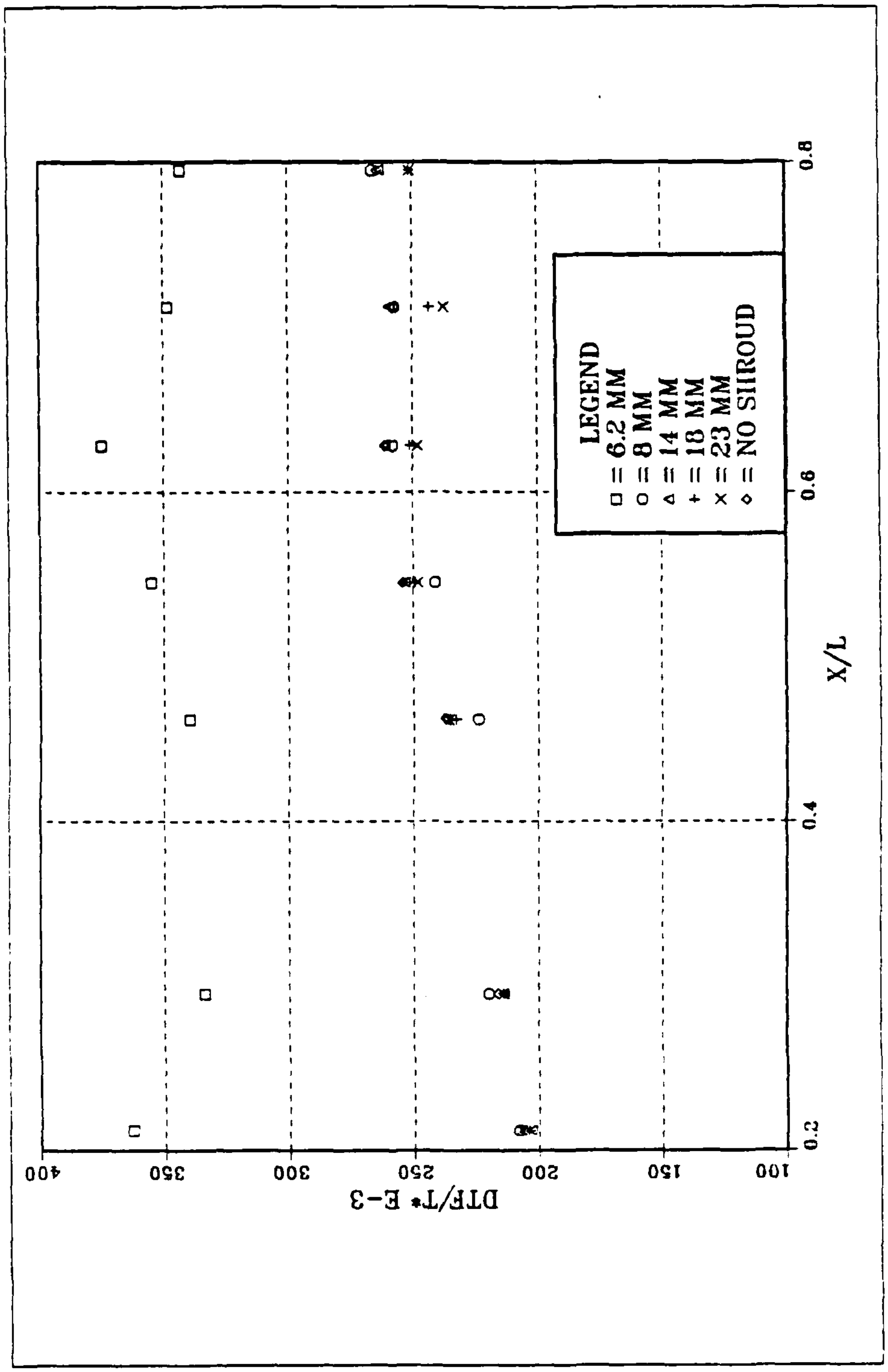

Figure 39. **Nondimensional Temperature Excess, 1.2 Watts, Various Spacings, Front Faces**

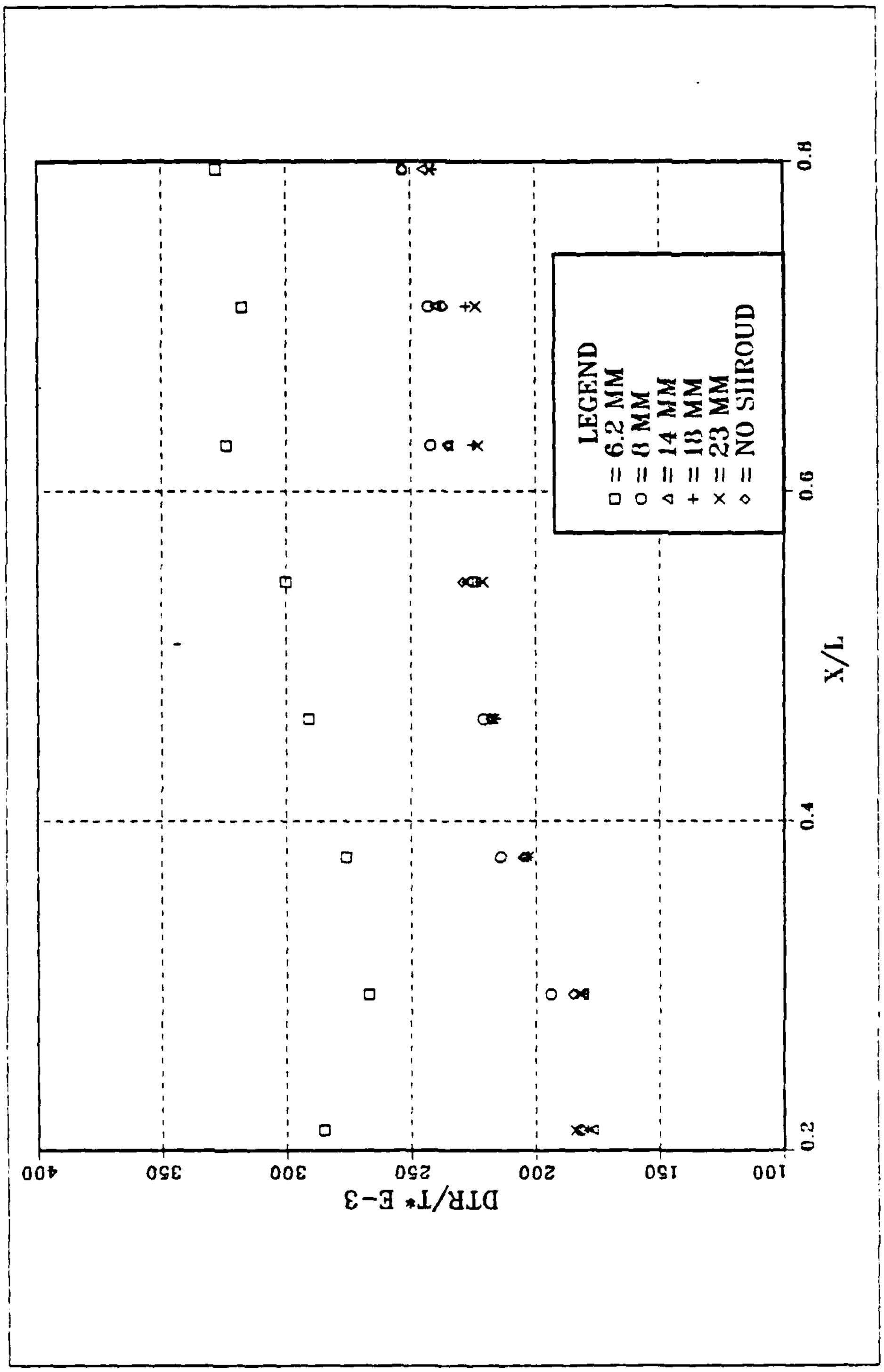

Figure 40. **Nondimensional Temperature Excess, 1.2 Watts, Various Spacings, Right Faces**

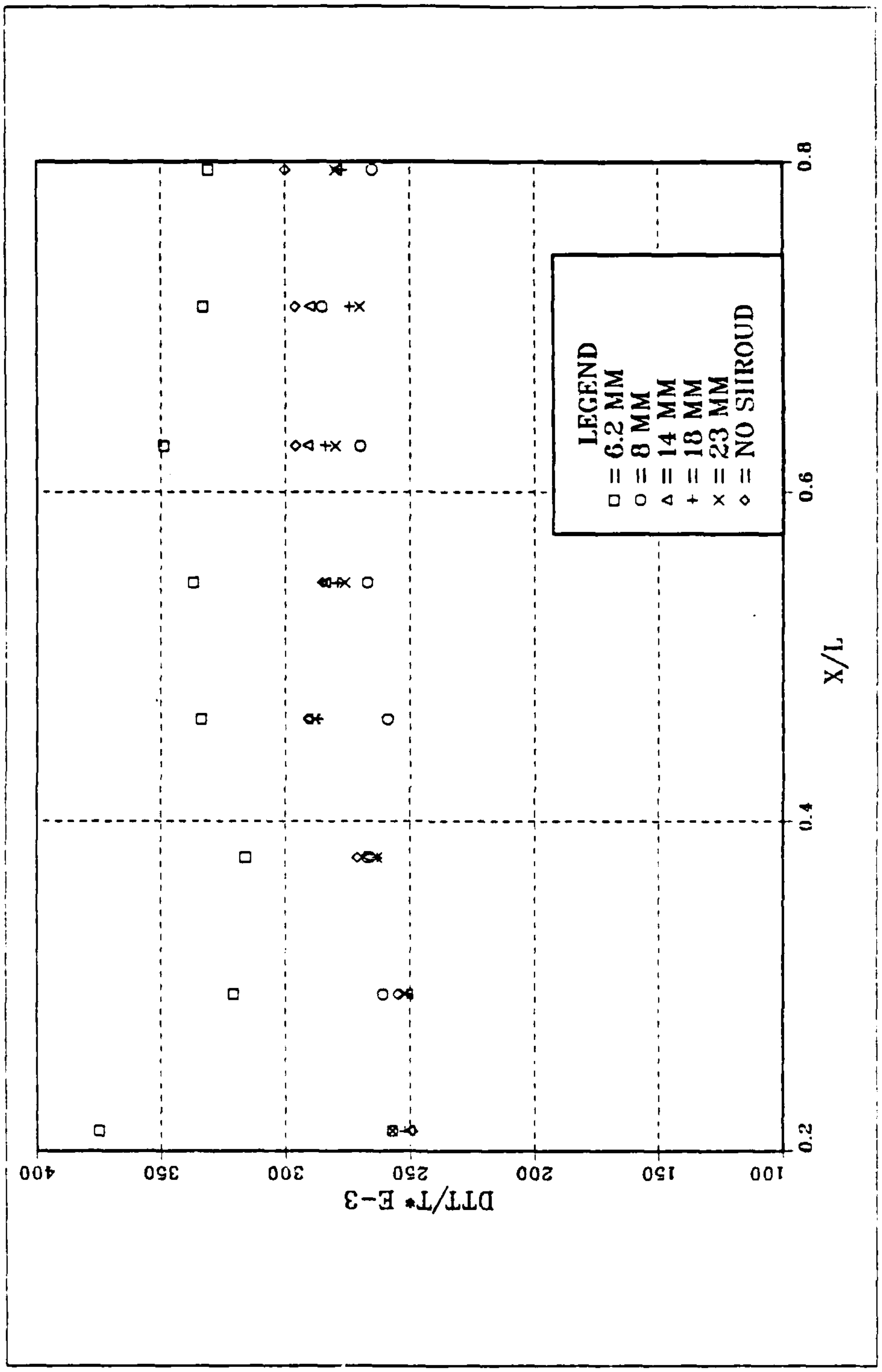

Figure 41. **Nondimensional Temperature Excess, 1.2 Watts, Various Spacings, Top Faces**

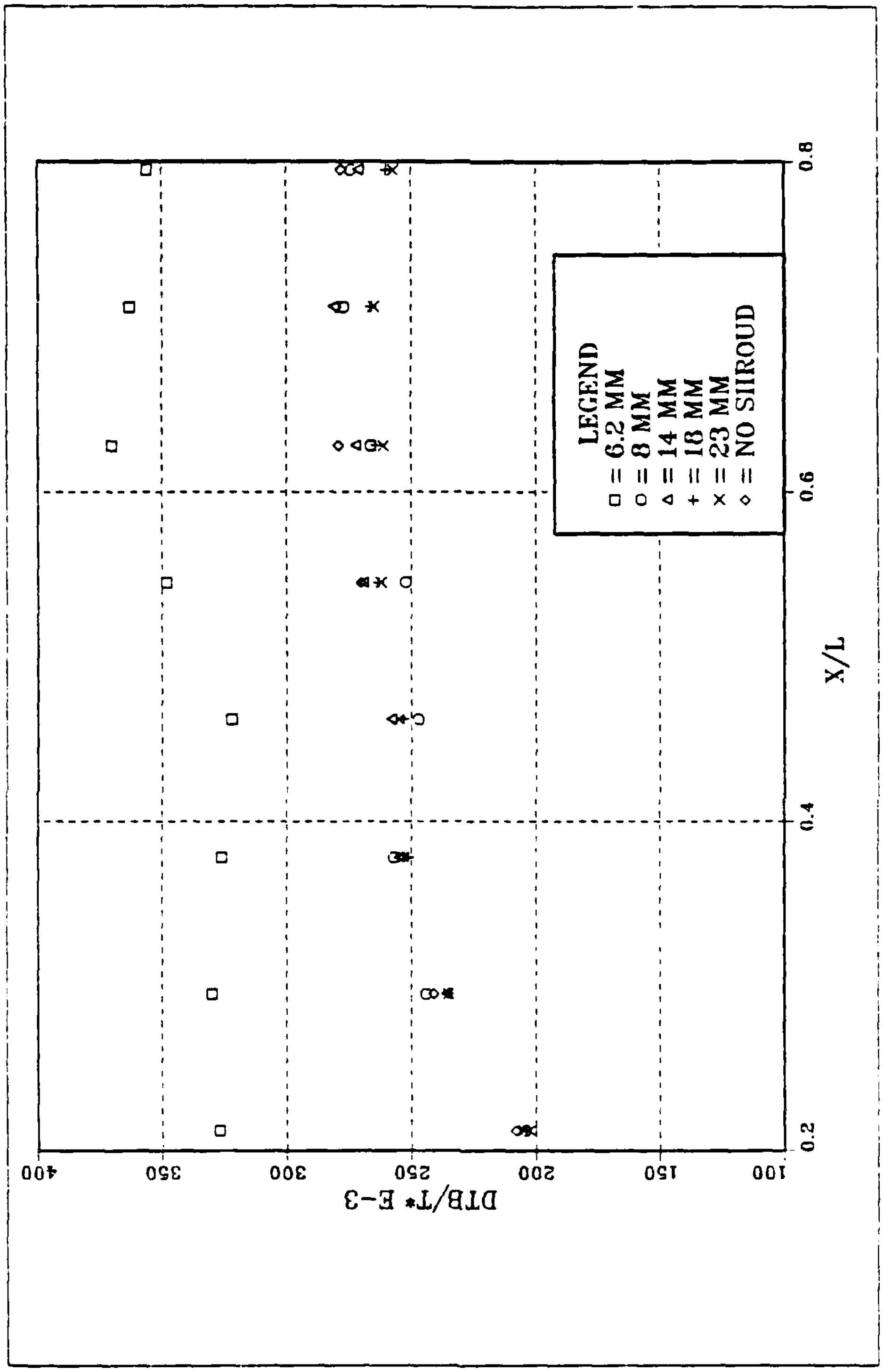

Figure 42. **Nondimensional Temperature Excess, 1.2 Watts, Various Spacings, Bottom Faces**

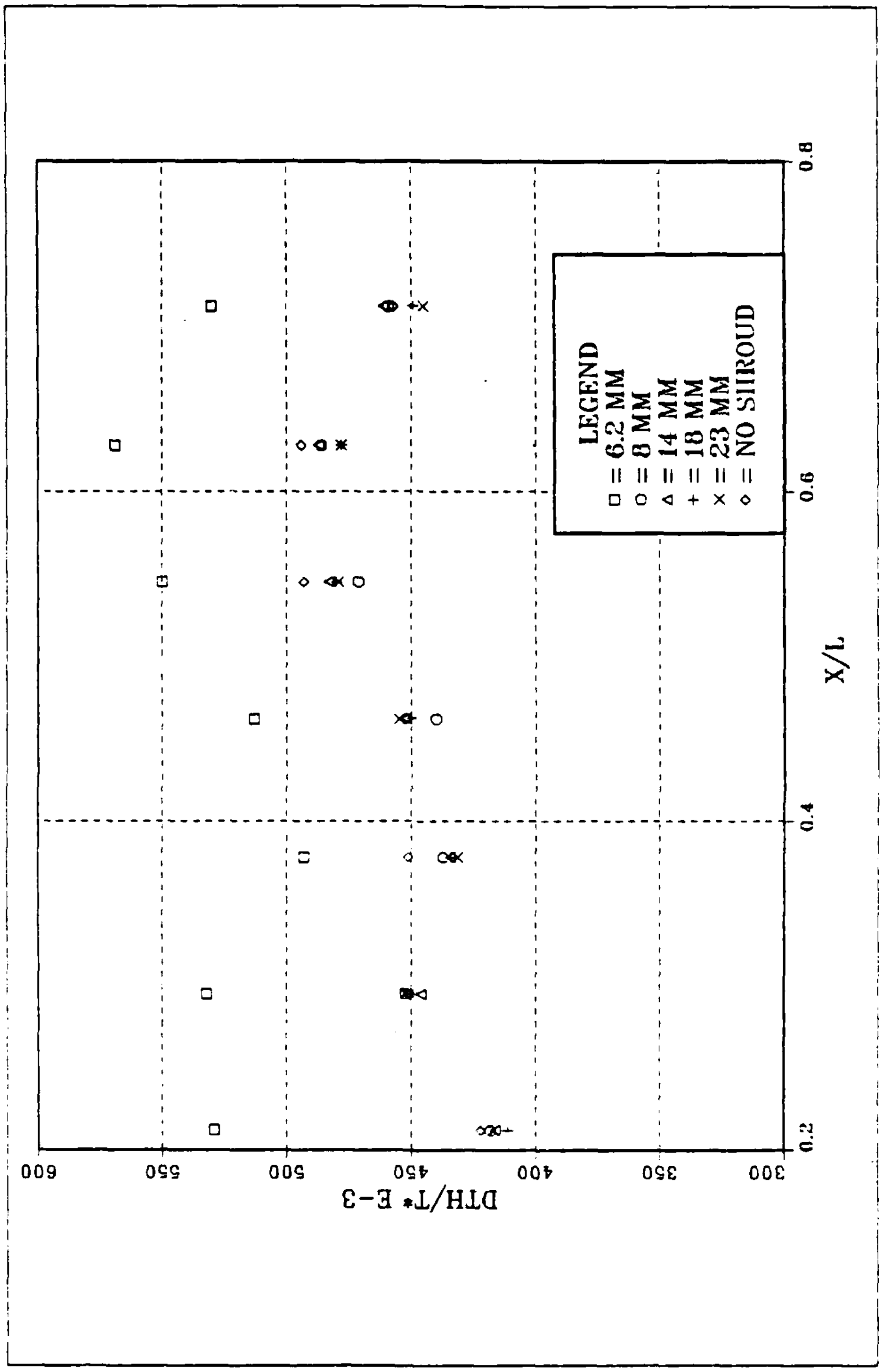

Figure 43. **Nondimensional Temperature Excess, 1.2 Watts, Various Spacings, Heaters**

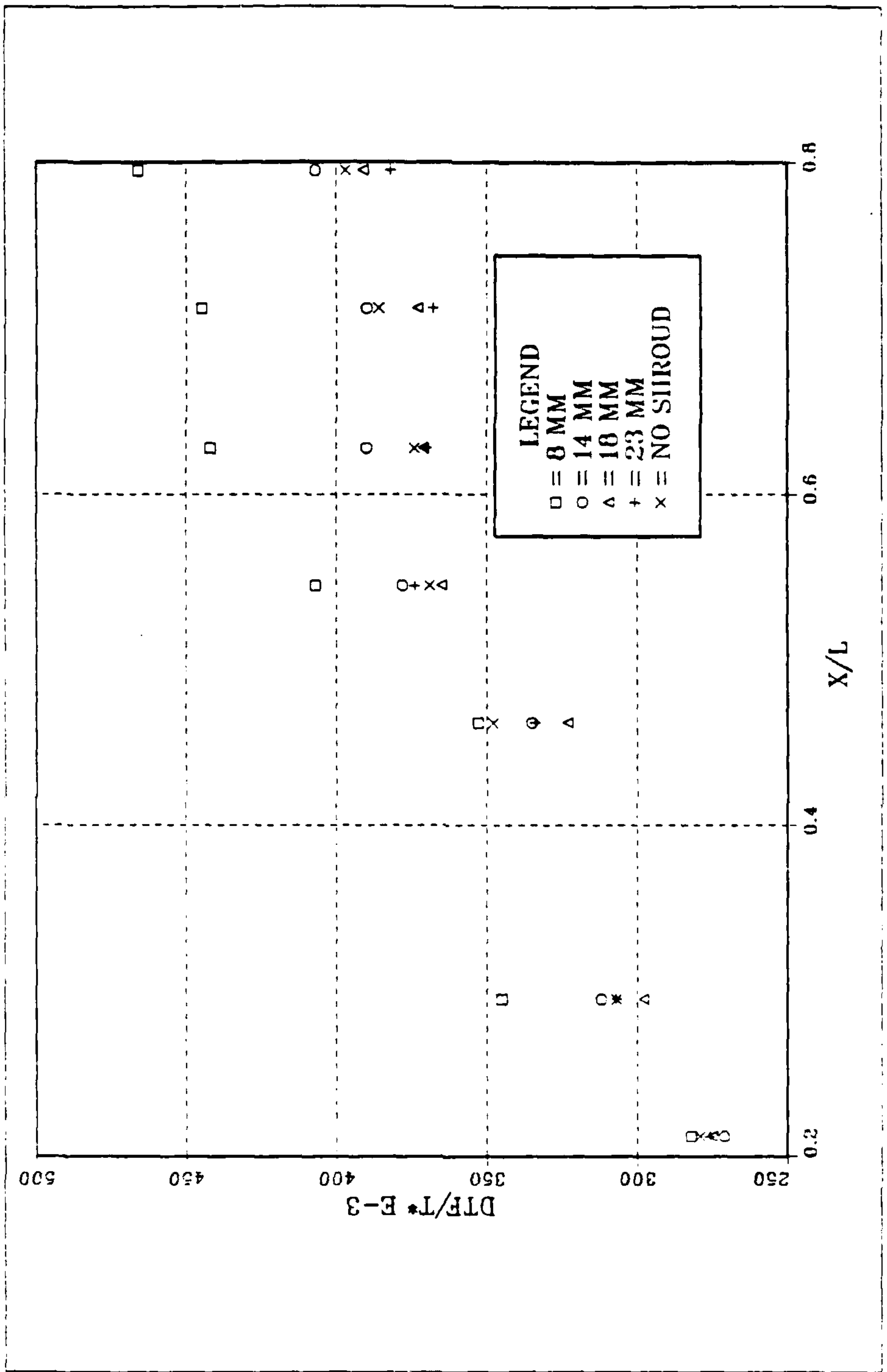

Figure 44. **Nondimensional Temperature Excess, 0.2 Watts, Excl. 6.2 mm, Front Faces**

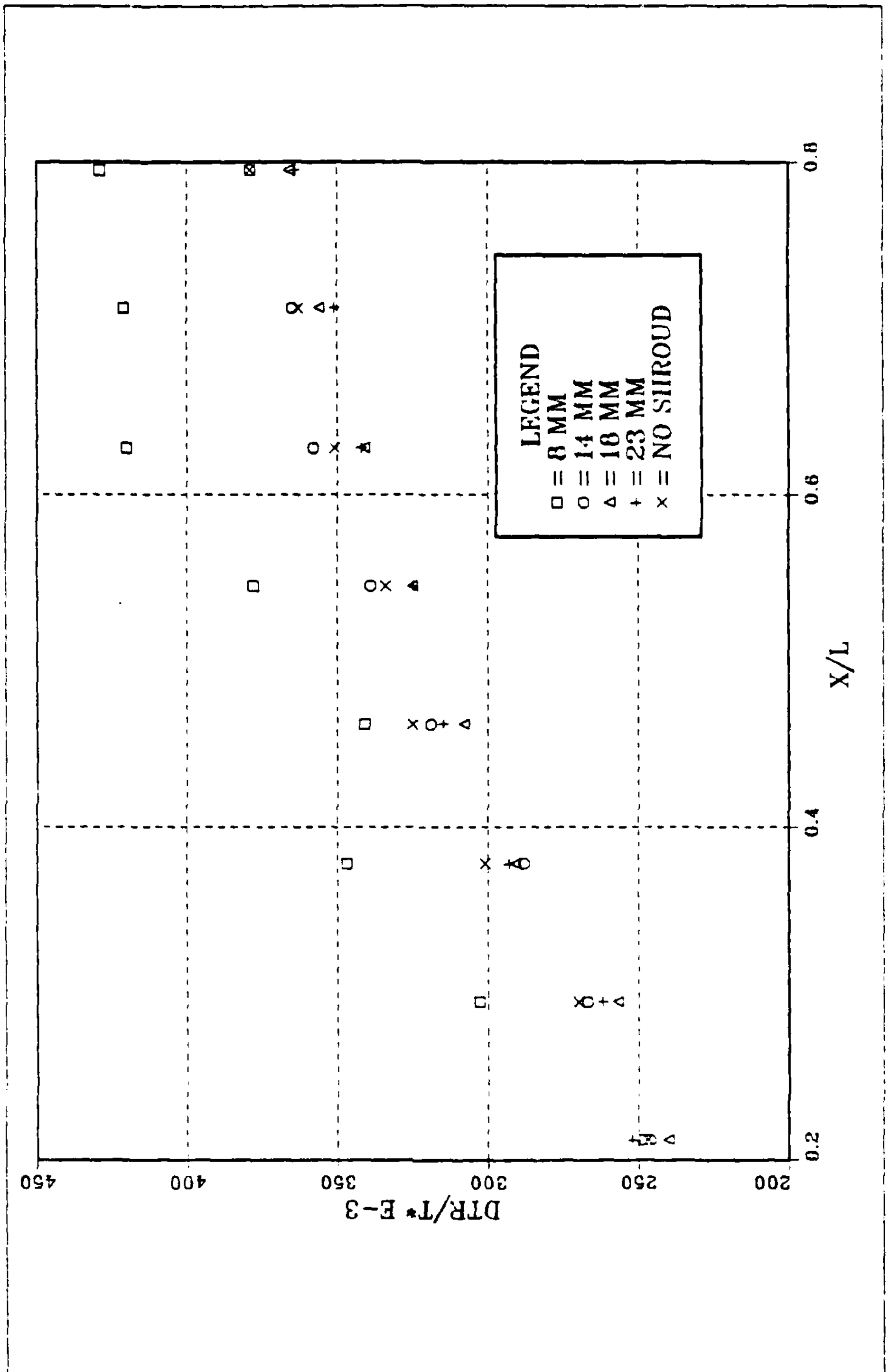

Figure 45. **Nondimensional Temperature Excess, 0.2 Watts, Excl. 6.2 mm, Right Faces**

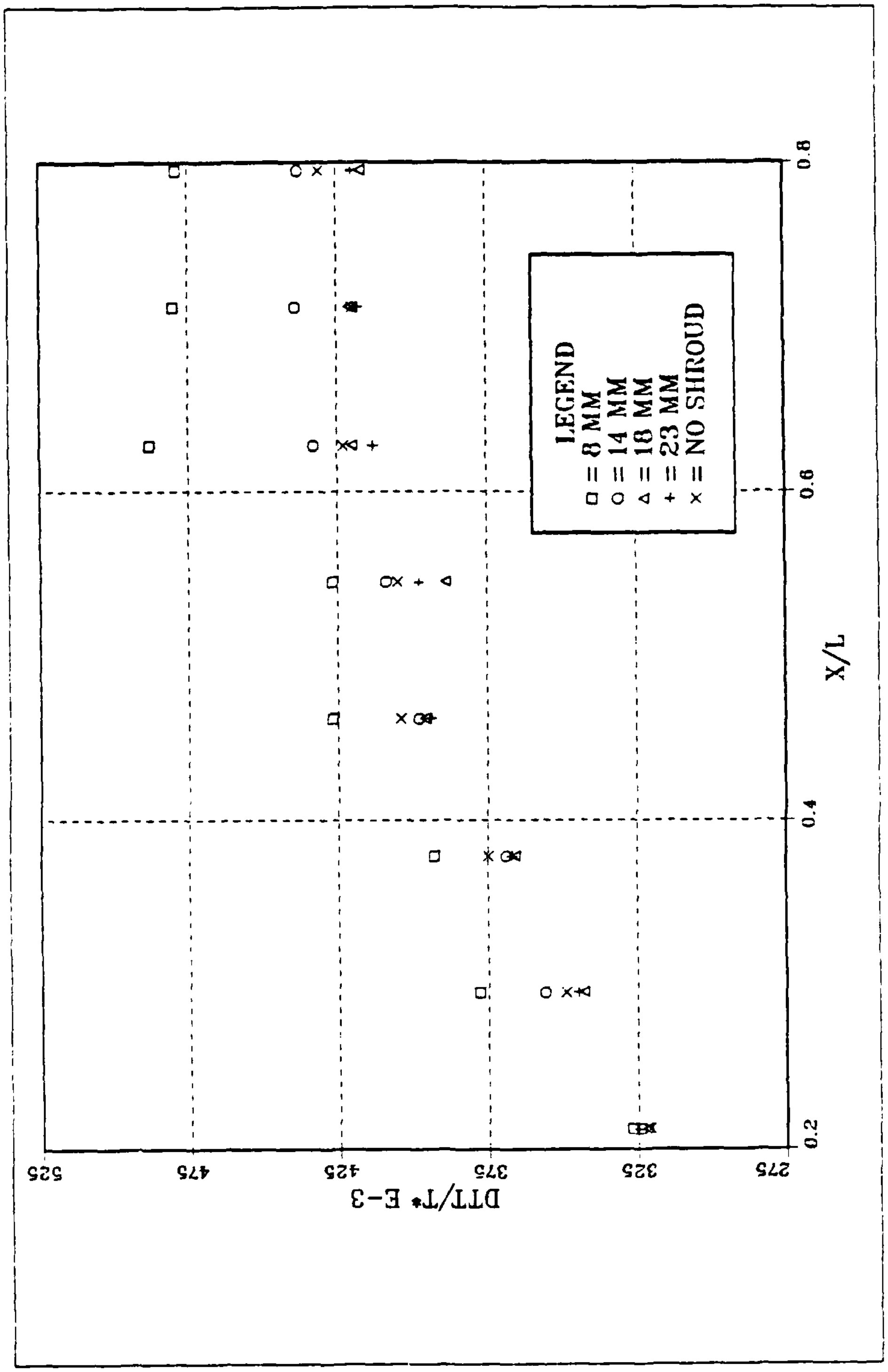

Figure 46. **Nondimensional Temperature Excess, 0.2 Watts, Excl. 6.2 mm, Top Faces**

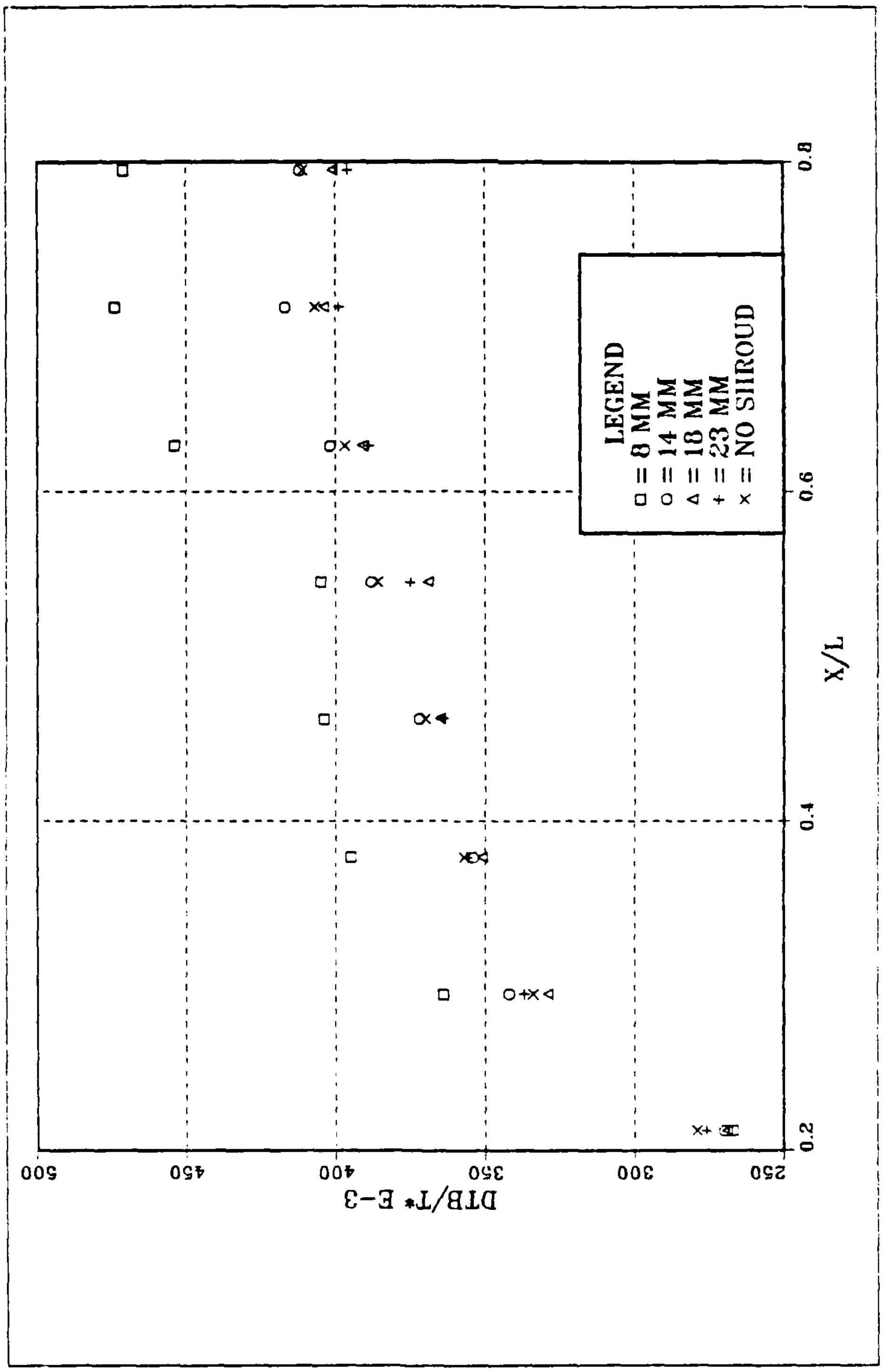

Figure 47. <u>**Nondimensional Temperature Excess, 0.2 Watts, Excl. 6.2 mm, Bottom Faces**</u>

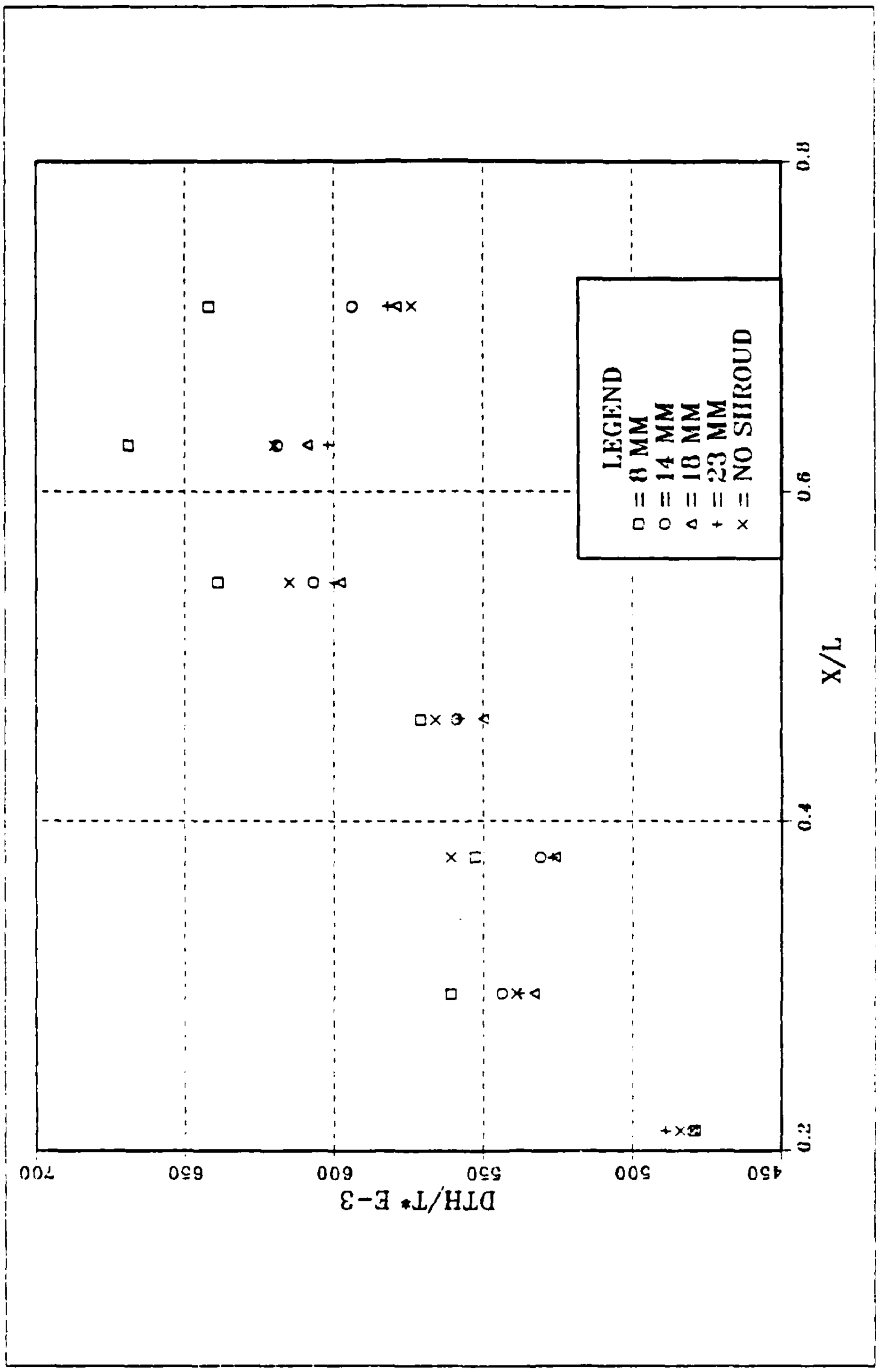

Figure 48. **Nondimensional Temperature Excess, 0.2 Watts, Excl. 6.2 mm. Heaters**

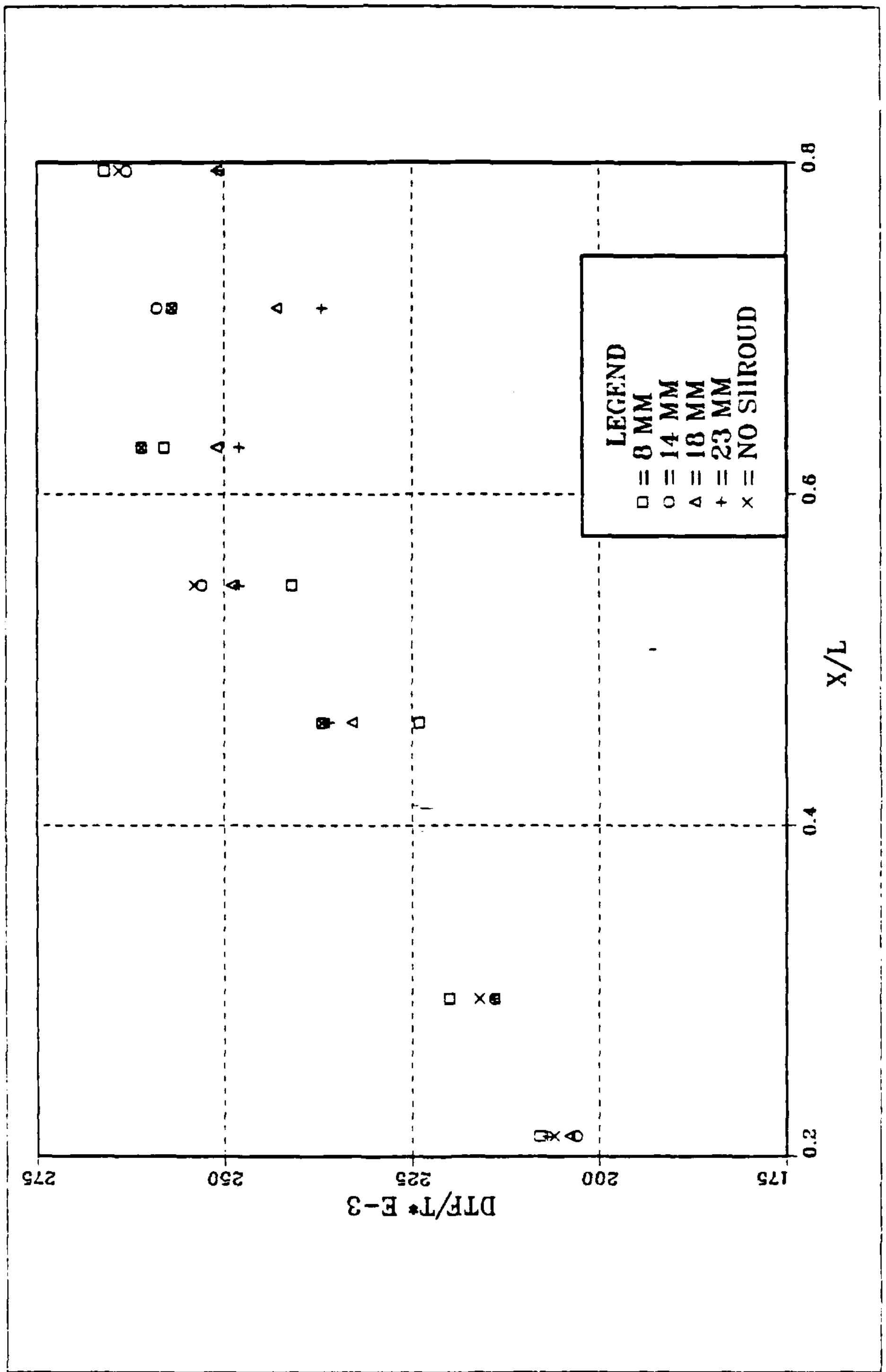

Figure 49. **Nondimensional Temperature Excess, 1.2 Watts, Excl. 6.2 mm, Front Faces**

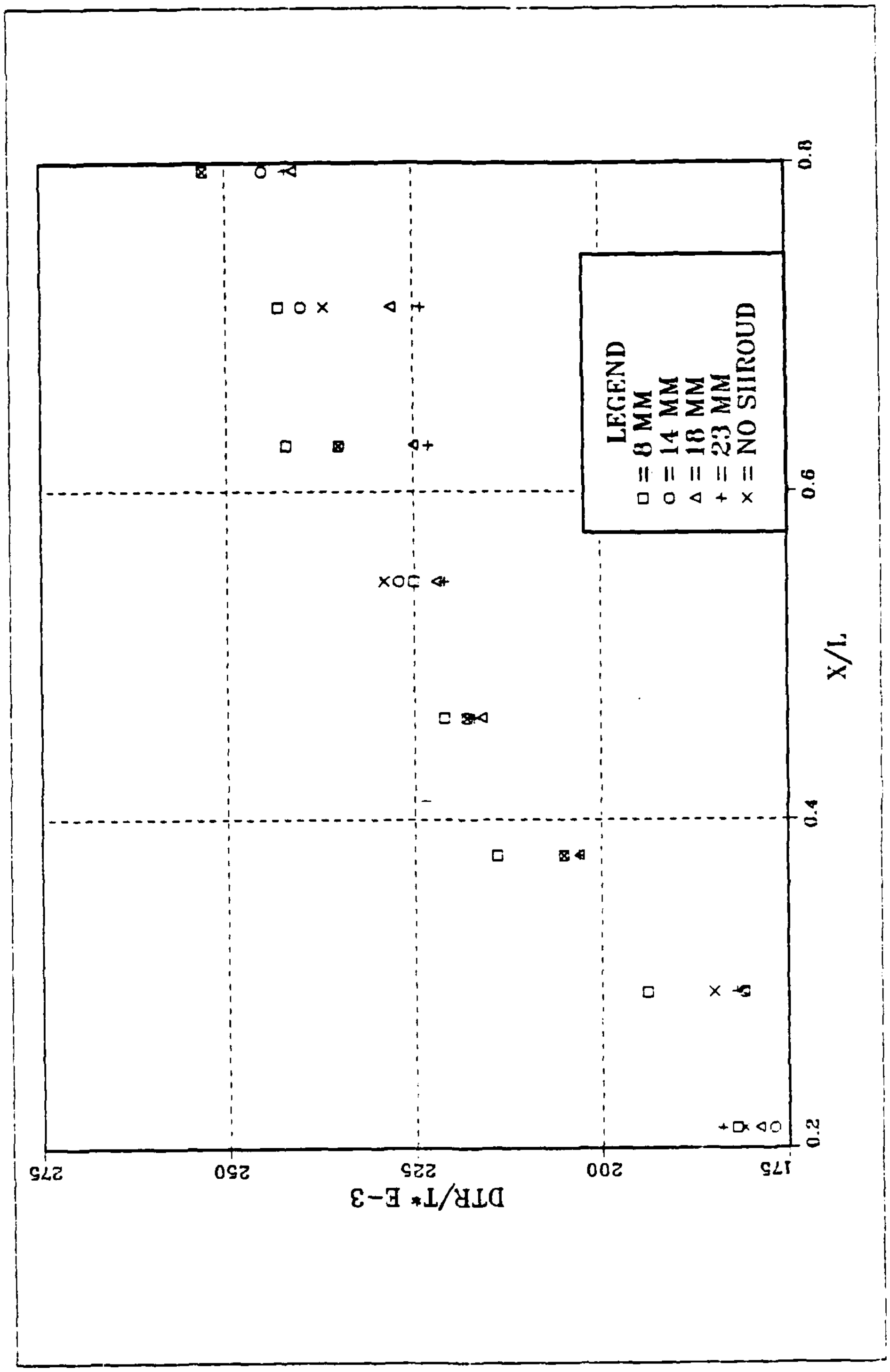

Figure 50. **Nondimensional Temperature Excess, 1.2 Watts, Excl. 6.2 mm, Right Faces**

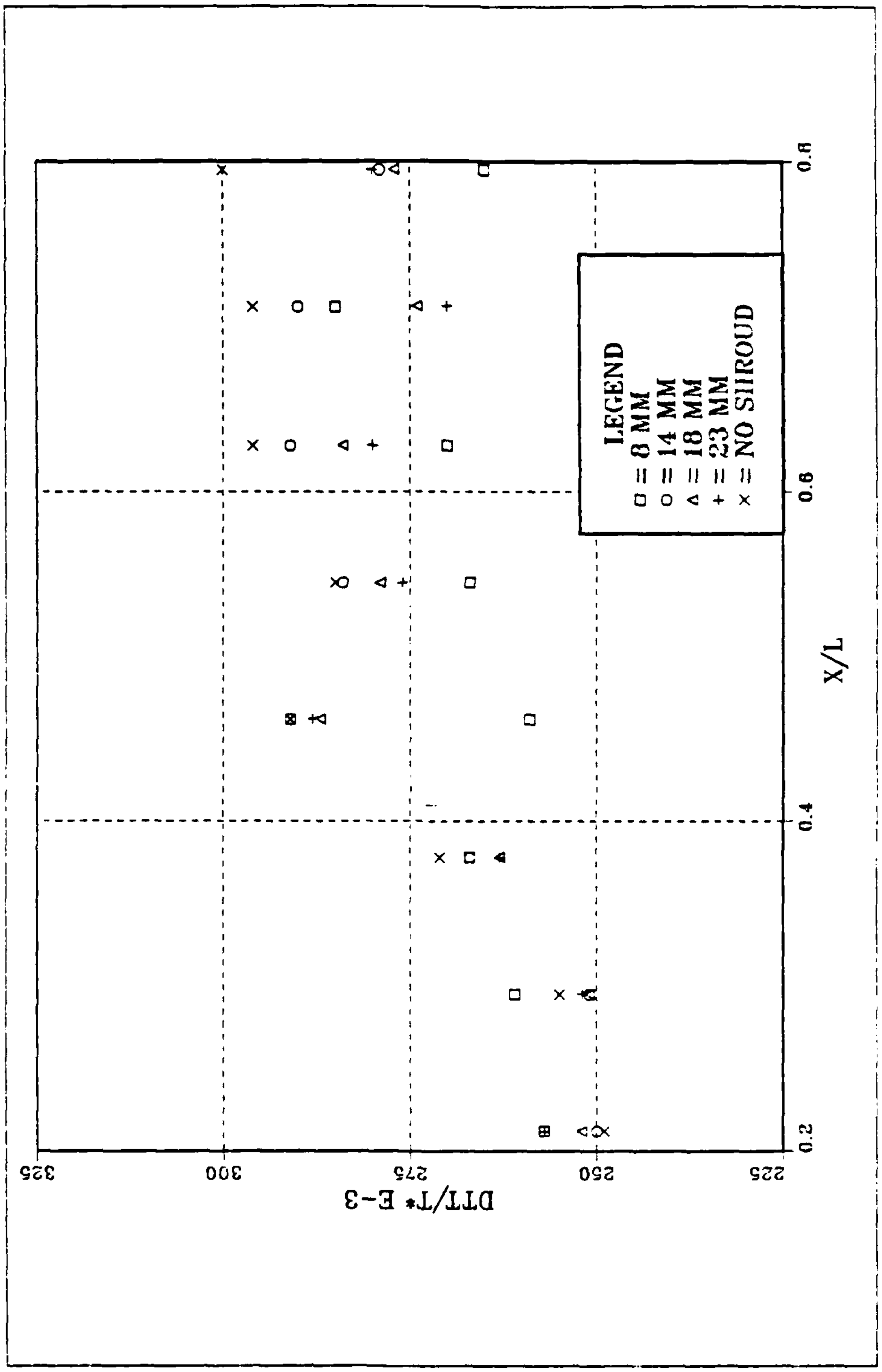

Figure 51. **Nondimensional Temperature Excess, 1.2 Watts, Excl. 6.2 mm, Top Faces**

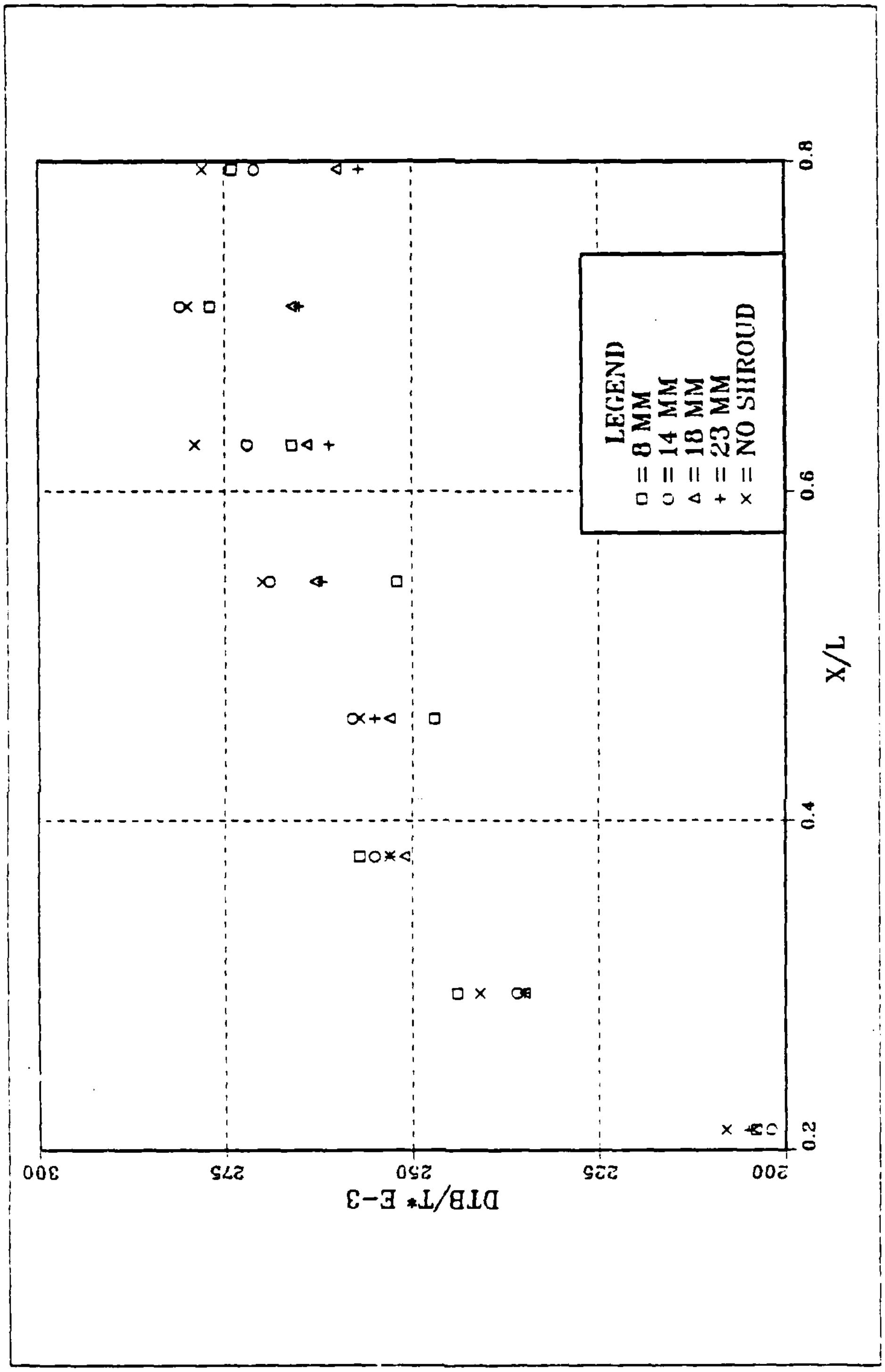

Figure 52. **Nondimensional Temperature Excess, 1.2 Watts, Excl. 6.2 mm, Bottom Faces**

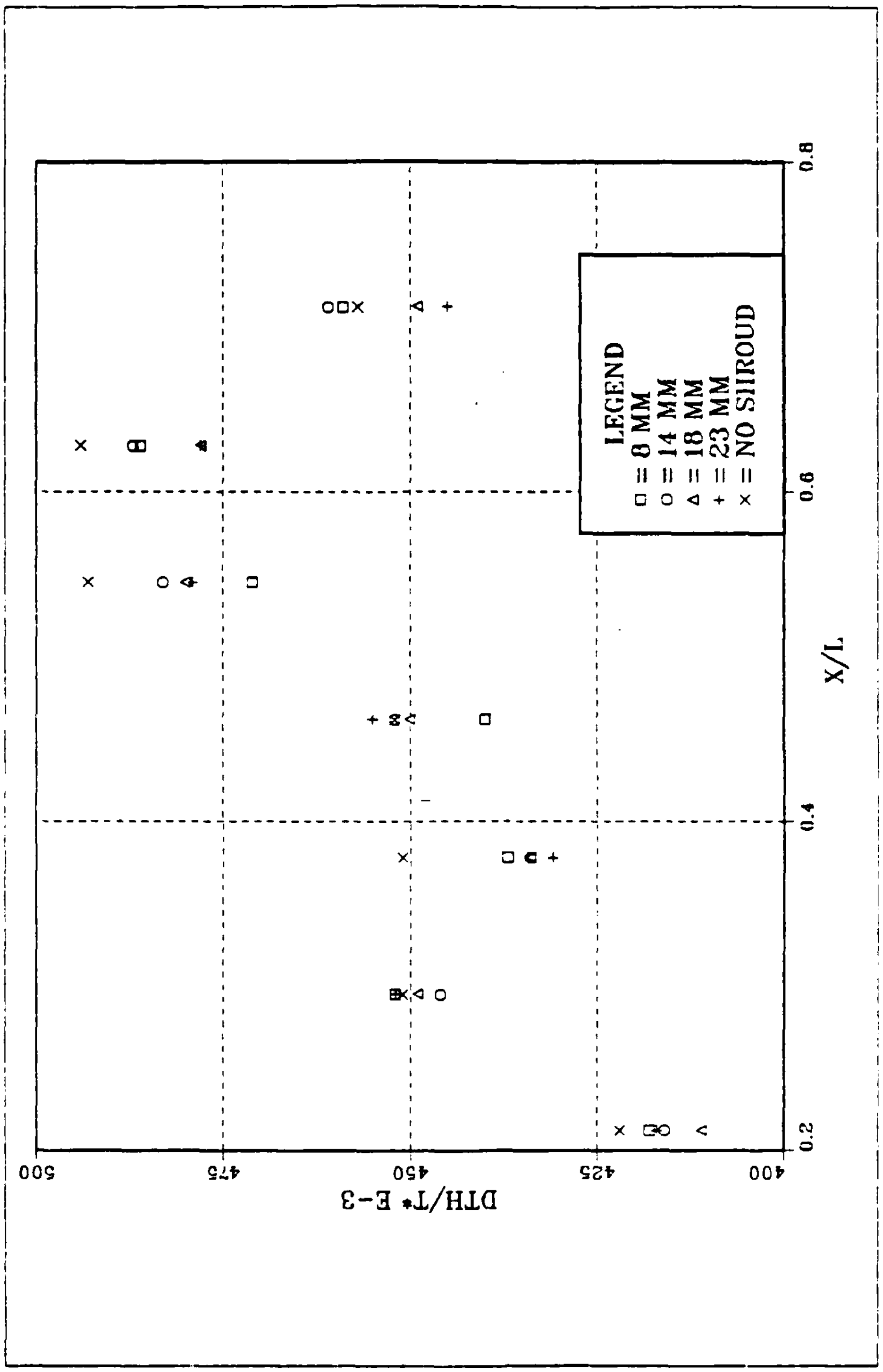

Figure 53. **Nondimensional Temperature Excess, 1.2 Watts, Excl. 6.2 mm. Heaters**

yield higher temperatures over the range of element positions. For higher spacings, there was no consistency in the relative position of the curves from one element position to the next. This indicates relative independence of transport on channel width for spacings greater than 8 mm. However, data for 1.2 watts includes even the 8 mm spacing within the mix of curves (its curve does not consistently yield higher temperatures). Therefore, for 1.2 watts the independence of transport extends below the 8 mm spacing. General patterns observed for both powers are:

- a steady rise in front and side face temperatures with element position as expected due to exposure to increasing convected energy at higher positions.
- a relative levelling of top and bottom temperatures at higher positions. This is perhaps due to increasing fluid velocities along the channel.
- the drop in heater temperatures at block 7, *which has four* percent less power on average.

The differences between the two powers result from the stronger driving force at 1.2 watts. Increased fluid velocities result in improved heat transfer characteristics, making 8 mm an acceptable spacing. This point is emphasized by referring to the graphs of component face temperature excess vs. shroud spacing for 0.2 watts (Figures 54-58) and 1.2 watts (Figures 59-63). Significantly, for the 1.2 watts there is no further temperature reduction for a spacing greater than 8 mm. Indeed, there is a slight rise in temperature of the latter blocks (7 and 8) when the shroud is removed. These higher

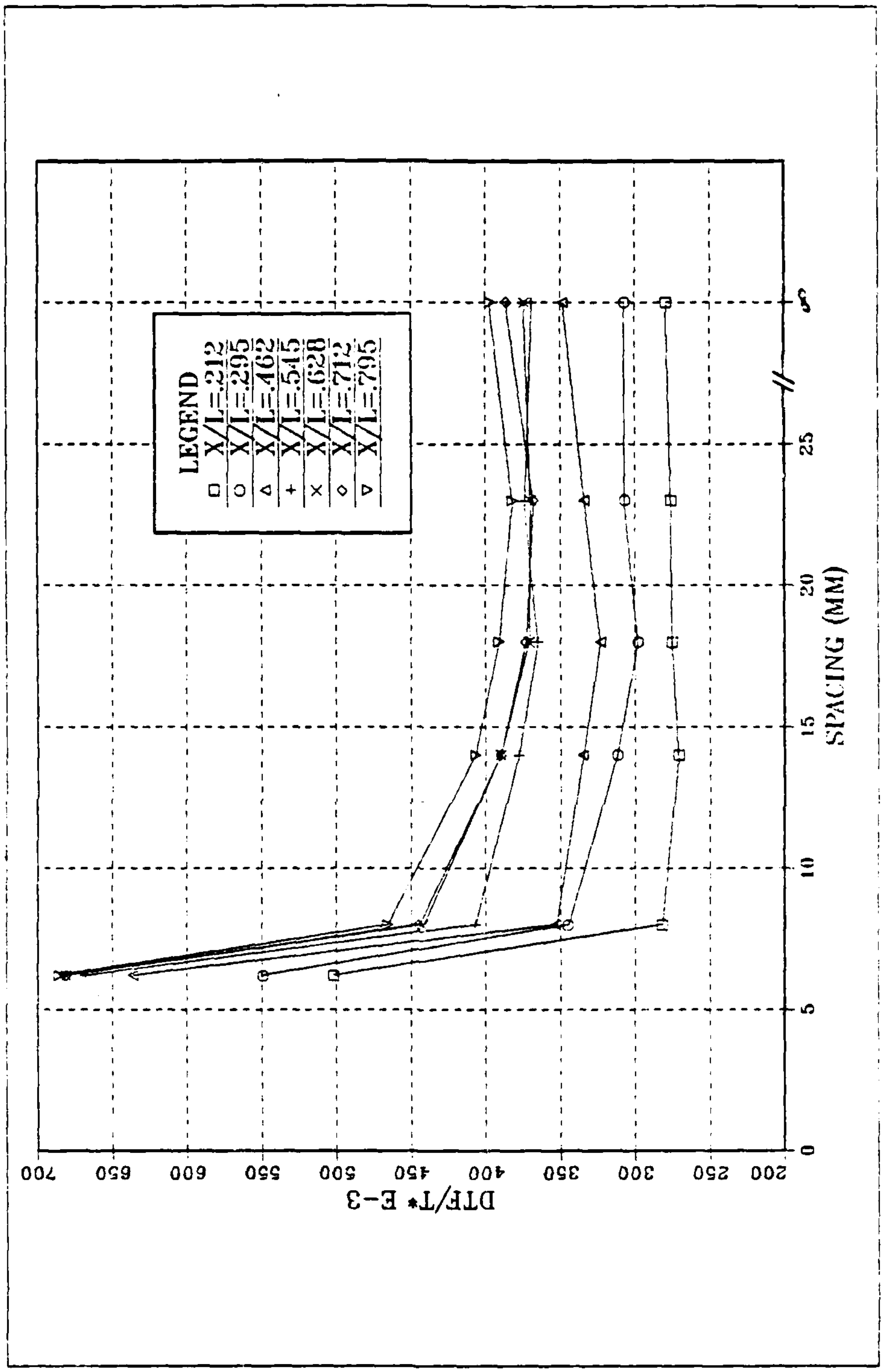

Figure 54. **Nondimensional Temperature Excess vs. Shroud Position, 0.2 Watts, Front Faces**

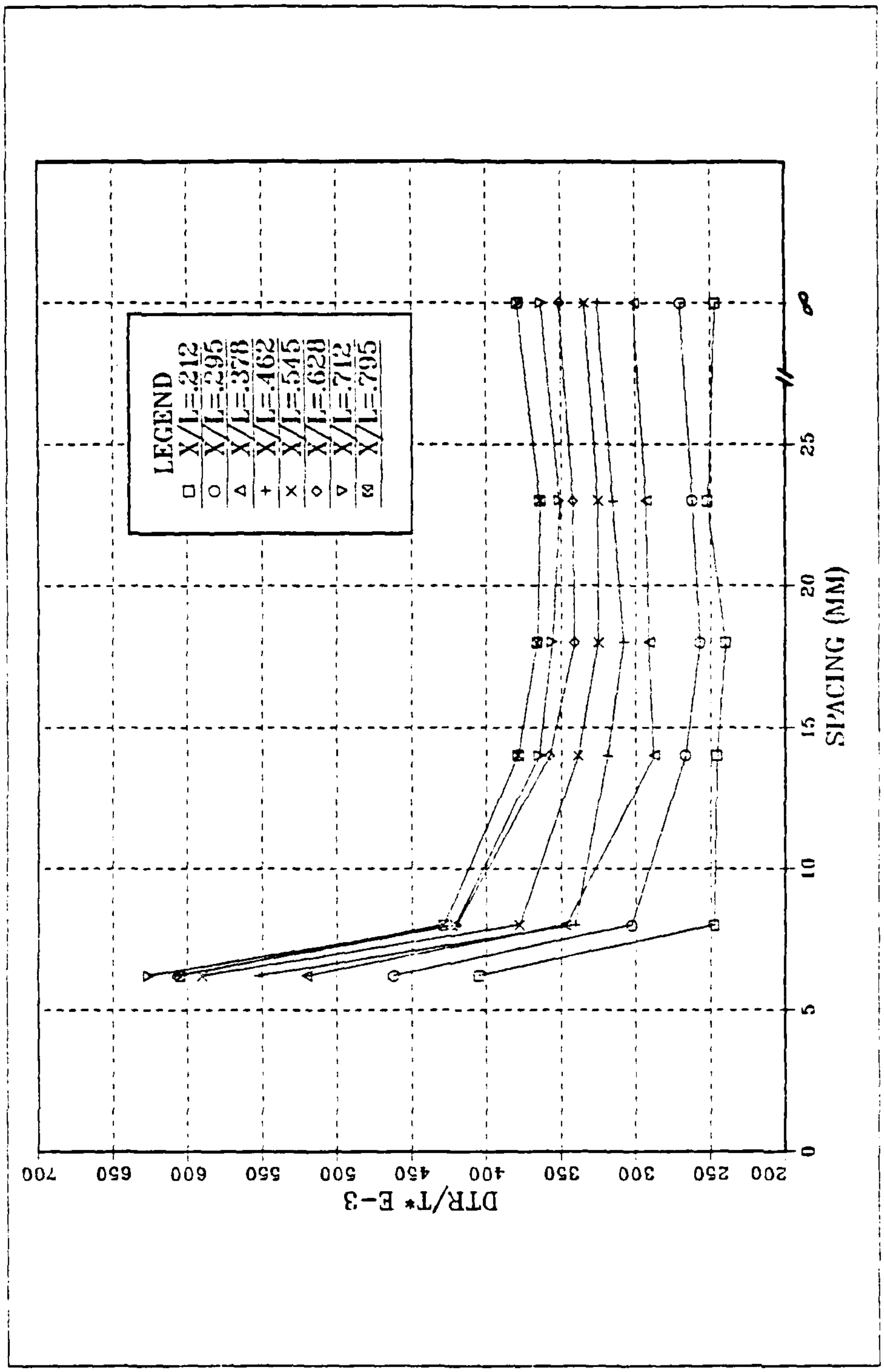

Figure 55. **Nondimensional Temperature Excess vs. Shroud Position, 0.2 Watts, Right Faces**

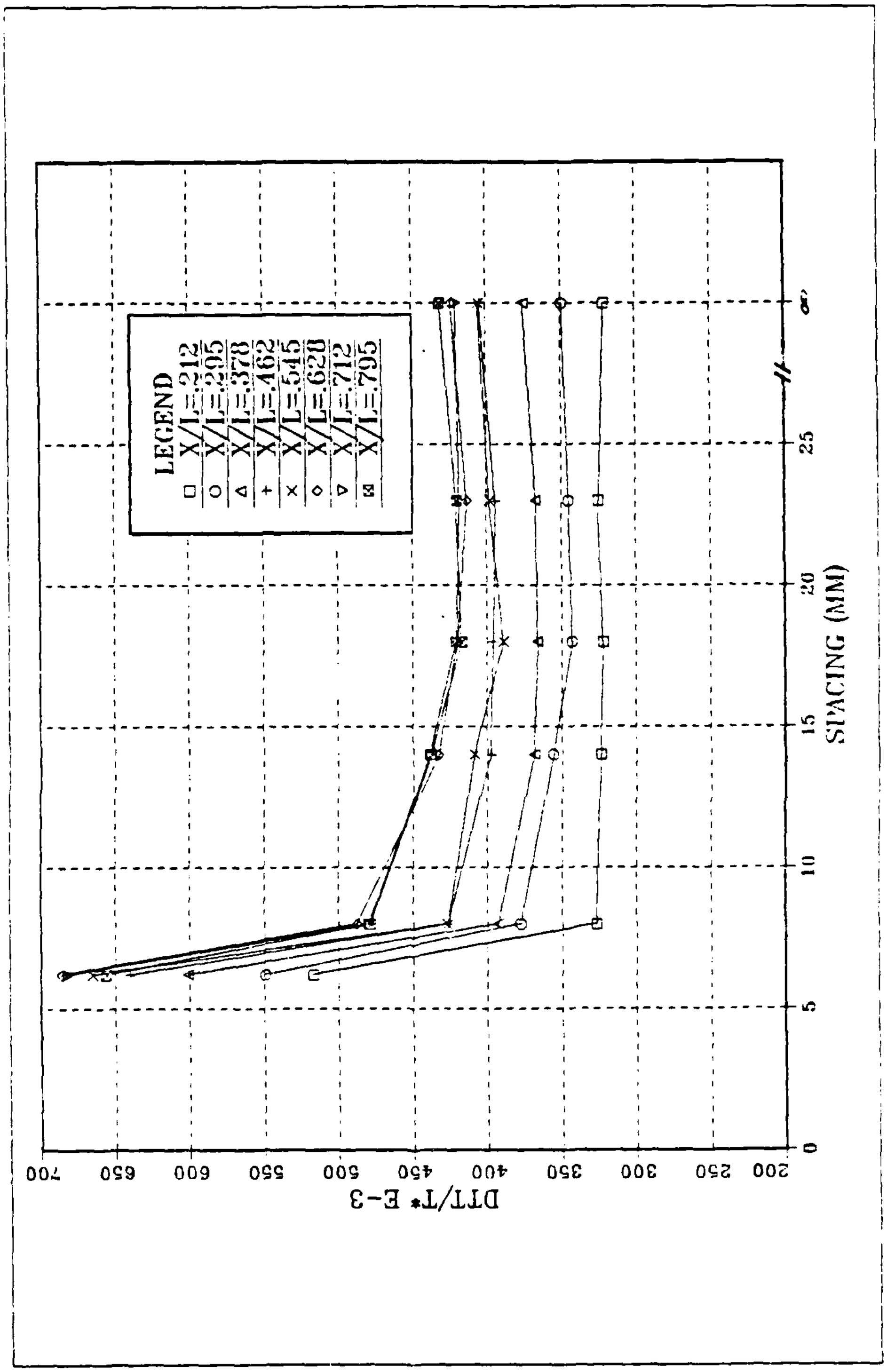

Figure 56. **Nondimensional Temperature Excess vs. Shroud Position, 0.2 Watts, Top Faces**

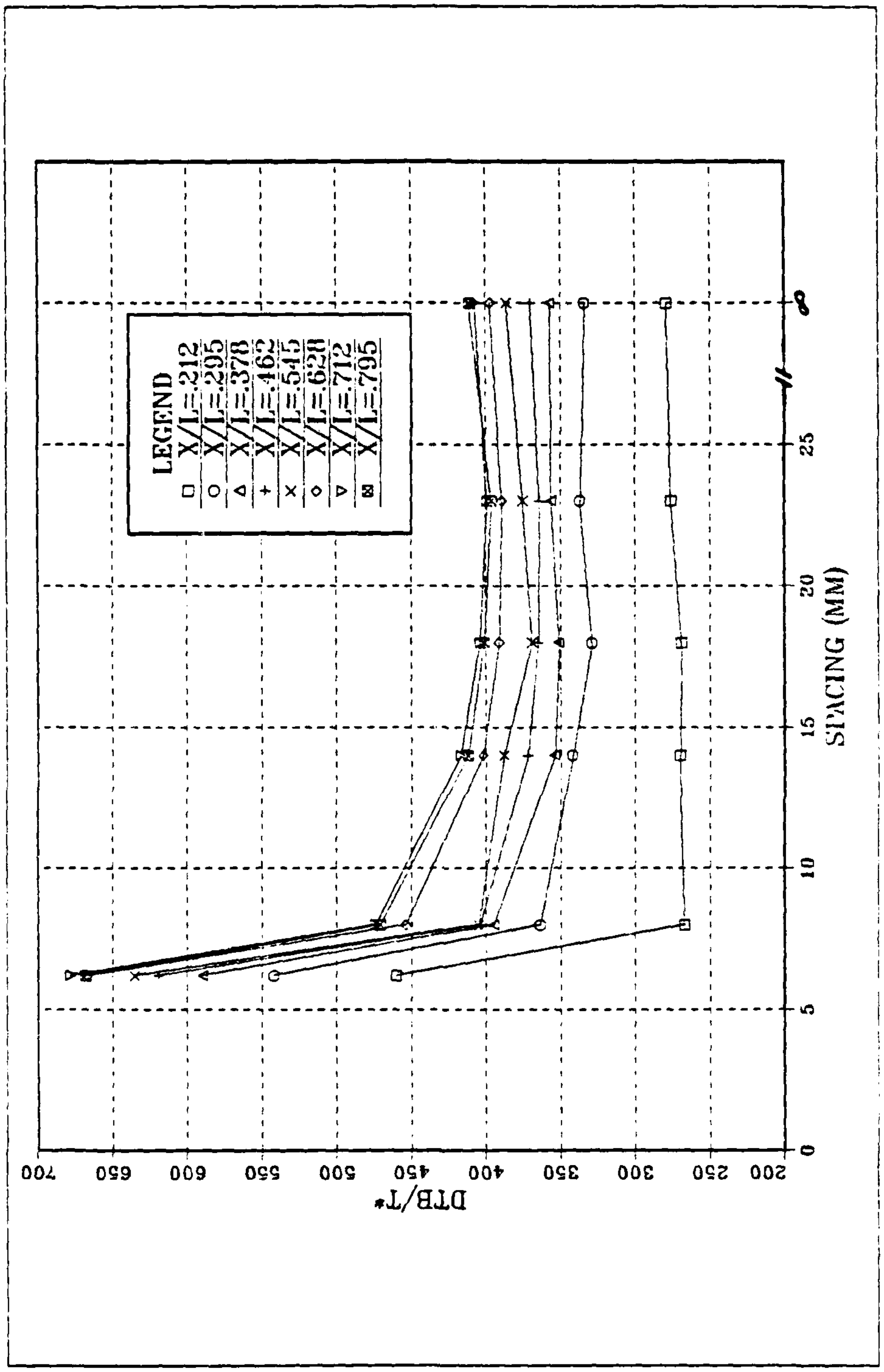

Figure 57. **Nondimensional Temperature Excess vs. Shroud Position, 0.2 Watts, Bottom Faces**

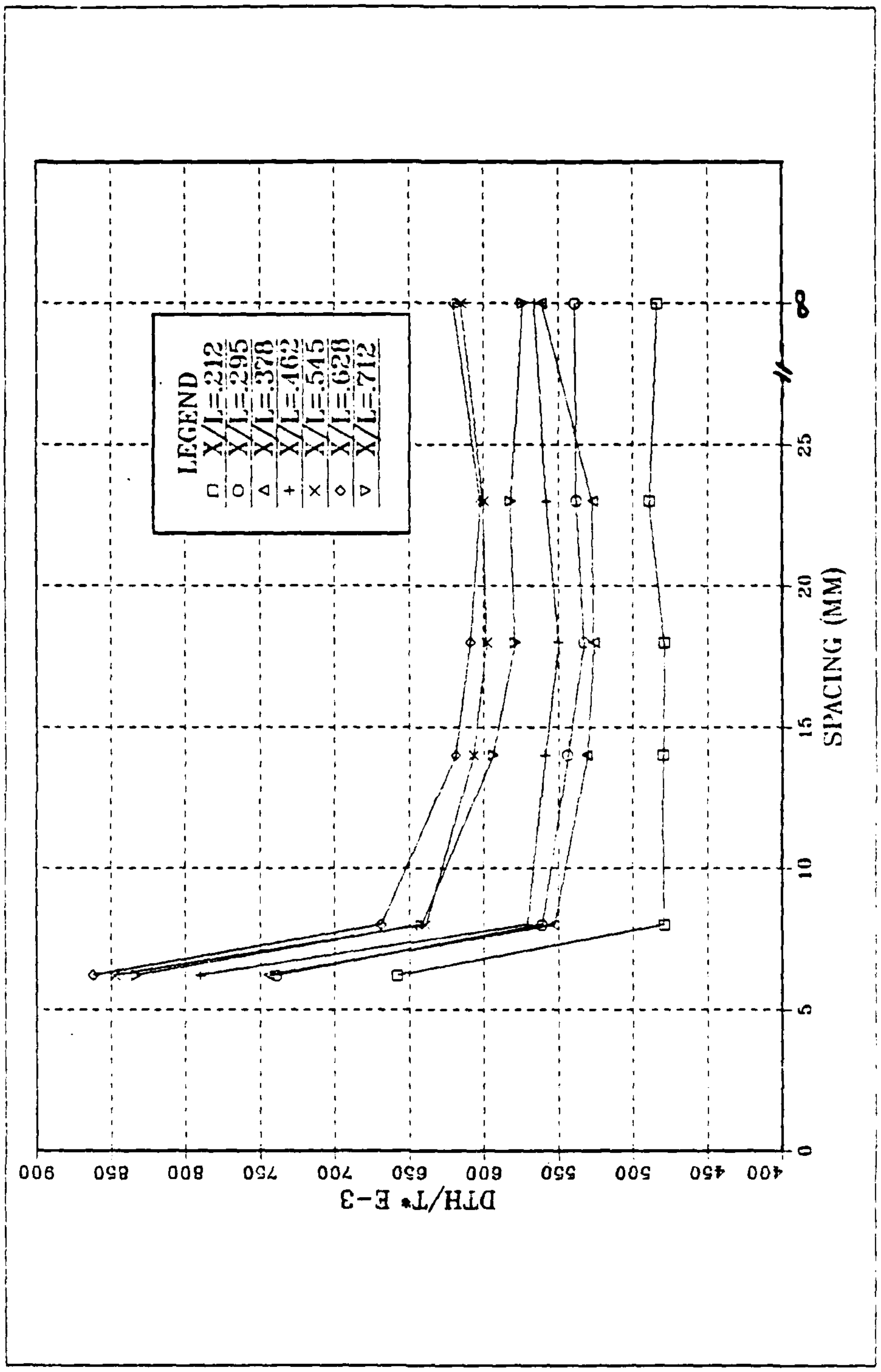

Figure 58. **Nondimensional Temperature Excess vs. Shroud Position, 0.2 Watts, Heaters**

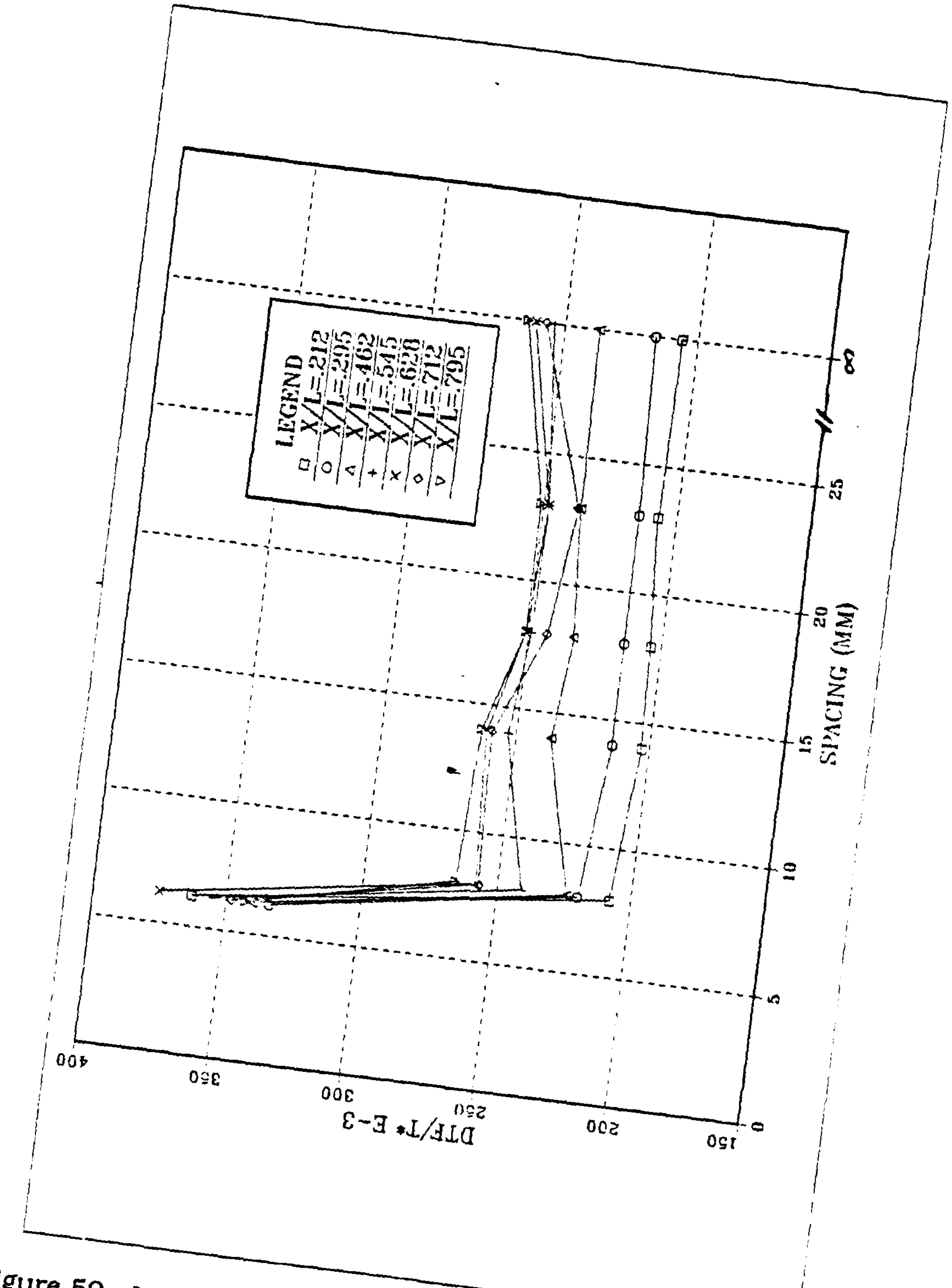

Figure 59. **Nondimensional Temperature Excess vs. Shroud Position, 1.2 Watts, Front Faces**

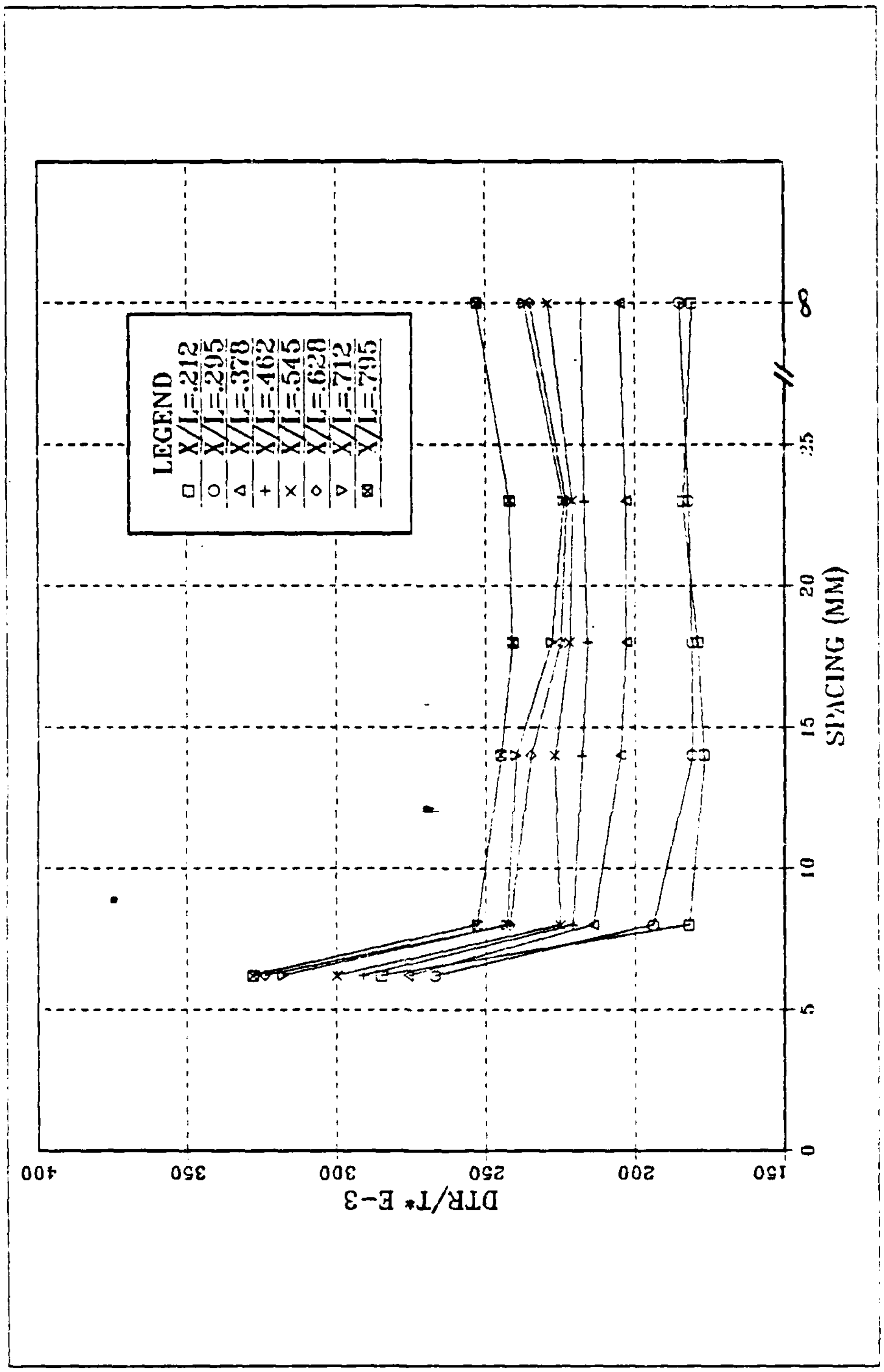

Figure 60. **Nondimensional Temperature Excess vs. Shroud Position, 1.2 Watts, Right Faces**

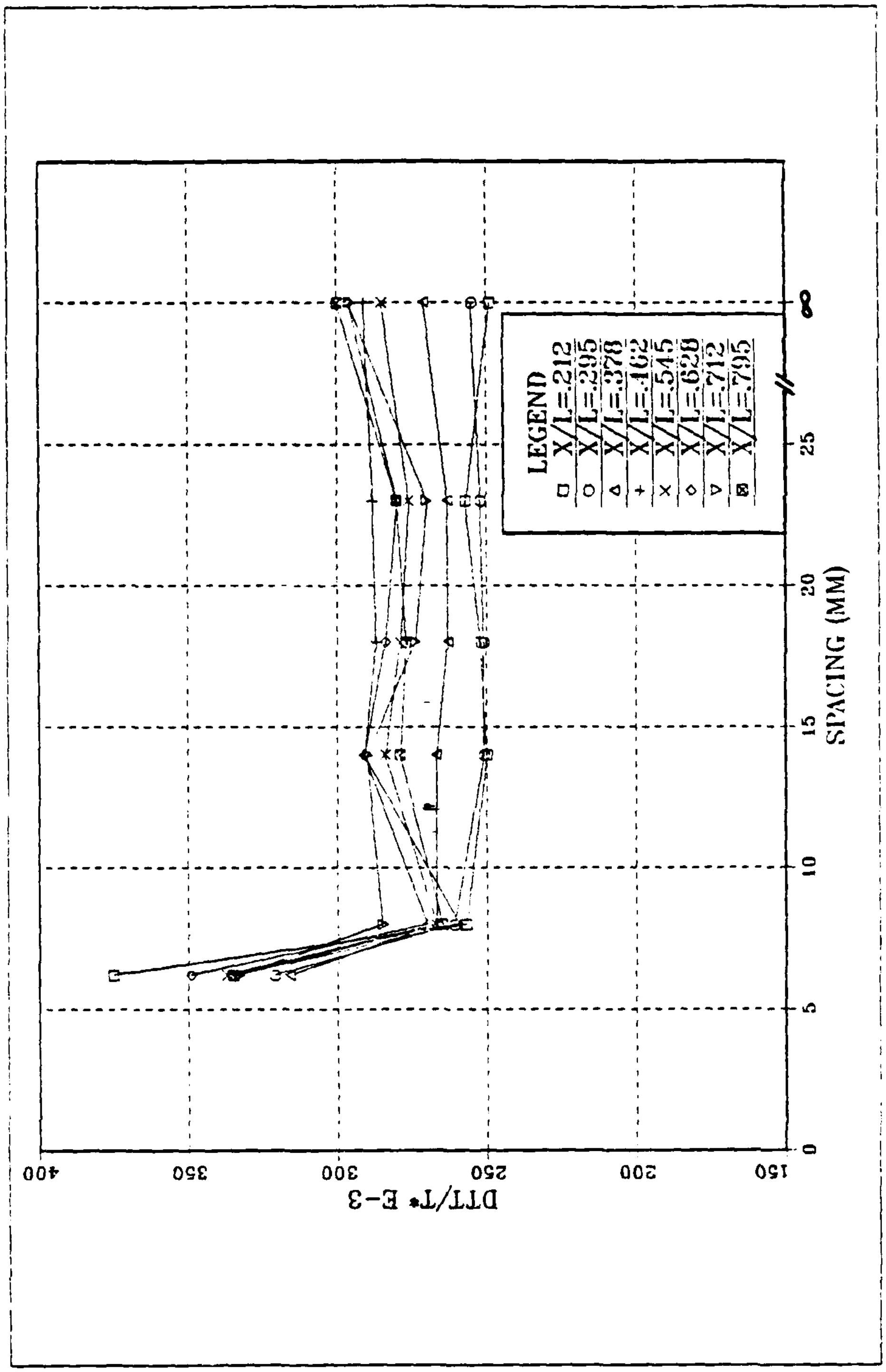

Figure 61. **Nondimensional Temperature Excess vs. Shroud Position, 1.2 Watts, Top Faces**

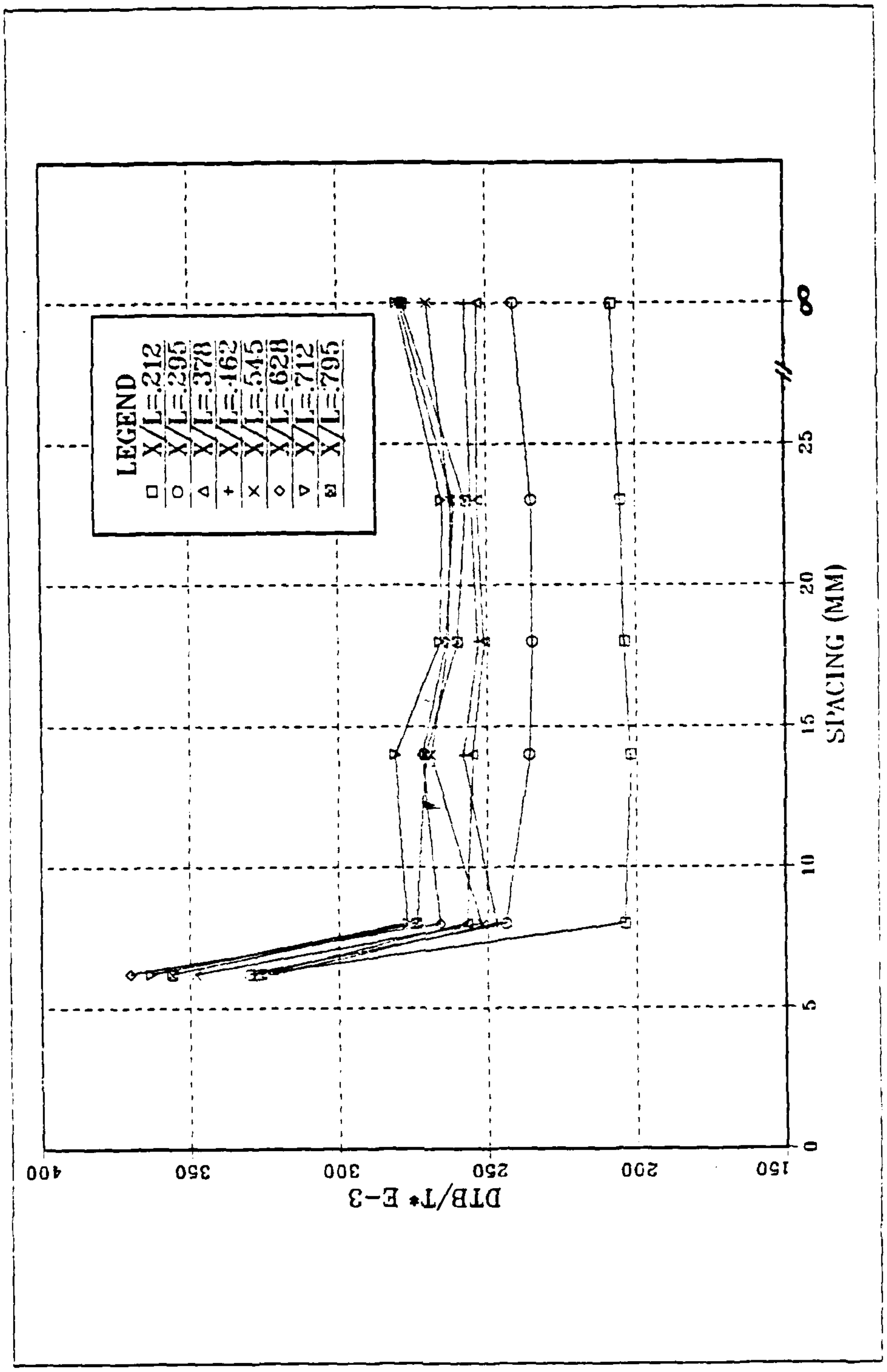

Figure 62. **Nondimensional Temperature Excess vs. Shroud Position, 1.2 Watts, Bottom Faces**

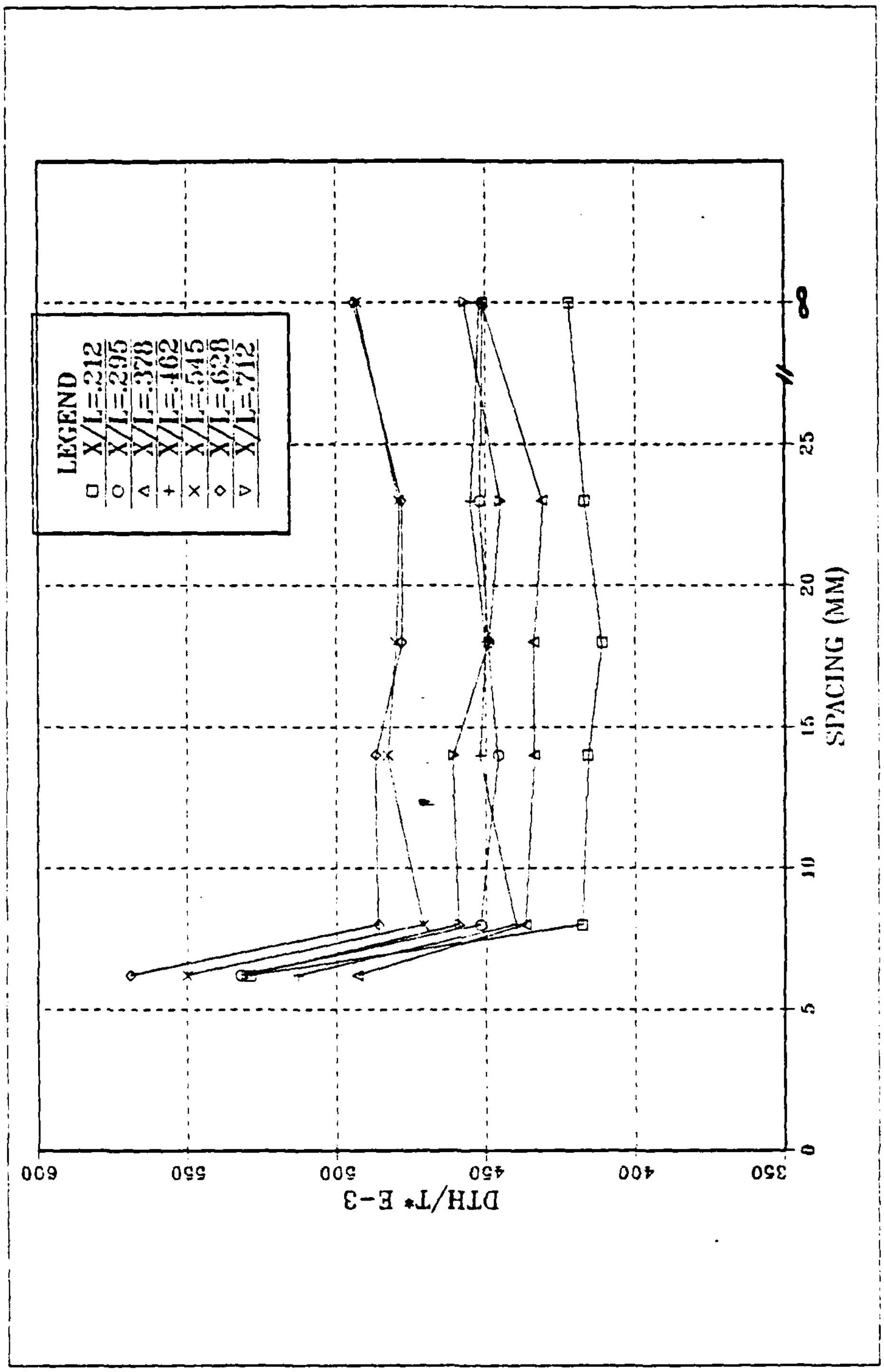

Figure 63. **Nondimensional Temperature Excess vs. Shroud Position, 1.2 Watts, Heaters**

temperatures (at the last blocks) are not observed when a shroud is in position because the global forced convection within the channel is driving the fluid more strongly past the last block. As seen from Figures 54 through 58, face temperatures at a power level of 0.2 watts for 8 mm are somewhat higher than for greater spacings. By 14 mm, the difference with larger spacings begins to become indistinguishable. Clearly for this geometry and for the power settings examined, a channel width of 2.5 times component depth is most satisfactory while a width of 1.3 times element depth may be acceptable. Further confirmation of the observation that spacings beyond 8 mm do not significantly affect heat transfer is seen in Figures 64 through 68. These show the Nu^* vs. Gr^* data along with the correlation, $Nu^* = 1.88 (Gr^*)^{.15}$, obtained in Chapter III. The correlation for an unshrouded surface holds very well through 14 mm. At 8 mm there is a slightly greater deviation. As anticipated, it is inapplicable for the smallest spacing of 6.2 mm.

B. INDIVIDUAL ELEMENTS POWERED

As in the absence of a shroud, individual blocks were powered to 1.0 watt, one at a time, but with a shroud spaced 14 mm from the substrate. The resultant data is displayed in Figures 69 through 73. The plots follow similar trends as for the no-shroud condition (Figures 21-25) but show somewhat smaller temperatures. Again, the protruding elements have minimal effect on the unheated starting length.

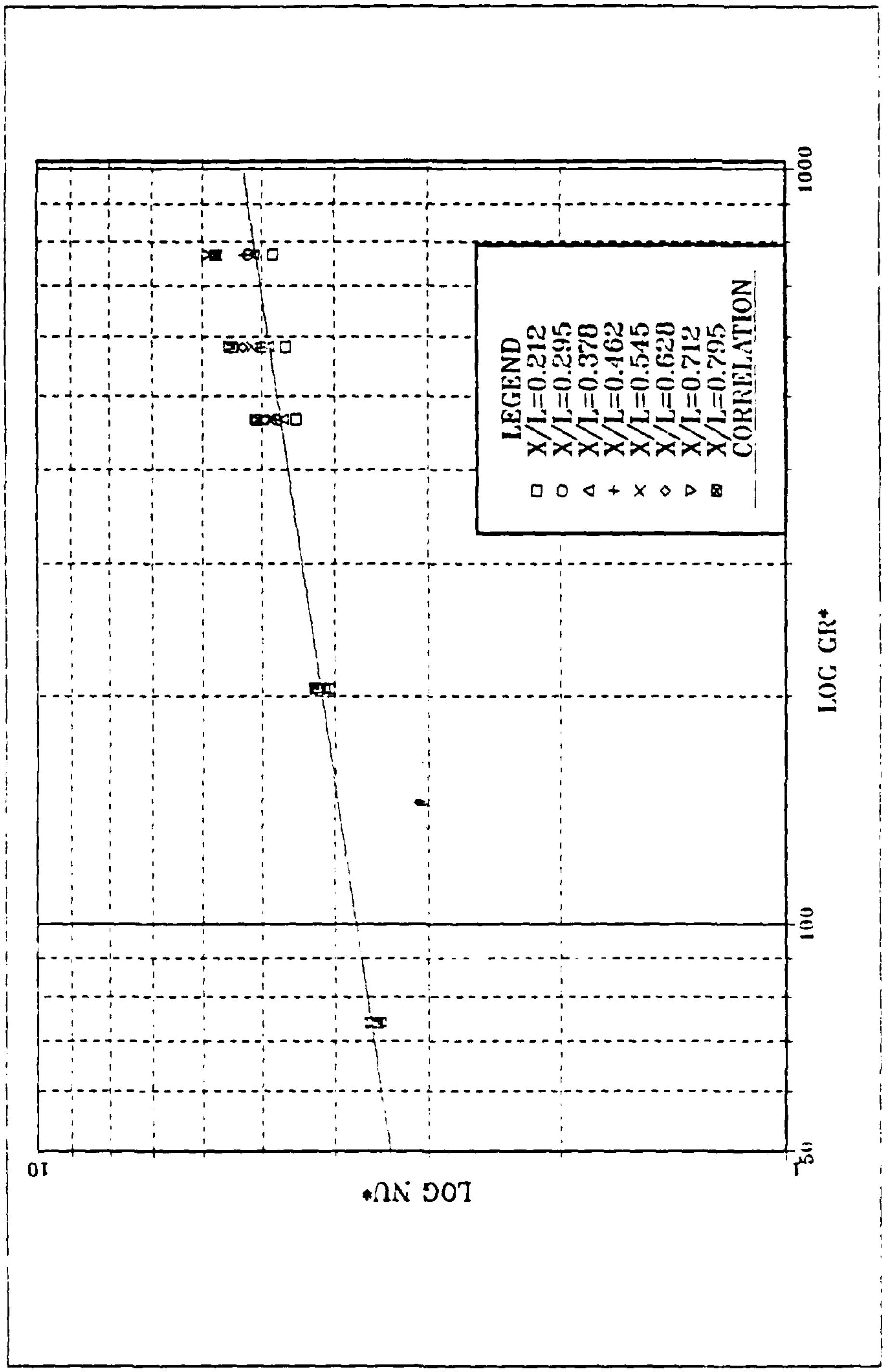

Figure 64. *Nu** **vs.** *Gr**, **With Correlation, 23 mm Channel Spacing**

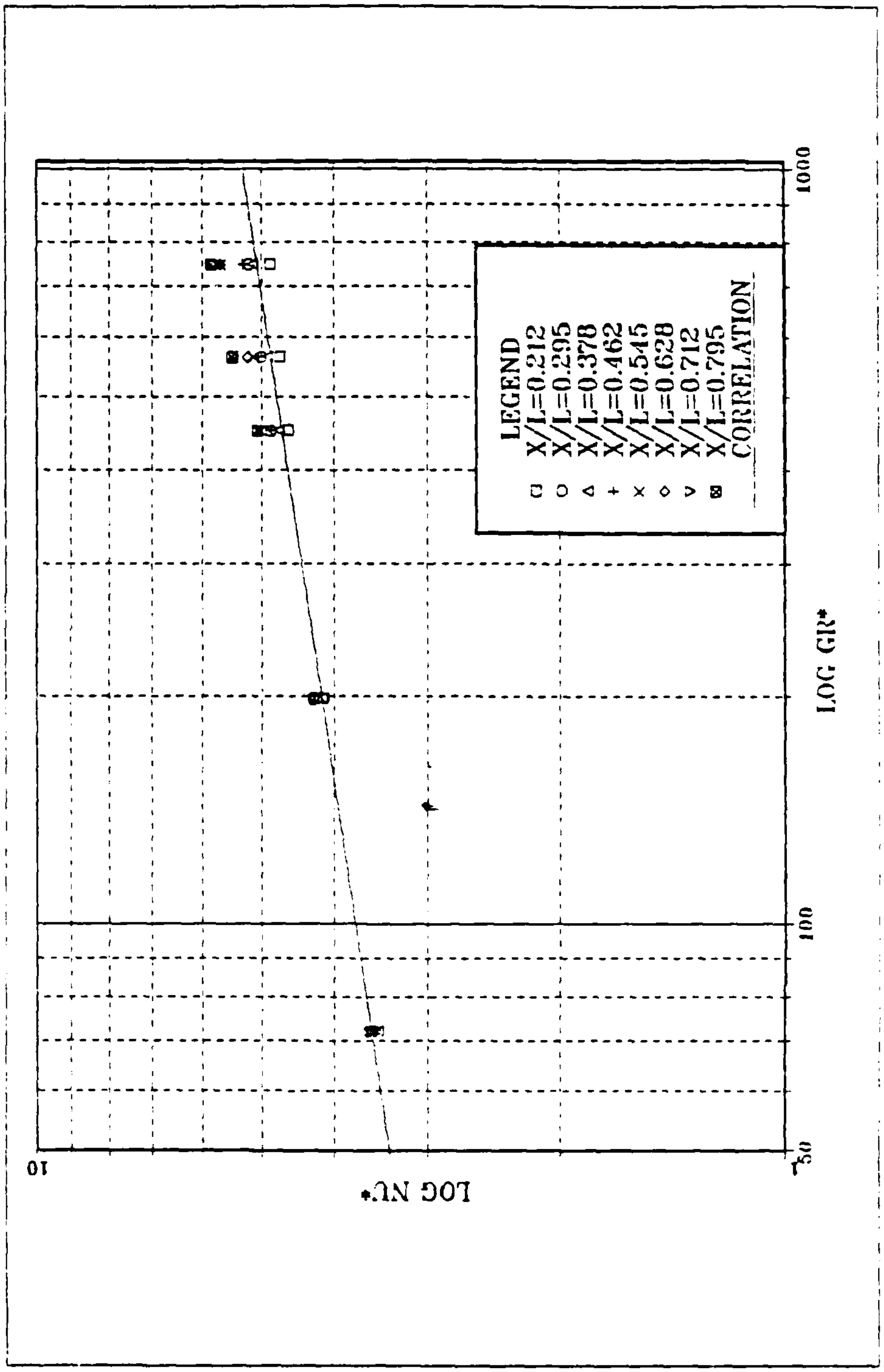

Figure 65. ***Nu* vs. Gr*, With Correlation, 18 mm Channel Spacing***

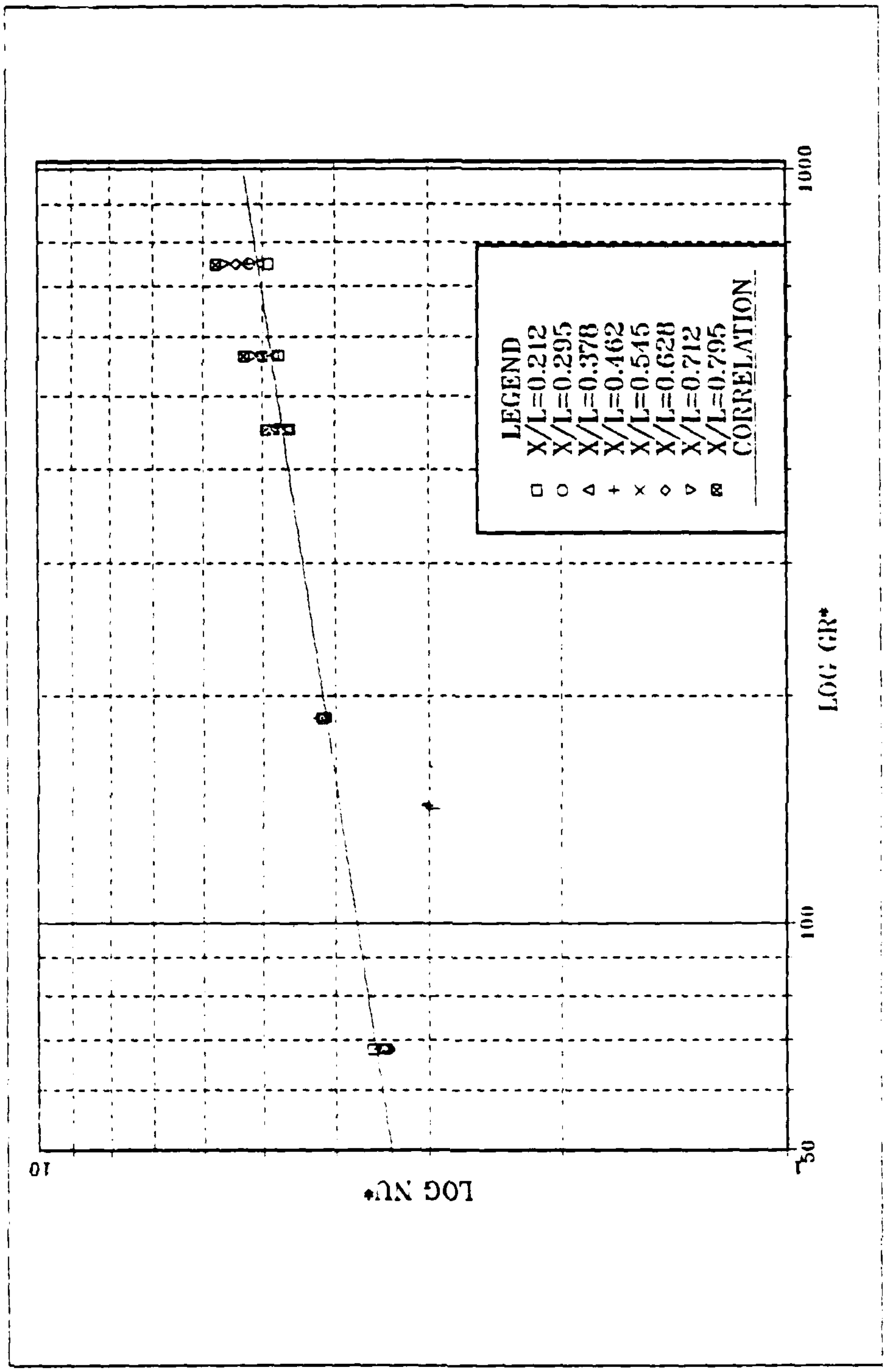

Figure 66. ***Nu* vs. *Gr*, With Correlation, 14 mm Channel Spacing***

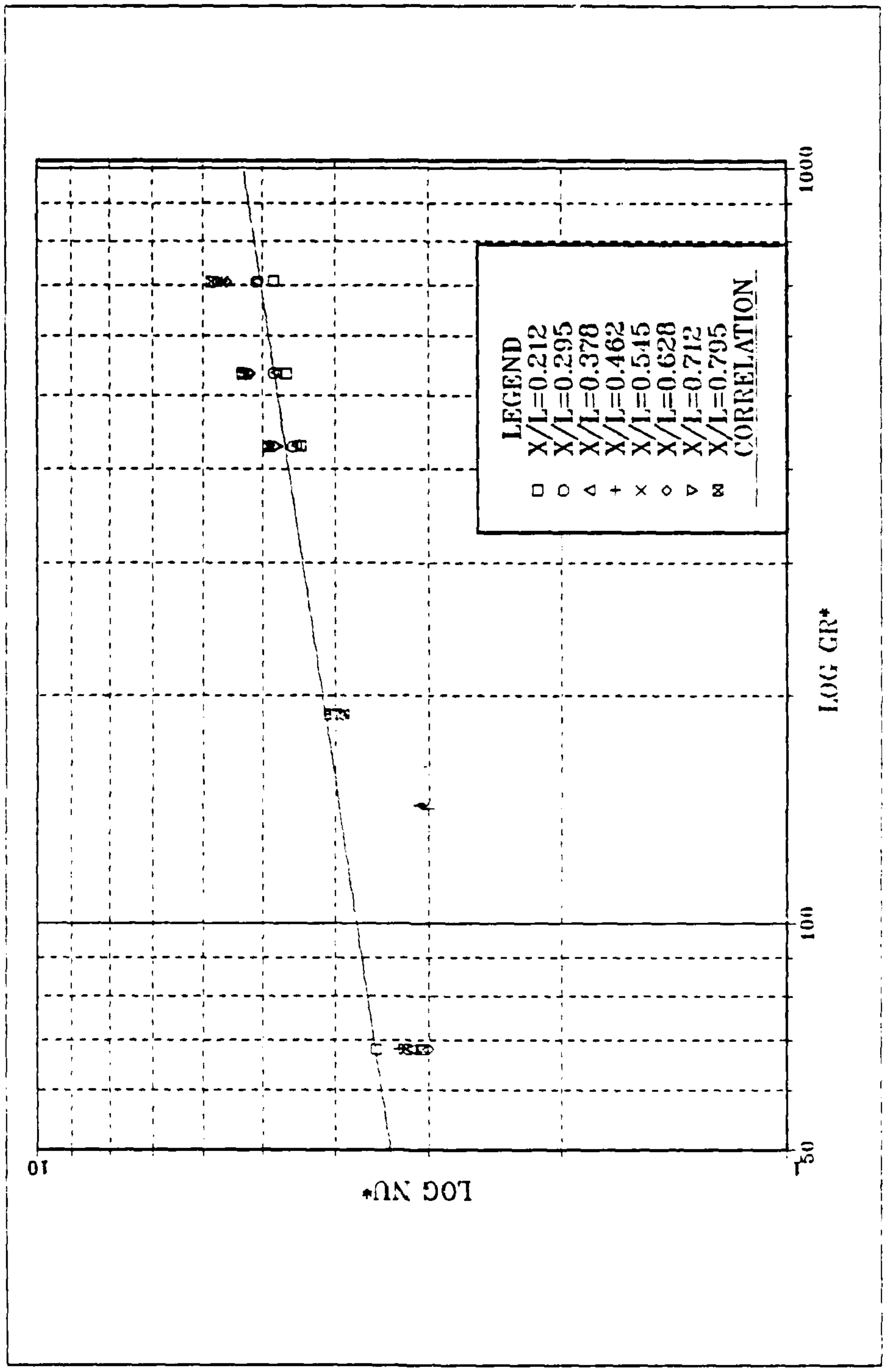

Figure 67. ***Nu* vs. Gr*, With Correlation, 8 mm Channel Spacing***

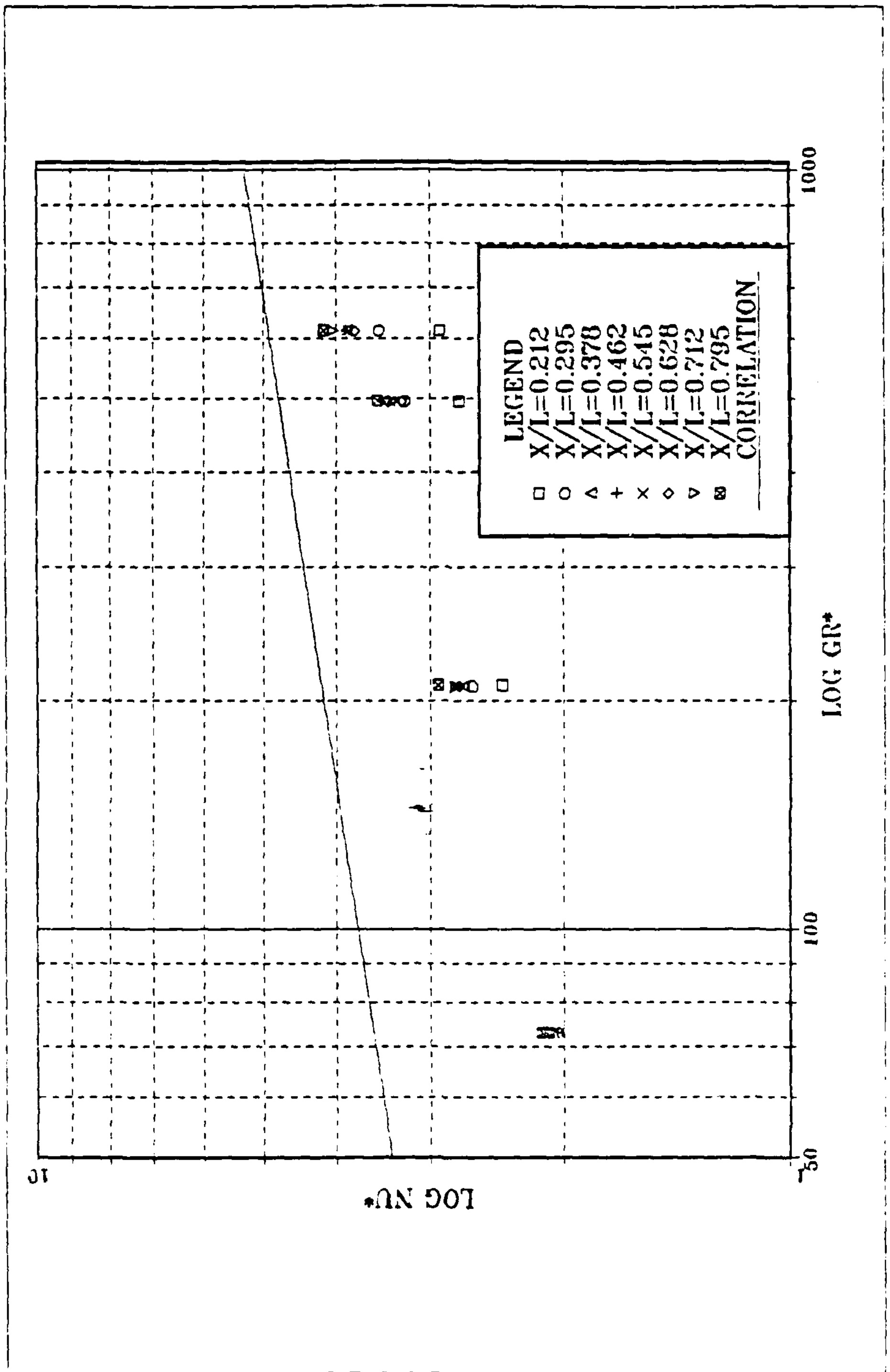

Figure 68. ***Nu* vs. Gr*, With Correlation, 6.2 mm Channel Spacing***

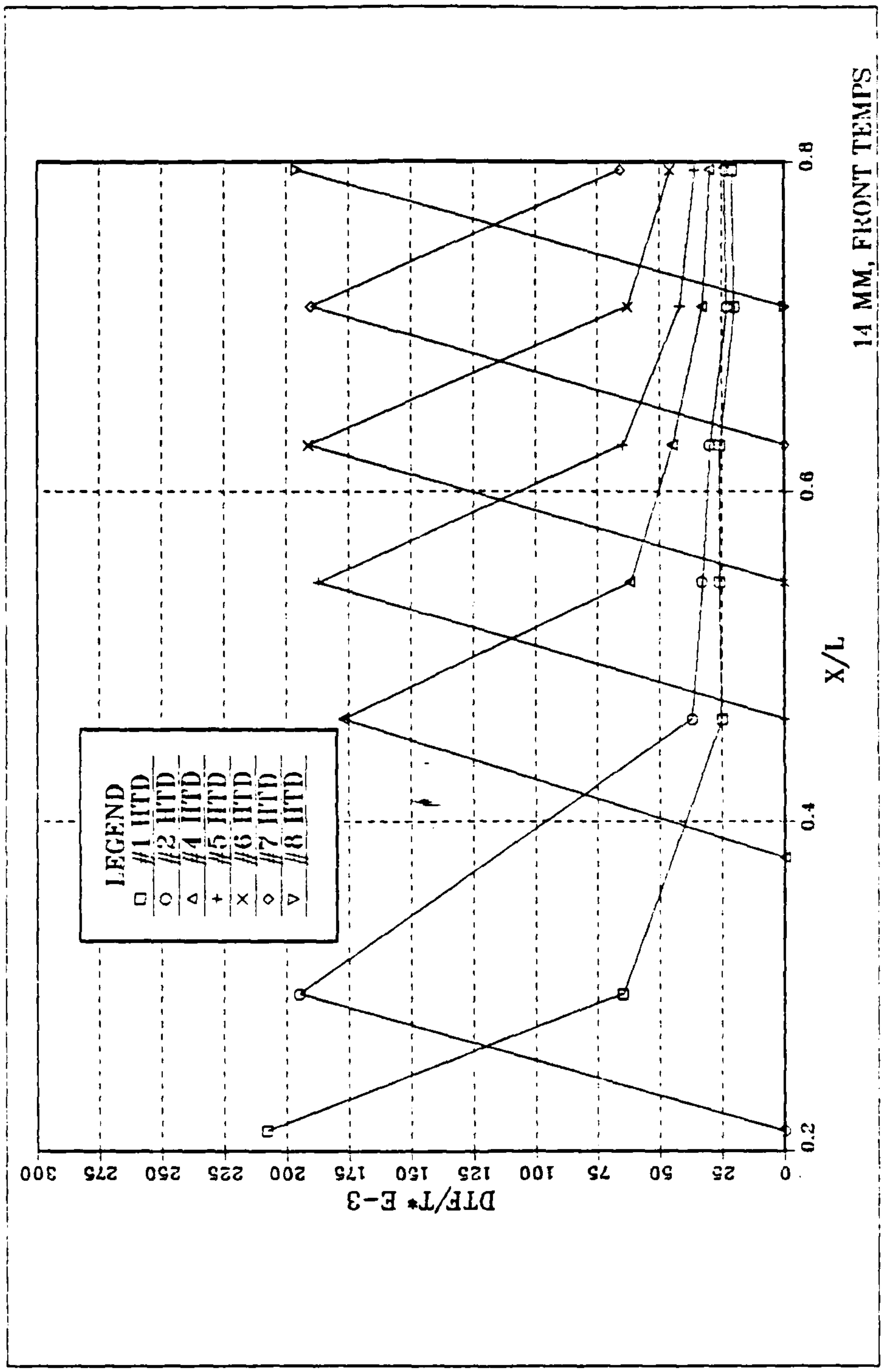

Figure 69. **Nondimensional Temperature Excess, Front Faces, Individually Heated Components, 14 mm Channel Spacing**

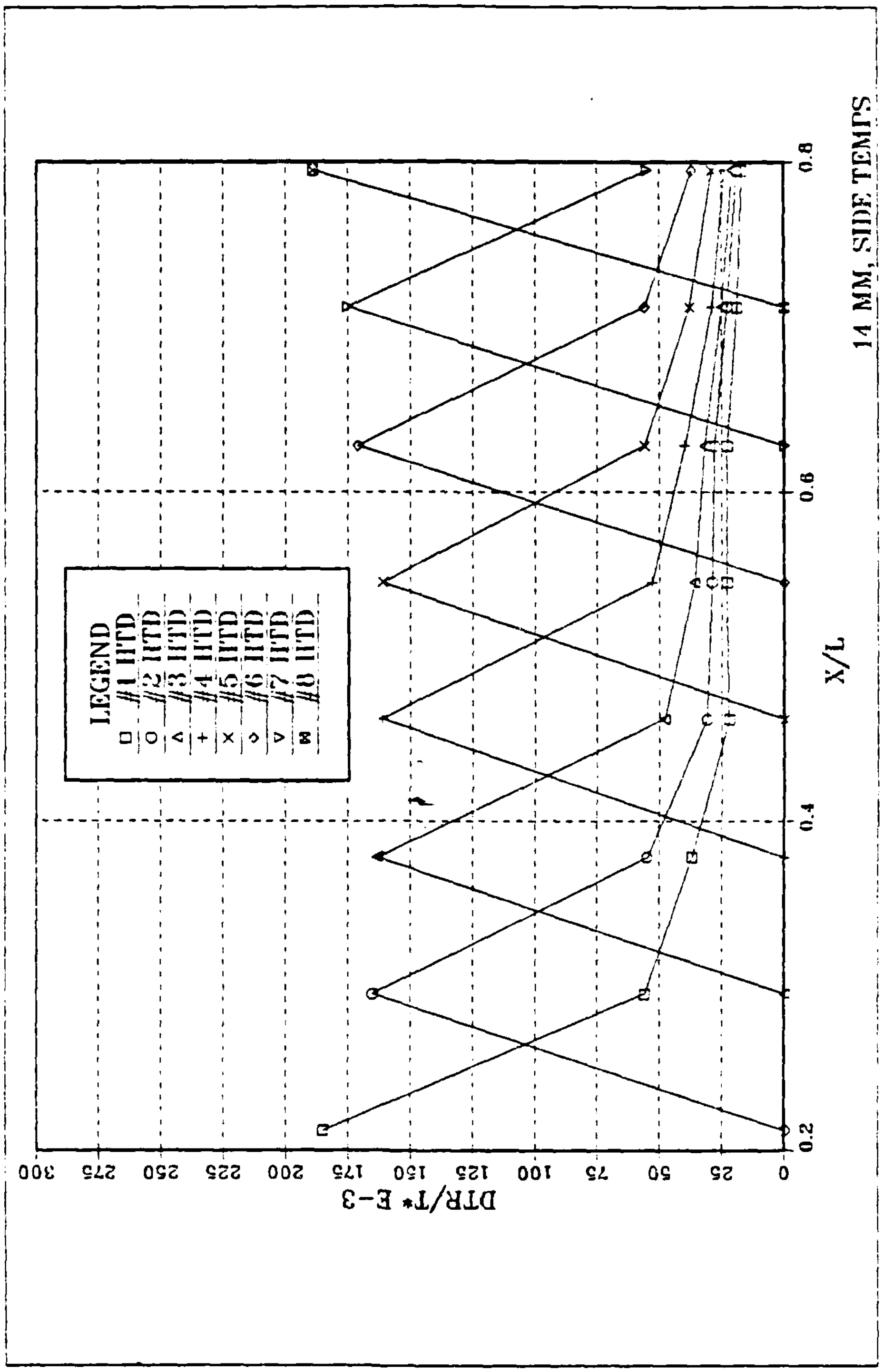

Figure 70. **<u>Nondimensional Temperature Excess, Right Faces, Individually Heated Components, 14 mm Channel Spacing</u>**

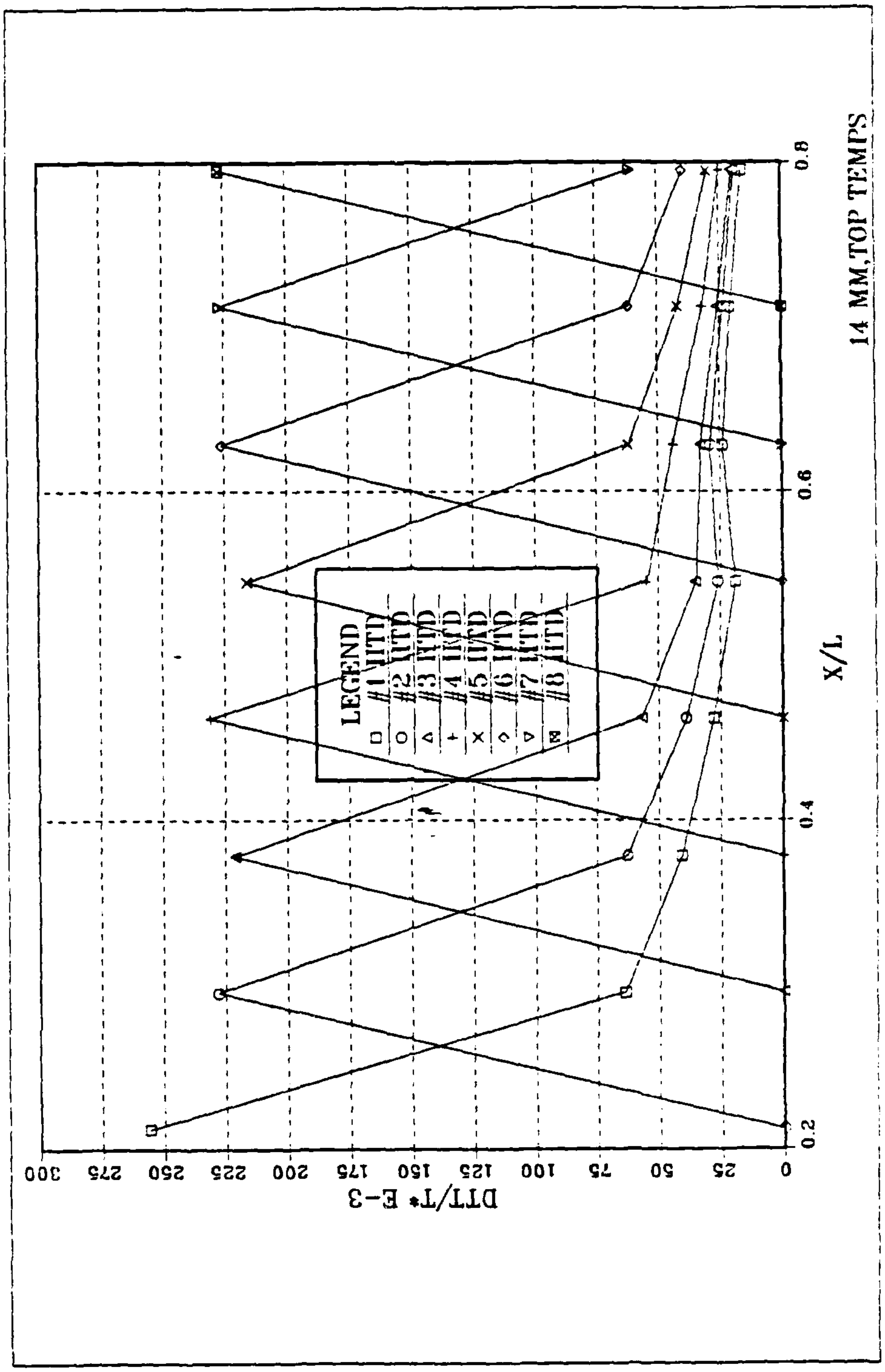

Figure 71. **Nondimensional Temperature Excess, Top Faces, Individually Heated Components, 14 mm Channel Spacing**

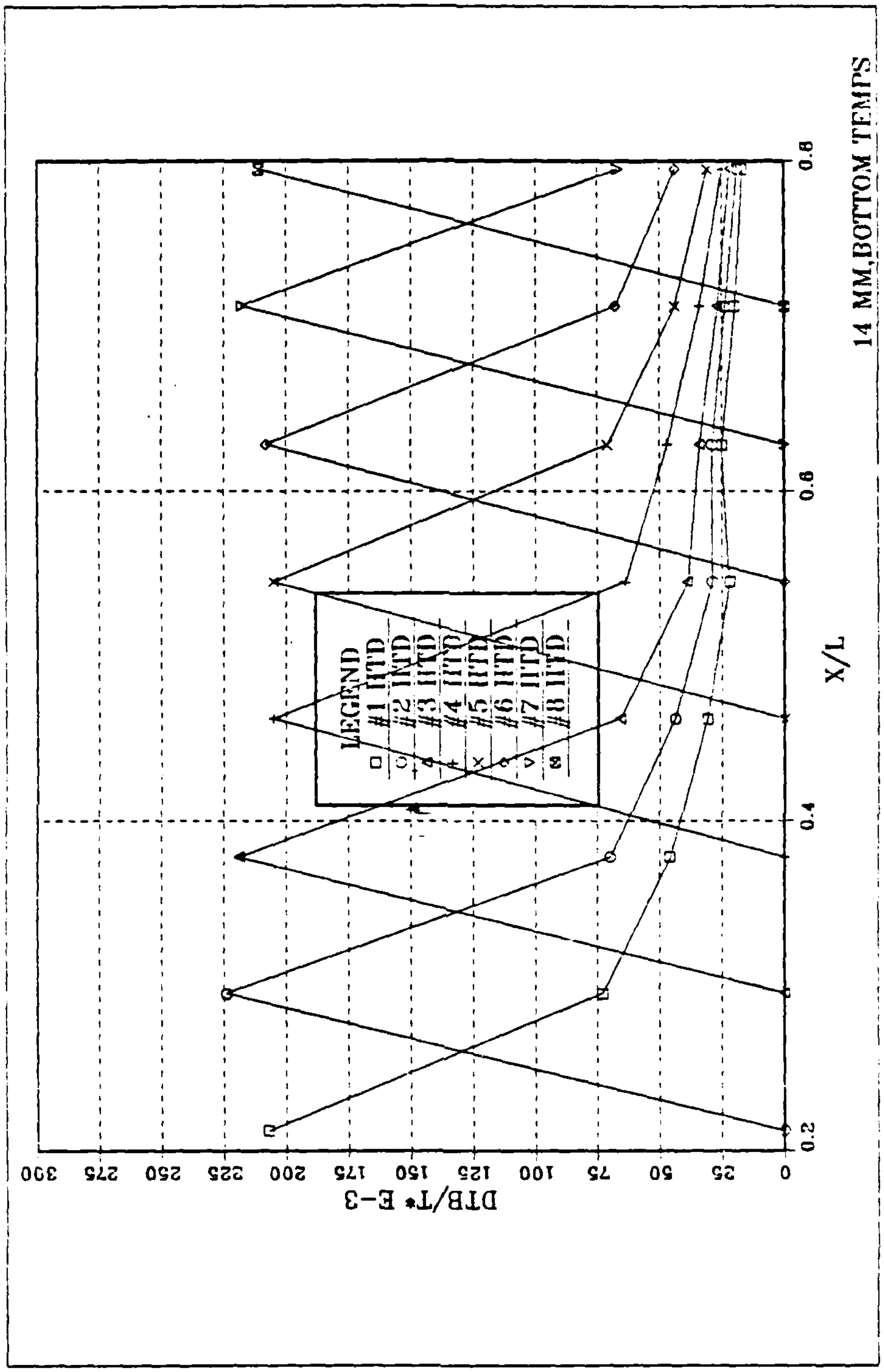

Figure 72. **Nondimensional Temperature Excess, Bottom Faces, Individually Heated Components, 14 mm Channel Spacing**

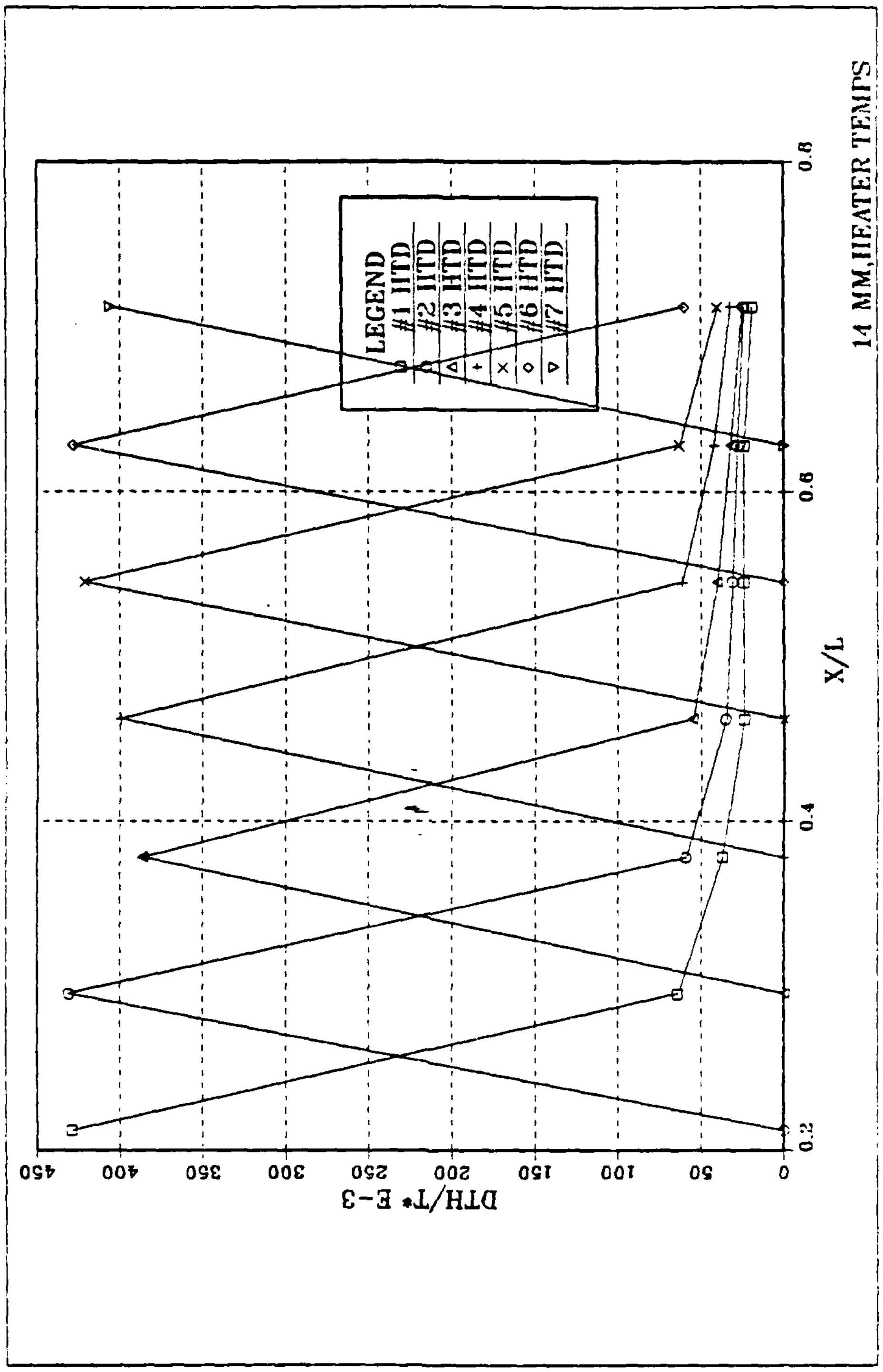

Figure 73. **Nondimensional Temperature Excess, Heaters, Individually Heated Components, 14 mm Channel Spacing**

C. COMBINATIONS OF ELEMENTS HEATED

In a manner identical to that without a shrouding wall, progression of elements heated was made up the array while all upstream blocks remained powered. Additionally, block 8 was powered throughout and a shroud 14 mm from the substrate was in place. The plots (Figures 74–78) reveal that for this channel width, as with no shroud, the powering of downstream components has minimal effect on those upstream components already powered. The plots further show a weak effect by a heated element (block 8) on those components between it and the ones powered upstream, which are heated only by the convective flow generated upstream of them.

D. ALL ELEMENTS POWERED, TRANSIENT

1. Flow Visualization

Figure 79 shows transient flow development in the x-y plane following 1.0 watt power step-up with a 19 mm spaced shroud in place. All exposures are for 20 seconds. The photographs from left to right are initiated at 0, 20, 40, 100, and 140 seconds following start of heating. In the first picture, parallel flow is developing over blocks 3 through 8 with relatively little movement at blocks 1 and 2. By picture number 3, the flow follows more closely the contours of the protruding blocks and originates further upstream. By photograph 5, the flow appears nearly fully developed.

The power step-down from 0.2 watts was again for a 19 mm channel width and 20-second exposures (Figure 80). The pictures

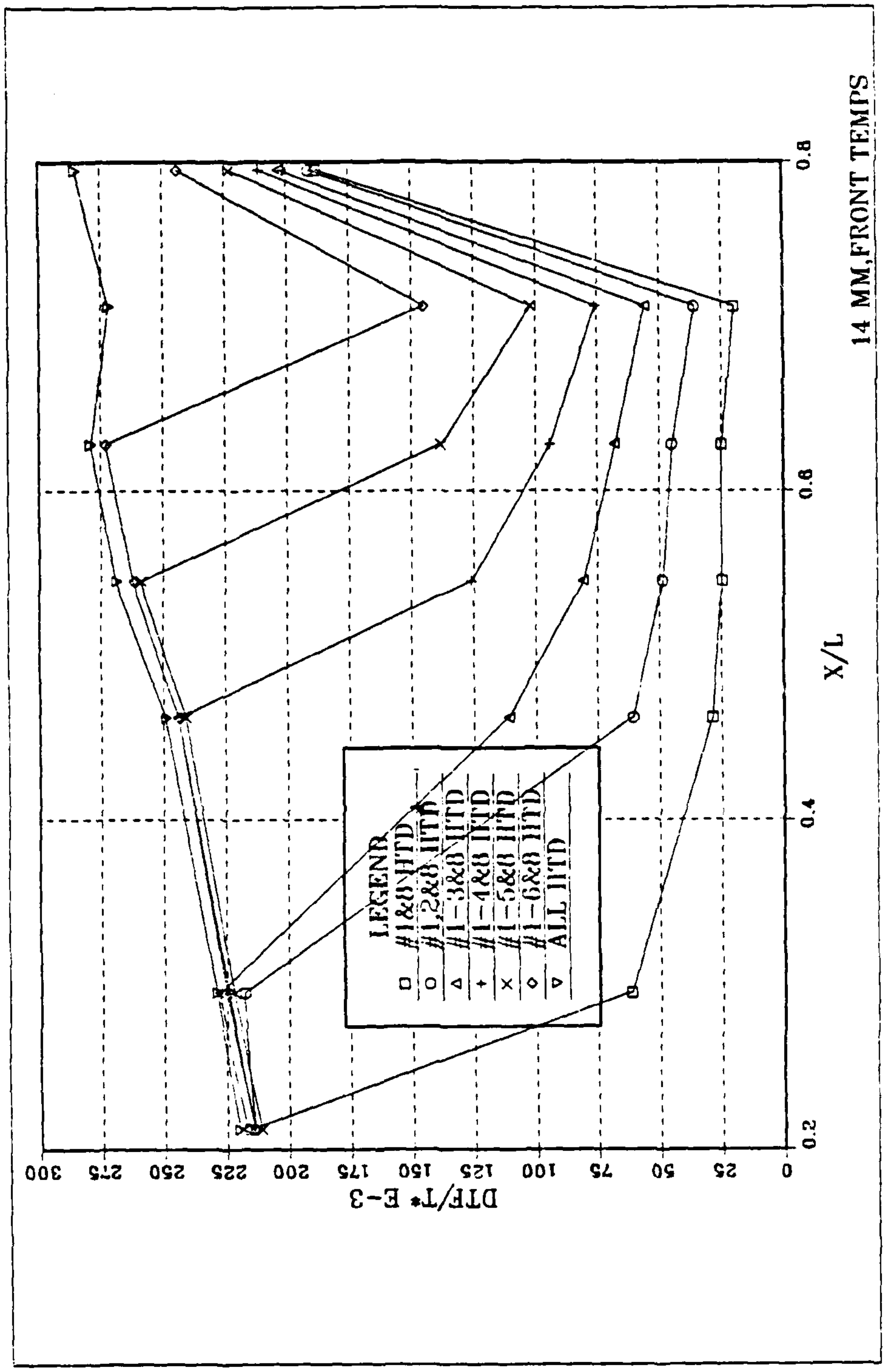

Figure 74. **Nondimensional Temperature Excess, Front Faces, Multiple Components Heated, 14 mm Channel Spacing**

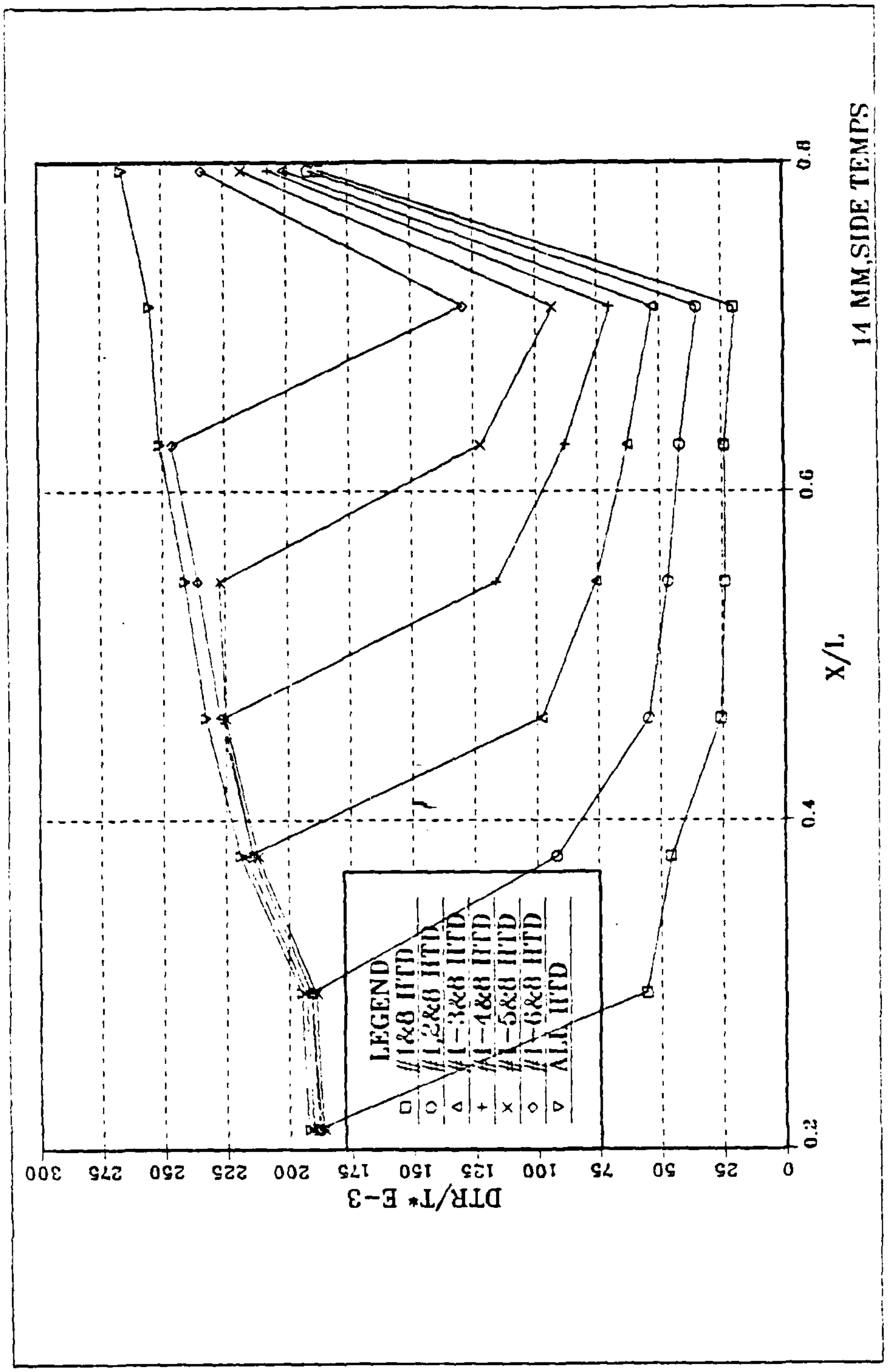

Figure 75. **Nondimensional Temperature Excess, Right Faces, Multiple Components Heated, 14 mm Channel Spacing**

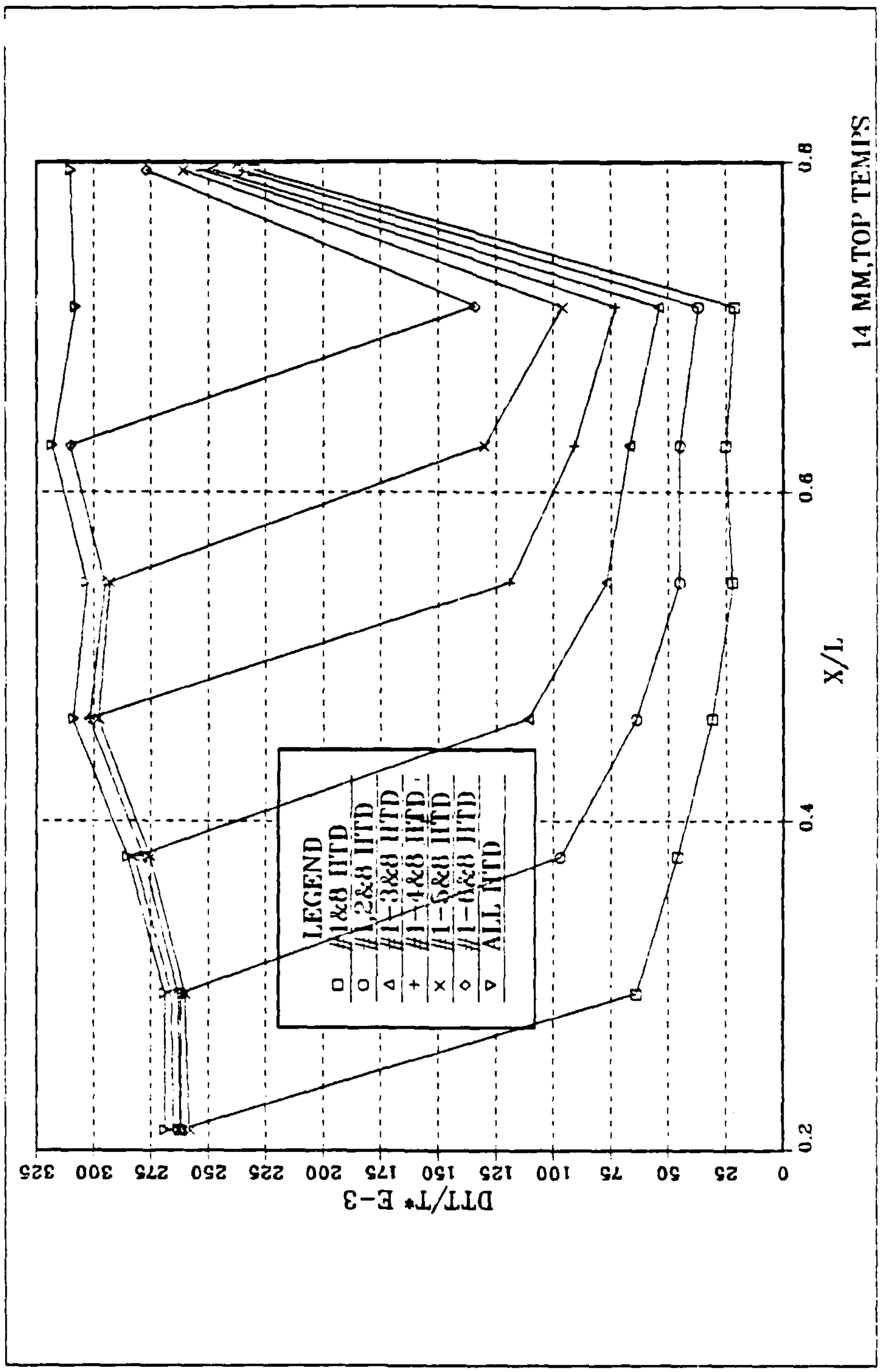

Figure 76. **Nondimensional Temperature Excess, Top Faces, Multiple Components Heated, 14 mm Channel Spacing**

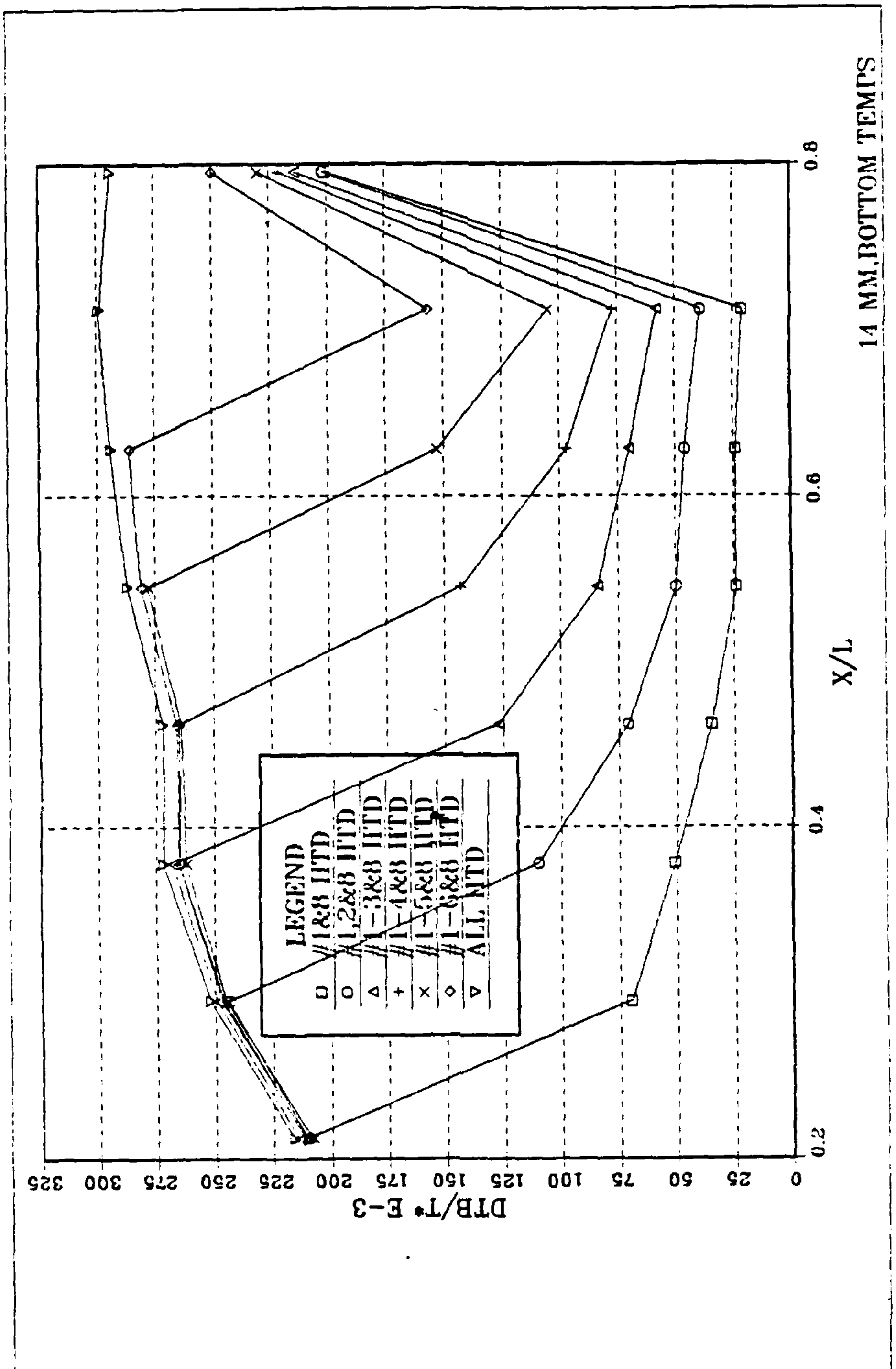

Figure 77. **Nondimensional Temperature Excess, Bottom Faces, Multiple Components Heated, 14 mm Channel Spacing**

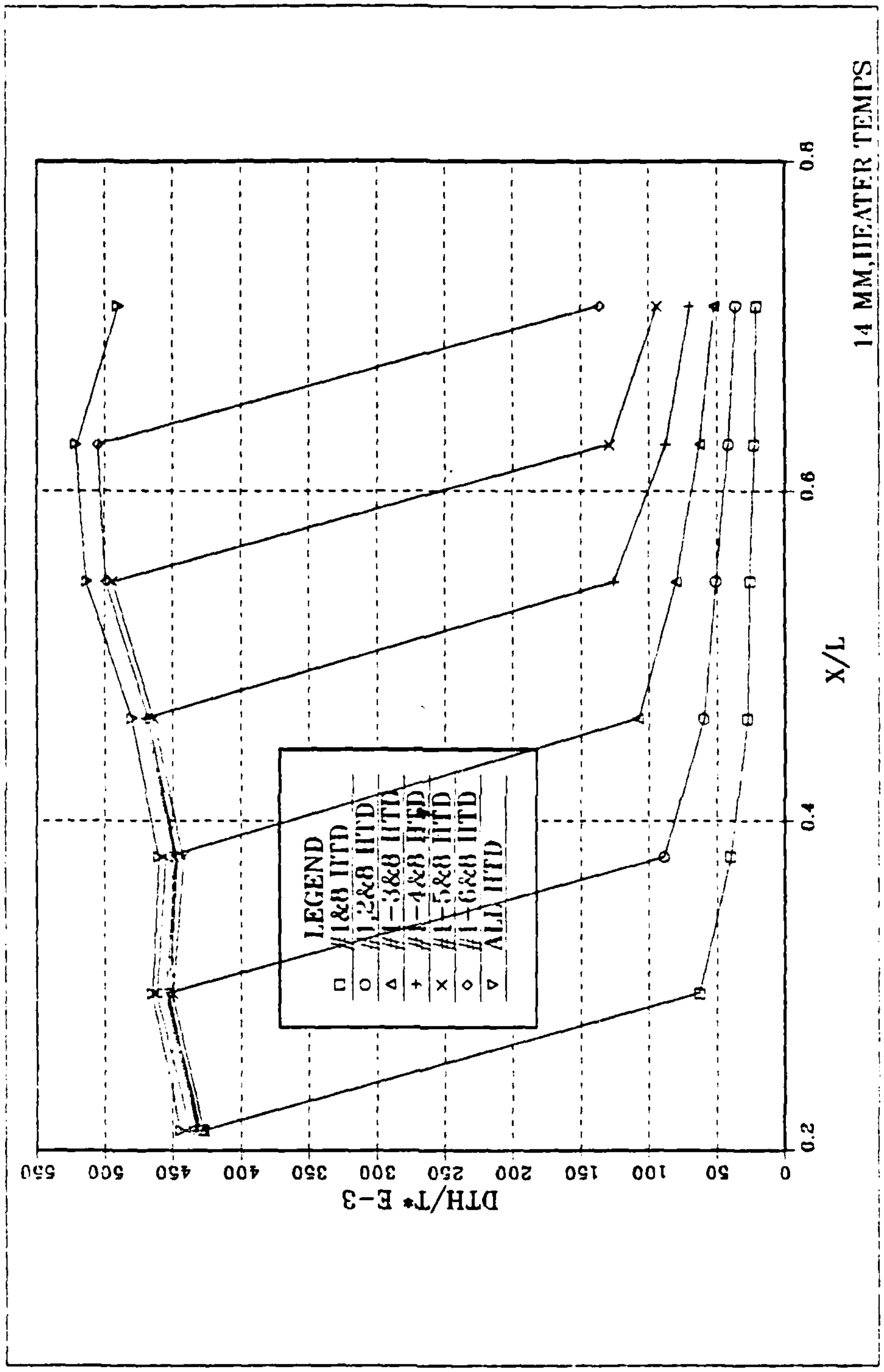

Figure 78. **Nondimensional Temperature Excess, Heaters, Multiple Components Heated, 14 mm Channel Spacing**

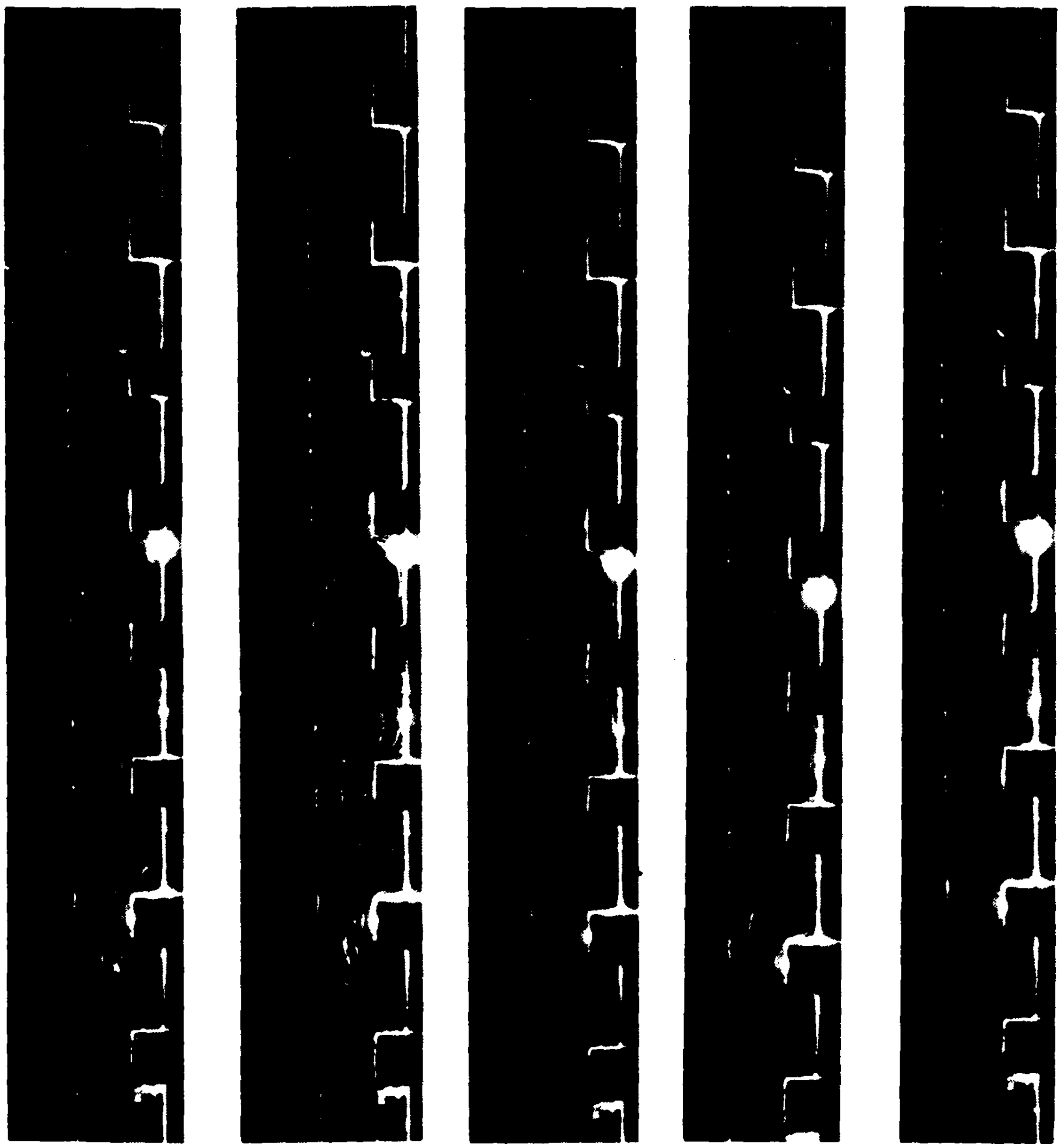

Figure 79. <u>**Flow Response During 1.0 Watt Step-Up Transient, 19 mm Channel**</u>

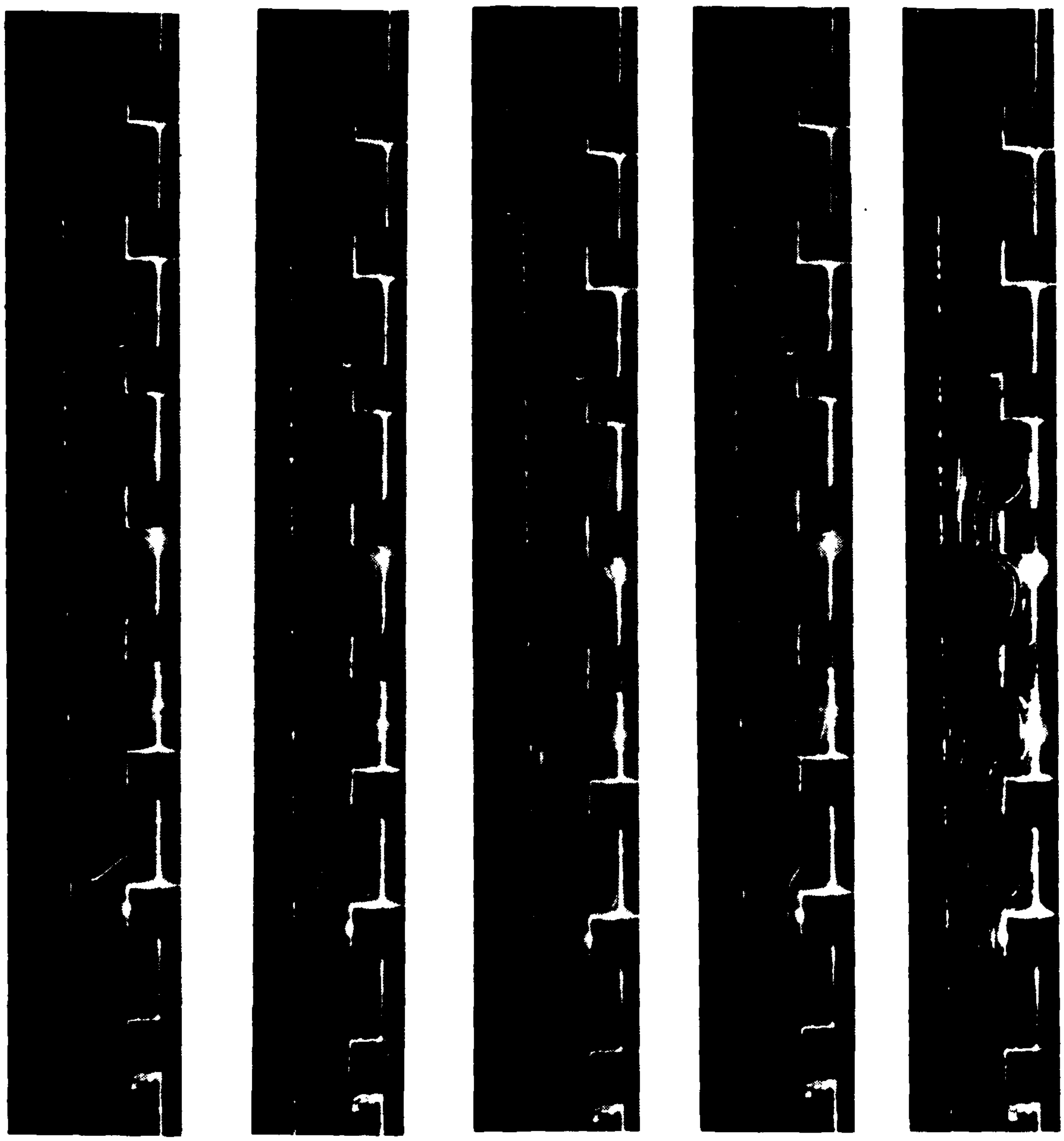

Figure 80. **Flow Response During 0.2 Watts Step-Down Transient, 19 mm Channel Spacing**

from left to right were initiated at 0, 60, 200, 320, and 460 seconds, respectively, following cessation of power. As with infinite channel width, the flow characteristic persists over the entire period observed. Only in the last picture does the flow begin to follow less closely the contour of blocks 7 and 8 and originate farther downstream.

2. Quantitative

The transient temperature response curves for powers of 1.0 and 0.2 watts and a shroud spacing of 19 mm (Figures 81 and 82) follow exactly the same pattern as those for no shroud (Figures 12 and 13). For the spacing examined, the shroud does not affect the transport evolution.

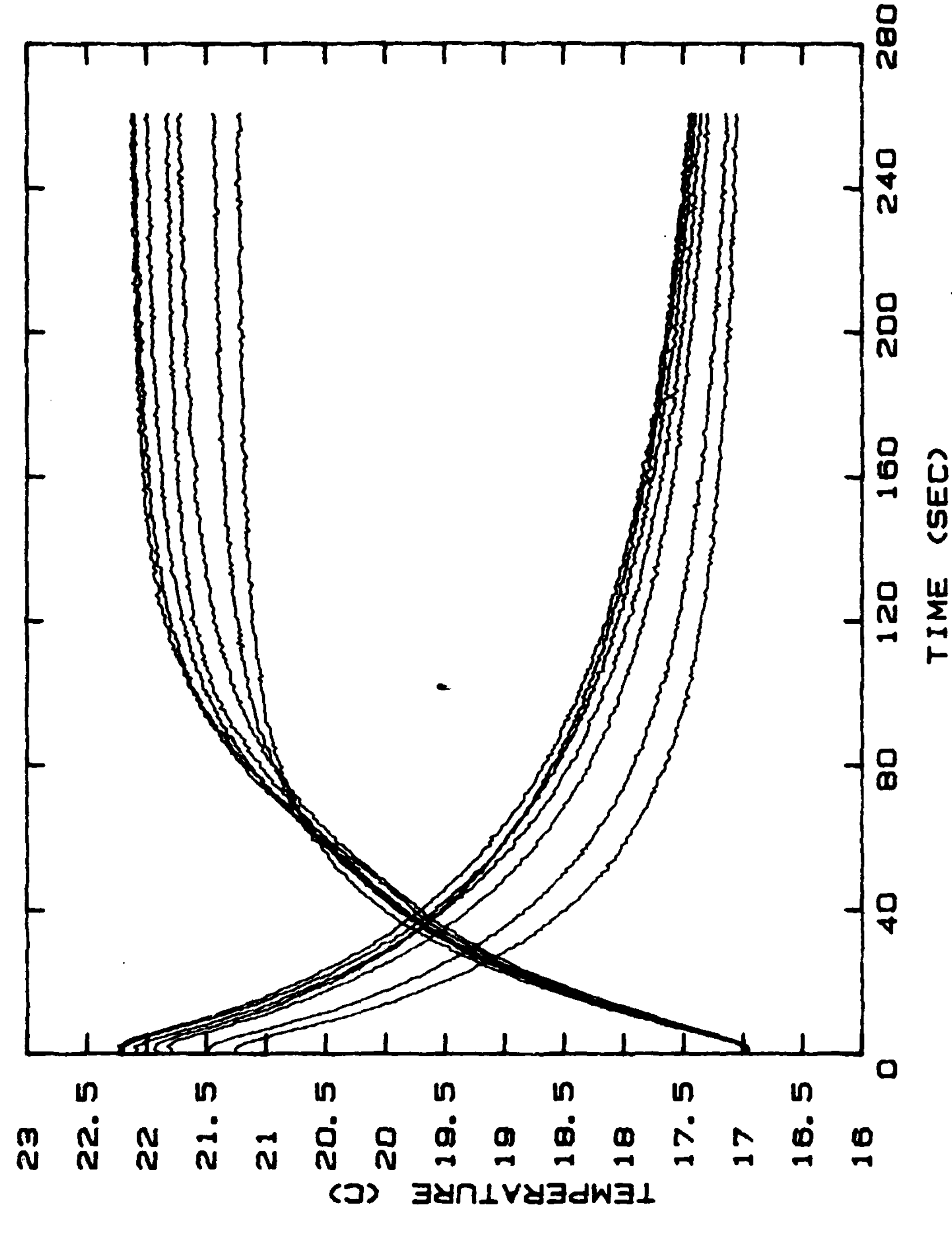

Figure 81. **Transient Temperature Response Following Initiation of Heating, 1.0 Watt**

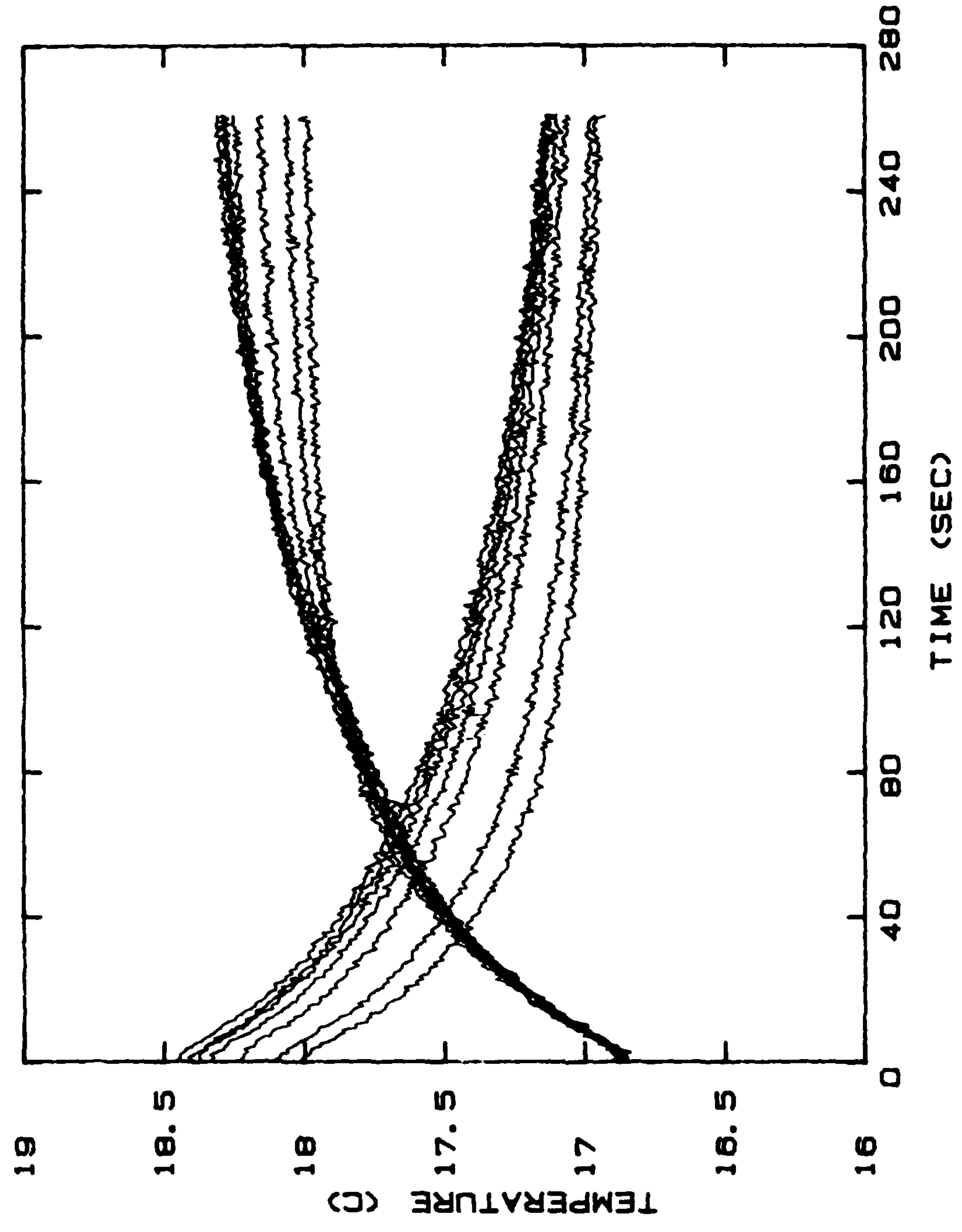

Figure 82. **Transient Temperature Response Following Cessation of Heating, 0.2 Watts**

V. CONCLUSIONS

Flow visualization in concert with quantitative analysis provided a number of significant determinations:

- The convective flow was three-dimensional.
- The flow was laminar.
- The thermal layer was imbedded within the momentum exchange region.
- Heated elements have minimal effect on those elements, upstream, which are already heated.
- There is no gain in heat transfer for channel widths greater than two times component depth.
- A correlation has been found to predict heat transfer rates for the subject geometry.

VI. RECOMMENDATIONS

It is suggested that the following areas of study be experimentally explored:

- Using the same test surface:
  - explore transient response for other block faces
  - with the traversing thermocouple probe, determine variation of temperature with position (in the thermal layer) for all blocks
- Construct new test surface and rerun the same battery of experiments to determine significant changes when:
  - heated elements are flush mounted
  - heated elements are spaced closer in the x-direction.

APPENDIX A

SOFTWARE

TEMPERATURE ACQUISITION PROGRAM

```
10    !!!!!!!!!!!!!!!!!!!!!!!!!!!!!!!!!!!!!!!!!!!!!!!!!!!!!!!!!!!!!!!!
20    !!                TEMPERATURE ACQUISITION PROGRAM             !!
30    !!                         (STEADY STATE)                     !!
40    !!!!!!!!!!!!!!!!!!!!!!!!!!!!!!!!!!!!!!!!!!!!!!!!!!!!!!!!!!!!!!!!
50    REAL Volts(60)
60    REAL Temp(59)
70    CREATE BDAT "THES____:,700,0,2",48
80    ASSIGN @Path3 TO "THES____:,700,0,2"
90    PRINT "                          BLOCK #8"
100   PRINT " "
110   OUTPUT 709;"CONFMEAS DCV,100,USE 0"
120   ENTER 709;Volts(60)
130   OUTPUT 709;"CONFMEAS DCV,100-105,USE 0"
140   FOR I=0 TO 5
150   ENTER 709;Volts(I)
160   Temp(I)=.0006797+(25825.1328*Volts(I))-(607789.2467*(Volts(I)*Volts(I)))-(
21952034.3364*(Volts(I)^3))+(8370810996.1874*(Volts(I)^4))
170   PRINT "T. C.  #";I+1,"  Volts D.C.  ";Volts(I),"Temp. DEG. C ";Temp(I)
180   NEXT I
190   PRINT " "
200   PRINT "                          BLOCK #7"
210   PRINT " "
220   OUTPUT 709;"CONFMEAS DCV,106-111,USE 0"
230   FOR I=6 TO 11
240   ENTER 709;Volts(I)
250   Temp(I)=.0006797+(25825.1328*Volts(I))-(607789.2467*(Volts(I)*Volts(I)))-(
21952034.3364*(Volts(I)^3))+(8370810996.1874*(Volts(I)^4))
260   PRINT "T. C.  #";I+1,"  Volts D.C.  ";Volts(I),"Temp. DEG. C ";Temp(I)
270   NEXT I
280   PRINT " "
290   PRINT "                          BLOCK #6"
300   PRINT " "
310   OUTPUT 709;"CONFMEAS DCV,112-117,USE 0"
320   FOR I=12 TO 17
330   ENTER 709;Volts(I)
340   Temp(I)=.0006797+(25825.1328*Volts(I))-(607789.2467*(Volts(I)*Volts(I)))-(
21952034.3364*(Volts(I)^3))+(8370810996.1874*(Volts(I)^4))
350   PRINT "T. C.  #";I+1,"  Volts D.C.  ";Volts(I),"Temp. DEG. C ";Temp(I)
360   NEXT I
370   PRINT " "
380   PRINT "                          BLOCK #5"
390   PRINT " "
400   OUTPUT 709;"CONFMEAS DCV,118-119,USE 0"
410   FOR I=18 TO 19
420   ENTER 709;Volts(I)
```

```
430   Temp(I)=.0006797+(25825.1328*Volts(I))-(607789.2467*(Volts(I)*Volts(I)))-(
21952034.3364*(Volts(I)^3))+(8370810996.1874*(Volts(I)^4))
440   PRINT "T. C.  #";I+1,"  Volts D.C.  ";Volts(I),"Temp. DEG. C ";Temp(I)
450   NEXT I
460   OUTPUT 709;"CONFMEAS DCV,200-203,USE 0"
470   FOR I=20 TO 23
480   ENTER 709;Volts(I)
490   Temp(I)=.0006797+(25825.1328*Volts(I))-(607789.2467*(Volts(I)*Volts(I)))-(
21952034.3364*(Volts(I)^3))+(8370810996.1874*(Volts(I)^4))
500   PRINT "T. C.  #";I+1,"  Volts D.C.  ";Volts(I),"Temp. DEG. C ";Temp(I)
510   NEXT I
520   PRINT " "
530   PRINT "                         BLOCK #4"
540   PRINT " "
550   OUTPUT 709;"CONFMEAS DCV,204-209,USE 0"
560   FOR I=24 TO 29
570   ENTER 709;Volts(I)
580   Temp(I)=.0006797+(25825.1328*Volts(I))-(607789.2467*(Volts(I)*Volts(I)))-(
21952034.3364*(Volts(I)^3))+(8370810996.1874*(Volts(I)^4))
590   PRINT "T. C.  #";I+1,"  Volts D.C.  ";Volts(I),"Temp. DEG. C ";Temp(I)
600   NEXT I
610   PRINT " "
620   PRINT "                         BLOCK #3"
630   PRINT " "
640   OUTPUT 709;"CONFMEAS DCV,210-215,USE 0"
650   FOR I=30 TO 35
660   ENTER 709;Volts(I)
670   Temp(I)=.0006797+(25825.1328*Volts(I))-(607789.2467*(Volts(I)*Volts(I)))-(
21952034.3364*(Volts(I)^3))+(8370810996.1874*(Volts(I)^4))
680   PRINT "T. C.  #";I+1,"  Volts D.C.  ";Volts(I),"Temp. DEG. C ";Temp(I)
690   NEXT I
700   FOR J=1 TO 14
710   PRINT " "
720   NEXT J
730   PRINT "                         BLOCK #2"
740   PRINT " "
750   OUTPUT 709;"CONFMEAS DCV,216-219,USE 0"
760   FOR I=36 TO 39
770   ENTER 709;Volts(I)
780   Temp(I)=.0006797+(25825.1328*Volts(I))-(607789.2467*(Volts(I)*Volts(I)))-(
21952034.3364*(Volts(I)^3))+(8370810996.1874*(Volts(I)^4))
790   PRINT "T. C.  #";I+1,"  Volts D.C.  ";Volts(I),"Temp. DEG. C ";Temp(I)
800   NEXT I
810   OUTPUT 709;"CONFMEAS DCV,300-301,USE 0"
820   FOR I=40 TO 41
830   ENTER 709;Volts(I)
840   Temp(I)=.0006797+(25825.1328*Volts(I))-(607789.2467*(Volts(I)*Volts(I)))-(
21952034.3364*(Volts(I)^3))+(8370810996.1874*(Volts(I)^4))
850   PRINT "T. C.  #";I+1,"  Volts D.C.  ";Volts(I),"Temp. DEG. C ";Temp(I)
860   NEXT I
870   PRINT " "
880   PRINT "                         BLOCK #1"
890   PRINT " "
900   OUTPUT 709;"CONFMEAS DCV,302-307,USE 0"
910   FOR I=42 TO 47
920   ENTER 709;Volts(I)
```

```
930   Temp(I)=.0006797+(25825.1328*Volts(I))-(607789.2467*(Volts(I)*Volts(I)))-(
21952034.3364*(Volts(I)^3))+(8370810996.1874*(Volts(I)^4))
940   PRINT "T. C.  #";I+1,"  Volts D.C.  ";Volts(I),"Temp. DEG. C ";Temp(I)
950   NEXT I
960   !
970   !
980   OUTPUT @Path3;Temp(*)
990   !
1000  !
1010  PRINT " "
1020  PRINT " "
1030  PRINT "                 BATH TEMPERATURES (TOP TO BOTTOM)"
1040  PRINT " "
1050  OUTPUT 709;"CONFMEAS DCV,317-319,USE 0"
1060  FOR I=57 TO 59
1070  ENTER 709;Volts(I)
1080  Temp(I)=.0006797+(25825.1328*Volts(I))-(607789.2467*(Volts(I)*Volts(I)))-(
21952034.3364*(Volts(I)^3))+(8370810996.1874*(Volts(I)^4))
1090  PRINT "VOLTS D.C.  ";Volts(I),"TEMP. DEG. C ";Temp(I)
1100  NEXT I
1110  END
```

DATA REDUCTION PROGRAM

```
10    !!!!!!!!!!!!!!!!!!!!!!!!!!!!!!!!!!!!!!!!!!!!!!!!!!!!!!!!!!!!!!!!!
20    !!                                                             !!
30    !!                 DATA REDUCING PROGRAM (BASIC)               !!
40    !!                                                             !!
50    !!!!!!!!!!!!!!!!!!!!!!!!!!!!!!!!!!!!!!!!!!!!!!!!!!!!!!!!!!!!!!!!!
60    REAL Temp(48),Tt(48),Qcond(8),Qconv(8),Qflux(8),H(8),Nu(8),Nustar(8)
70    REAL Gr(8),Ttt(8),At(8),Dtf(8),Dtr(8),Dtl(8),Dtt(8),Dtb(8),Dth(8),Bl(8)
80    REAL Jstar(8),Jp(8),Grstar(8)
90    REAL Power,Space,Dxpg,Dxr,Kpg,Kr,Block
100   REAL A,G,Dis,Try,KhZo,Beta,Kinvisc,Pr
110   INTEGER I,J,K,L,M,N,O
120   !
130   Dxpg=.006731
140   Dxr=.003175
150   Kpg=.1421
160   Kr=.0389
170   Chpht=.00787
180   Chpdpth=.00610
190   Chpwdth=.02388
200   Prim=(2*(Chpht+Chpwdth))+(2*(2*(Chpht+Chpdpth)))+(2*(2*(Chpwdth+Chpdpth)))
210   A1=Chpwdth*Chpht
220   A2=Chpwdth*Chpdpth
230   A3=Chpht*Chpdpth
240   Atotal=A1+(2.*A2)+(2.*A3)
250   Atotala=(2.*A2)+(2.*A3)
260   G=9.81
270   !!!!!!!!!!!!!!!!!!!!!!!!!!!!!!!!!!!!!!!!!!!!!!!!!!!!!!!!!!!!!!!!!!!!!!!!!
280   !!                  CALCULATE CHARACTERISTIC LENGTH                    !!
290   !!!!!!!!!!!!!!!!!!!!!!!!!!!!!!!!!!!!!!!!!!!!!!!!!!!!!!!!!!!!!!!!!!!!!!!!!
300   Lbar=Atotal/Prim
310   !
320   R1=Dxpg/(Kpg*A1)
330   R2=Dxr/(Kr*A1)
340   !
350   PRINTER IS 1
360   PRINT "INPUT RUN #, INTEGER ONLY"
370   INPUT Try
380   PRINT " "
390   PRINT " "
400   PRINT "INPUT POWER VALUE IN WATTS"
410   INPUT Power
420   PRINT " "
430   PRINT " "
440   PRINT "INPUT BLOCK #'S POWERED"
450   INPUT Blnp$
460   PRINT " "
470   PRINT " "
480   PRINT "INPUT SPACING IN MM"
490   INPUT Space$
500   PRINT " "
```

```
510   PRINT " "
520   PRINT "INPUT AMBIENT TEMPERATURE"
530   INPUT Tinf
540   PRINT " "
550   PRINT " "
560   !  PRINT "INPUT NEW FILENAME$"
570   !  INPUT Newfile$
580   !  PRINT " "
590   !  PRINT " "
600   PRINT "INPUT OLD FILENAME$"
610   INPUT Oldfile$
620   !
630   !
640   !  CREATE BDAT Newfile$,128
650   !  ASSIGN @Road TO Newfile$
660   !
670   ASSIGN @Street TO Oldfile$
680   ENTER @Street;Temp(*)
690   FOR I=0 TO 47
700   J=J+1
710   !PRINT J,Temp(I)
720   NEXT I
730   !
740   !
750   !!!!!!!!!!!!!!!!!!!!!!!!!!!!!!!!!!!!!!!!!!!!!!!!!!!!!!!!!!!!!!!!
760   !!          CALCULATE AVERAGE SURFACE TEMPERATURES              !!
770   !!!!!!!!!!!!!!!!!!!!!!!!!!!!!!!!!!!!!!!!!!!!!!!!!!!!!!!!!!!!!!!!
780   !   PRINT "AVG. SURFACE TEMPERATURE"
790   J=0
800   FOR I=1 TO 8
810      IF I=6 THEN
820         At(I)=((Temp(J+1)*A3)+(Temp(J+2)*A3)+(Temp(J+3)*A2)+(Temp(J+4)*A2))/
Atotala
830      ELSE
840         At(I)=((Temp(J)*A1)+(Temp(J+1)*A3)+(Temp(J+2)*A3)+(Temp(J+3)*A2)+(Te
mp(J+4)*A2))/Atotal
850      END IF
860   !  PRINT At(I)
870   J=J+6
880   NEXT I
890   !
900   !!!!!!!!!!!!!!!!!!!!!!!!!!!!!!!!!!!!!!!!!!!!!!!!!!!!!!!!!!!!!!!!
910   !!                   CALCULATE TFILM                            !!
920   !!!!!!!!!!!!!!!!!!!!!!!!!!!!!!!!!!!!!!!!!!!!!!!!!!!!!!!!!!!!!!!!
930   J=1
940   Tbar=(At(J)+At(J+1)+At(J+2)+At(J+3)+At(J+4)+At(J+5)+At(J+6)+At(J+7))/8.0
950   Tfilmc=((Tbar+Tinf)/2.0)
960   Tfilm=Tfilmc+273.15
970   !   PRINT "TFILM DEGREES C",Tfilmc
980   !   PRINT "TFILM",Tfilm
990   !!!!!!!!!!!!!!!!!!!!!!!!!!!!!!!!!!!!!!!!!!!!!!!!!!!!!!!!!!!!!!!!
1000  !!                 CALCULATE WATER PROPERTIES                   !!
```

```
1010  !!!!!!!!!!!!!!!!!!!!!!!!!!!!!!!!!!!!!!!!!!!!!!!!!!!!!!!!!!!!!!!!!!
1020  Beta=(-7.9448548E-8*(Tfilm^2))+(5.7356479E-5*Tfilm)-.0097810563
1030  Spvol=(4.69699E-9*(Tfilm^2))+(-2.53745E-6*Tfilm)+.001341903
1040  Dynvisc=(3.2348511E-7*(Tfilm^2))+(-.00021474487*Tfilm)+.036166792
1050  Kinvisc=Spvol*Dynvisc
1060  Kh2o=(1.418181818E-3*Tfilm)+.1866
1070  Pr=(4.65706E-3*(Tfilm^2))+(-2.922094*Tfilm)+463.3319
1080  !!!!!!!!!!!!!!!!!!!!!!!!!!!!!!!!!!!!!!!!!!!!!!!!!!!!!!!!!!!!!!!!!!
1090  !!                  CALCULATE TEMP-TINF                         !!
1100  !!!!!!!!!!!!!!!!!!!!!!!!!!!!!!!!!!!!!!!!!!!!!!!!!!!!!!!!!!!!!!!!!!
1110  !   PRINT "TEMP-TINF"
1120  FOR I=0 TO 47
1130     IF I=5 THEN
1140       Tt(I)=888.888
1150     ELSE
1160        IF I=30 THEN
1170          Tt(I)=888.888
1180        ELSE
1190       Tt(I)=Temp(I)-Tinf
1200     END IF
1210     END IF
1220  !  PRINT Tt(I)
1230  NEXT I
1240  !!!!!!!!!!!!!!!!!!!!!!!!!!!!!!!!!!!!!!!!!!!!!!!!!!!!!!!!!!!!!!!!!!!
1250  !!    CALCULATE CONDUCTION LOSSES THROUGH THE TEST SURFACE       !!
1260  !!!!!!!!!!!!!!!!!!!!!!!!!!!!!!!!!!!!!!!!!!!!!!!!!!!!!!!!!!!!!!!!!!!
1270  !   PRINT "QCOND"
1280  L=5
1290  FOR I=1 TO 8
1300     IF I=1 THEN
1310        Qcond(I)=.015*Power
1320     ELSE
1330        Qcond(I)=Tt(L)*(1.0/(R1+R2))
1340     END IF
1350  !  PRINT Qcond(I)
1360   L=L+6
1370   NEXT I
1380   !!!!!!!!!!!!!!!!!!!!!!!!!!!!!!!!!!!!!!!!!!!!!!!!!!!!!!!!!!!!!!!!!!
1390   !!              CALCULATE CONVECTED HEAT FLUX                    !!
1400   !!!!!!!!!!!!!!!!!!!!!!!!!!!!!!!!!!!!!!!!!!!!!!!!!!!!!!!!!!!!!!!!!!
1410   !   PRINT "QCONV"
1420   FOR I=1 TO 8
1430   Qconv(I)=Power-Qcond(I)
1440   Qflux(I)=Qconv(I)/A1
1450   NEXT I
1460   !!!!!!!!!!!!!!!!!!!!!!!!!!!!!!!!!!!!!!!!!!!!!!!!!!!!!!!!!!!!!!!!!!
1470   !!             CALCULATE TEMPERATURE SCALING FACTOR              !!
1480   !!!!!!!!!!!!!!!!!!!!!!!!!!!!!!!!!!!!!!!!!!!!!!!!!!!!!!!!!!!!!!!!!!
1490   !  PRINT "T*"
1500   FOR I=1 TO 8
```

```
1510   Tstar(I)=Qflux(I)*Lbar/Kh2o
1520  !   PRINT TSTAR(I)
1530  NEXT I
1540  !!!!!!!!!!!!!!!!!!!!!!!!!!!!!!!!!!!!!!!!!!!!!!!!!!!!!!!!!!!!!!!!!!
1550  !!                CALCULATE MODIFIED GRASHOF NUMBER              !!
1560  !!!!!!!!!!!!!!!!!!!!!!!!!!!!!!!!!!!!!!!!!!!!!!!!!!!!!!!!!!!!!!!!!!
1570  FOR I=1 TO 8
1580   Grstar(I)=G*Beta*Qflux(I)*(Lbar^4)/(Kh2o*(Kinvisc^2))
1590  NEXT I
1600  !!!!!!!!!!!!!!!!!!!!!!!!!!!!!!!!!!!!!!!!!!!!!!!!!!!!!!!!!!!!!!!!!!
1610  !!               CALCULATE HEAT TRANSFER COEFFICIENT              !!
1620  !!!!!!!!!!!!!!!!!!!!!!!!!!!!!!!!!!!!!!!!!!!!!!!!!!!!!!!!!!!!!!!!!!
1630  FOR I=1 TO 8
1640   H(I)=Qflux(I)/(At(I)-Tinf)
1650  NEXT I
1660  !!!!!!!!!!!!!!!!!!!!!!!!!!!!!!!!!!!!!!!!!!!!!!!!!!!!!!!!!!!!!!!!!!!
1670  !!                     CALCULATE NUSSELT NUMBER                    !!
1680  !!!!!!!!!!!!!!!!!!!!!!!!!!!!!!!!!!!!!!!!!!!!!!!!!!!!!!!!!!!!!!!!!!!
1690  FOR I=1 TO 8
1700   Nu(I)=H(I)*Lbar/Kh2o
1710  NEXT I
1720  !!!!!!!!!!!!!!!!!!!!!!!!!!!!!!!!!!!!!!!!!!!!!!!!!!!!!!!!!!!!!!!!!!!
1730  !!                 CALCULATE NUSSELT SCALING FACTOR                !!
1740  !!!!!!!!!!!!!!!!!!!!!!!!!!!!!!!!!!!!!!!!!!!!!!!!!!!!!!!!!!!!!!!!!!!
1750  FOR I=1 TO 8
1760   Js=9-I
1770   Nustar(I)=Nu(I)*Js^(1/6)
1780  NEXT I
1790  !!!!!!!!!!!!!!!!!!!!!!!!!!!!!!!!!!!!!!!!!!!!!!!!!!!!!!!!!!!!!!!!!!
1800  !!                     GENERATE OUTPUT DATA FILES                !!
1810  !!!!!!!!!!!!!!!!!!!!!!!!!!!!!!!!!!!!!!!!!!!!!!!!!!!!!!!!!!!!!!!!!!
1820  !
1830     PRINTER IS 701
1840  !
1850  PRINT USING """RUN NUMBER"",15X,DD";Try
1860  PRINT USING """POWER IN WATTS"",11X,Z.D";Power
1870  PRINT USING """SPACING IN MM"",12X,10A";Space$
1880  PRINT USING """BLOCK #'s POWERED"",8X,10A";Blnp$
1890  PRINT USING """AMBIENT TEMP. DEG. C"",5X,DD.DD";Tinf
1900  PRINT USING """FILM TEMPERATURE"",9X,DDD.DD";Tfilm
1910  PRINT USING """FILM TEMPERATURE, C"",6X,DD.DD";Tfilmc
1920  PRINT USING """THERMAL COND. OF WATER"",3X,Z.DDD";Kh2o
1930  PRINT USING """EXPANSION COEFFICIENT,B"",2X,3DE";Beta
1940  PRINT USING """KINEMATIC VISCOSITY"",6X,3DE";Kinvisc
1950  PRINT USING """PRANDTL NUMBER"",11X,DD.DD";Pr
1960  PRINT " "
1970  PRINT " "
1980  PRINT " "
1990  PRINT "BLOCK #","QCOND","QCONV","GR *","T*","H","NU *","NU*"
2000  FOR I=1 TO 8
```

```
2010   Block=9-I
2020   PRINT USING "3X,D,3X,S3DE,3X,SZ.DDD,3X,S3DE,2X,S3DE,3X,S3DE,2X,S3DE,2X,S3
DE";Block,Qcond(I),Qconv(I),Grstar(I),Tstar(I),H(I),Nu(I),Nustar(I)
2030   NEXT I
2040   PRINT " "
2050   PRINT " "
2060   PRINT " "
2070   PRINT " "
2080   !!!!!!!!!!!!!!!!!!!!!!!!!!!!!!!!!!!!!!!!!!!!!!!!!!!!!!!!!!!!!!!!!!!!!!!!!!!!!!!
2090   !!         CALCULATE TEMPERATURE DIFFERENCES                              !!
2100   !!!!!!!!!!!!!!!!!!!!!!!!!!!!!!!!!!!!!!!!!!!!!!!!!!!!!!!!!!!!!!!!!!!!!!!!!!!!!!!
2110   K=0
2120   FOR N=1 TO 8
2130     Dtf(N)=Tt(K)
2140     Dtr(N)=Tt(K+1)
2150     Dtl(N)=Tt(K+2)
2160     Dtt(N)=Tt(K+3)
2170     Dtb(N)=Tt(K+4)
2180     Dth(N)=Tt(K+5)
2190     K=K+6
2200   NEXT N
2210   PRINT "BLOCK #","DTF","DTR","DTL","DTT","DTB","DTH"
2220   FOR I=1 TO 8
2230   Block=9-I
2240   PRINT USING "3X,D,3X,S3DE,3X,S3DE,3X,S3DE,3X,S3DE,2X,S3DE,2X,S3DE";Block,
Dtf(I),Dtr(I),Dtl(I),Dtt(I),Dtb(I),Dth(I)
2250   NEXT I
2260   !!!!!!!!!!!!!!!!!!!!!!!!!!!!!!!!!!!!!!!!!!!!!!!!!!!!!!!!!!!!!!!!!!!!!!!!!!!!!!
2270   !!       CALCULATE NON DIMENSIONAL TEMPERATURE DIFFERENCES              !!
2280   !!!!!!!!!!!!!!!!!!!!!!!!!!!!!!!!!!!!!!!!!!!!!!!!!!!!!!!!!!!!!!!!!!!!!!!!!!!!!!
2290   FOR I=1 TO 8
2300   !     IF I=1 THEN
2310   !     Dthn(I)=88888
2320   !     ELSE
2330   !    IF I=6 THEN
2340   !      Dtfn(I)=88888
2350     Dtfn(I)=Dtf(I)/Tstar(I)
2360     Dtrn(I)=Dtr(I)/Tstar(I)
2370     Dtln(I)=Dtl(I)/Tstar(I)
2380     Dttn(I)=Dtt(I)/Tstar(I)
2390     Dtbn(I)=Dtb(I)/Tstar(I)
2400     Dthn(I)=Dth(I)/Tstar(I)
2410        IF I=1 THEN
2420          Dthn(I)=88888
2430         ELSE
2440           IF I=6 THEN
2450            Dtfn(I)=88888
2460          END IF
2470          END IF
2480   NEXT I
2490   PRINT " "
2500   PRINT " "
```

```
2510   PRINT "X/L","DTFN","DTRN","DTLN","DTTN","DTBN","DTHN"
2520   Xs=.795
2530   Gap=.0254/.3048
2540   FOR I=1 TO 8
2550   X1=Xs-((I-1)*Gap)
2560   PRINT USING ".DDD,3X  3DE,3X,S3DE,3X,S3DE,3X,S3DE,2X,S3DE,2X,S3DE";X1,Dtf
n(I),Dtrn(I),Dtln(I),Dttn(I.  )tbn(I),Dthn(I)
2570   NEXT I
2580   PRINT " "
2590   PRINT " "
2600   PRINT "DTR = RIGHT T. C. - TINF, etc."
2610   PRINT "T* IS TEMPERATURE SCALING FACTOR"
2620   PRINT "GR # IS MODIFIED GRASHOF NUMBER"
2630   PRINT "H IS HEAT TRANSFER COEFFICIENT"
2640   PRINT "NU # IS NUSSELT NUMBER"
2650   !        OUTPUT @Road;Qcond(*),Qconv(*),Gr(*),Ttt(*),Bl(*),Dtf(*),Dtr(*),
Dtl(*),Dtt(*),Dtb(*),Dth(*)
2660   !
2670   !!  NOTE THIS PROGRAM IS USED IN CONJUNCTION WITH THE
2680   !!  THE DATA AQUISITION PROGRAM AND ACCOUNTS FOR THE
2690   !!  INOPERATIVE THERMOCOUPLES ON BLOCKS 3&8
2700   !
2710   END
```

<u>THERMOCOUPLE VARIATION WITH TIME PROGRAM</u>

```
10    !!!!!!!!!!!!!!!!!!!!!!!!!!!!!!!!!!!!!!!!!!!!!!!!!!!!!!!!!!!!!!!!!!
20    !!         TEMPERATURE TRANSIENT RESPONSE PROGRAM             !!
30    !!!!!!!!!!!!!!!!!!!!!!!!!!!!!!!!!!!!!!!!!!!!!!!!!!!!!!!!!!!!!!!!!!
40    REAL T2(575),T3(575),T4(575),T5(575),T6(575),T7(575),T8(575)
50    REAL V2(575),V3(575),V4(575),V5(575),V6(575),V7(575),V8(575)
60    REAL G(575)
70    N=575
80    PRINTER IS 701
90    CREATE BDAT "TRANS_____:,700,0,1",502
100   ASSIGN @Trail1 TO "TRANS_____:,700,0,1"
110   !!!!!!!!!!!!!!!!!!!!!!!!!!!!!!!!!!!!!!!!!!!!!!!!!!!!!!!!!!!!!!!!!!!!!!!!!!!!
120   BEEP
130   FOR J=1 TO 5
140      OUTPUT 709;"CONFMEAS DCV,___,USE 0"
150        ENTER 709;V1(J)
160      OUTPUT 709;"CONFMEAS DCV,___,USE 0"
170        ENTER 709;V2(J)
180      OUTPUT 709;"CONFMEAS DCV,___,USE 0"
190        ENTER 709;V3(J)
200      OUTPUT 709;"CONFMEAS DCV,___,USE 0"
210        ENTER 709;V4(J)
220      OUTPUT 709;"CONFMEAS DCV,___,USE 0"
230        ENTER 709;V5(J)
240      OUTPUT 709;"CONFMEAS DCV,___,USE 0"
250        ENTER 709;V6(J)
260      OUTPUT 709;"CONFMEAS DCV,___,USE 0"
270        ENTER 709;V7(J)
280      OUTPUT 709;"CONFMEAS DCV,___,USE 0"
290        ENTER 709;V8(J)
300        NEXT J
310        BEEP
320        FOR J=6 TO N
330      OUTPUT 709;"CONFMEAS DCV,___,USE 0"
340        ENTER 709;V1(J)
350      OUTPUT 709;"CONFMEAS DCV,___,USE 0"
360        ENTER 709;V2(J)
370      OUTPUT 709;"CONFMEAS DCV,___,USE 0"
380        ENTER 709;V3(J)
390      OUTPUT 709;"CONFMEAS DCV,___,USE 0"
400        ENTER 709;V4(J)
410      OUTPUT 709;"CONFMEAS DCV,___,USE 0"
420        ENTER 709;V5(J)
430      OUTPUT 709;"CONFMEAS DCV,___,USE 0"
440        ENTER 709;V6(J)
450      OUTPUT 709;"CONFMEAS DCV,___,USE 0"
460        ENTER 709;V7(J)
470      OUTPUT 709;"CONFMEAS DCV,___,USE 0"
480        ENTER 709;V8(J)
490        IF J=N THEN
500        BEEP 2450.97*Tone,1.5
510        END IF
520        NEXT J
```

```
530   A=.0006797
540   B=25825.1328
550   C=-607789.2467
560   D=-21952034.3364
570   E=8370810996.1874
580    FOR J=1 TO N
590    IF J<5 THEN
600    G(J)=0
610    ELSE
620    G(J)=(J-5)*Tim
630    !  Tim IS TIME BASED ON TIME PROGRAM RUNS FROM 2ND BEEP TO TONE DIVDED
640    !  BY N-5, E.G. FOR 7 THERMOCOUPLES Tim IS .745, FOR 8 IT IS .852
650    END IF
660   NEXT J
670   PRINT " "
680   PRINT " "
690   FOR J=1 TO N
700   T1(J)=A+(B*V1(J))+(C*(V1(J)^2))+(D*(V1(J)^3))+(E*(V1(J)^4))
710   T2(J)=A+(B*V2(J))+(C*(V2(J)^2))+(D*(V2(J)^3))+(E*(V2(J)^4))
720   T3(J)=A+(B*V3(J))+(C*(V3(J)^2))+(D*(V3(J)^3))+(E*(V3(J)^4))
730   T4(J)=A+(B*V4(J))+(C*(V4(J)^2))+(D*(V4(J)^3))+(E*(V4(J)^4))
740   T5(J)=A+(B*V5(J))+(C*(V5(J)^2))+(D*(V5(J)^3))+(E*(V5(J)^4))
750   T6(J)=A+(B*V6(J))+(C*(V6(J)^2))+(D*(V6(J)^3))+(E*(V6(J)^4))
760   T7(J)=A+(B*V7(J))+(C*(V7(J)^2))+(D*(V7(J)^3))+(E*(V7(J)^4))
770   T8(J)=A+(B*V8(J))+(C*(V8(J)^2))+(D*(V8(J)^3))+(E*(V8(J)^4))
780    PRINT USING "1X,DDD,1X,4DE,1X,4DE,1X,4DE,1X,4DE,1X,4DE,1X,4DE,1X,4DE,1X,4
DE";G(J),T1(J),T2(J),T3(J),T4(J),T5(J),T6(J),T7(J),T8(J)
790  NEXT J
800  OUTPUT @Trail1;G(*),T1(*),T2(*),T3(*),T4(*),T5(*),T6(*),T7(*),T8(*)
810    END
```

APPENDIX B

EQUATIONS FOR DETERMINING FLUID PROPERTIES

$$\beta = -7.945\text{E}{-10}\, T_{FILM}^2 + 5.736\text{E}{-5}\, T_{FILM} - 9.781\text{E}{-3}$$

$$\nu = 4.697\text{E}{-9}\, T_{FILM}^2 - 2.537\text{E}{-6}\, T_{FILM} + 1.342\text{E}{-3}$$

$$\mu = 3.235\,\text{E}{-7}\; T_{FILM}^2 - 2.147\,\text{E}{-3}\; T_{FILM} + 0.03617$$

$$V = \nu\mu$$

$$k = 1.42\text{E}{-3} T_{FILM} + 0.187$$

$$Pr = 4.66\text{E}{-3}\, T_{FILM}^2 - 2.92\, T_{FILM} + 463$$

Curve fits were determined for range of temperatures from 280 to 300 K.

APPENDIX C

SAMPLE CALCULATIONS

The calculations were based on temperatures derived from a run with all blocks powered to 1.0 watt, no shroud in place. When appropriate, values are calculated for block number 6.

A. CHARACTERISTIC DIMENSIONS

$$\text{Perimeter} = \begin{bmatrix} 2(0.00787 + 0.02388) + (2(2(0.00787 + 0.00610))) \\ + (2(2(0.02388 + 0.00610))) \end{bmatrix} = 0.2393\,\text{m}$$

$$A_1 = (0.02388)(0.00787) = 1.879 \times 10^{-4}\, m^2$$

$$A_2 = (0.02388)(0.00610) = 1.457 \times 10^{-4}\, m^2$$

$$A_3 = (0.00787)(0.00610) = 4.80 \times 10^{-5}\, m^2$$

$$A_{TOTAL} = (1.879 \times 10^{-4}) + (2)(1.457 \times 10^{-4}) + (2)(4.80 \times 10^{-5}) = 5.75 \times 10^{-4} m^2$$

$$A_{TOTALA} = (5.75 \times 10^{-4} - 1.879 \times 10^{-4}) = 3.87 \times 10^{-4}\, m^2$$

$$\bar{L} = \frac{5.75 \times 10^{-4}}{0.2393} = 2.40 \times 10^{-3}\, m$$

B. SURFACE AVERAGED TEMPERATURES

$$T_{AVG\,(8)} = \frac{\begin{bmatrix}(19.82)(1.879\times 10^{-4}) + (19.48)(4.80\times 10^{-5}) \\ + (19.49)(4.80\times 10^{-5}) + (20.62)(1.457\times 10^{-4}) \\ + (20.26)(1.457\times 10^{-4})\end{bmatrix}}{(5.75\times 10^{-4})} = 20.08\,^{\circ}\mathrm{C}$$

$$T_{AVG\,(7)} = \frac{\begin{bmatrix}(19.41)(1.879\times 10^{-4}) + (18.99)(4.80\times 10^{-5}) \\ + (19.05)(4.80\times 10^{-5}) + (19.88)(1.457\times 10^{-4}) \\ + (20.08)(1.457\times 10^{-4})\end{bmatrix}}{(5.75\times 10^{-4})} = 19.64\,^{\circ}\mathrm{C}$$

$$T_{AVG\,(6)} = \frac{\begin{bmatrix}(19.16)(1.879\times 10^{-4}) + (18.67)(4.80\times 10^{-5}) \\ + (18.61)(4.80\times 10^{-5}) + (20.00)(1.457\times 10^{-4}) \\ + (19.57)(1.457\times 10^{-4})\end{bmatrix}}{(5.75\times 10^{-4})} = 19.40\,^{\circ}\mathrm{C}$$

$$T_{AVG\,(5)} = \frac{\begin{bmatrix}(18.96)(1.879\times 10^{-4}) + (18.33)(4.80\times 10^{-5}) \\ + (18.47)(4.80\times 10^{-5}) + (19.68)(1.457\times 10^{-4}) \\ + (19.37)(1.457\times 10^{-4})\end{bmatrix}}{(5.75\times 10^{-4})} = 19.16\,^{\circ}\mathrm{C}$$

$$T_{AVG\,(4)} = \frac{\begin{bmatrix}(18.65)(1.879\times 10^{-4}) + (18.30)(4.80\times 10^{-5}) \\ + (18.39)(4.80\times 10^{-5}) + (19.75)(1.457\times 10^{-4}) \\ + (19.06)(1.457\times 10^{-4})\end{bmatrix}}{(5.75\times 10^{-4})} = 18.99\,^{\circ}\mathrm{C}$$

$$T_{AVG\,(3)} = \frac{\begin{bmatrix}(17.76)(4.80\times 10^{-5}) + (18.10)(4.80\times 10^{-5}) \\ + (19.18)(1.457\times 10^{-4}) + (18.87)(1.457\times 10^{-4})\end{bmatrix}}{(3.87\times 10^{-4})} = 18.77\,^{\circ}C$$

$$T_{AVG\,(2)} = \frac{\begin{bmatrix}(18.07)(1.879\times 10^{-4}) + (17.40)(4.80\times 10^{-5}) \\ + (17.79)(4.80\times 10^{-5}) + (18.85)(1.457\times 10^{-4}) \\ + (18.56)(1.457\times 10^{-4})\end{bmatrix}}{(5.75\times 10^{-4})} = 18.32\,^{\circ}C$$

$$T_{AVG\,(1)} = \frac{\begin{bmatrix}(17.73)(1.879\times 10^{-4}) + (17.25)(4.80\times 10^{-5}) \\ + (17.25)(4.80\times 10^{-5}) + (18.60)(1.457\times 10^{-4}) \\ + (17.78)(1.457\times 10^{-4})\end{bmatrix}}{(5.75\times 10^{-4})} = 17.89\,^{\circ}C$$

C. TFILM

$$\bar{T} = \frac{20.08 + 19.64 + 19.40 + 19.16 + 18.99 + 18.77 + 18.32 + 17.89}{8} = 19.03^{\circ}C$$

$$T_{FILM} = \frac{19.03 + 13.23}{2} = 16.13^{\circ}C$$

D. TEMPERATURE EXCESSES

Using data from block 6, temperature excess is evaluated as:

$$\Delta T_F = 19.16 - 13.23 = 5.93\,^{\circ}C$$

$$\Delta T_R = 18.67 - 13.23 = 5.44\,^{\circ}C$$

$$\Delta T_L = 18.61 - 13.23 = 5.38\,^\circ\mathrm{C}$$

$$\Delta T_T = 20.00 - 13.23 = 6.77\,^\circ\mathrm{C}$$

$$\Delta T_B = 19.57 - 13.23 = 6.34^\circ\,\mathrm{C}$$

$$\Delta T_H = 24.20 - 13.23 = 10.97\,^\circ\mathrm{C}$$

E. CONVECTED HEAT FLUX

$$q'' = \frac{0.984}{1.879 \times 10^{-4}} = 5240 \frac{w}{m^2}$$

F. TEMPERATURE SCALING FACTOR

$$T^* = \frac{(5240)(2.40 \times 10^{-3})}{(0.597)} = 21.1^\circ\mathrm{C}$$

G. MODIFIED GRASHOF NUMBER

$$Gr^* = \frac{(9.81)(163 \times 10^{-6})(5240)(2.40 \times 10^{-3})^4}{(0.597)(112 \times 10^{-8})^2} = 371$$

H. HEAT TRANSFER COEFFICIENT

$$h = \frac{(5240)}{(19.40 - 13.23)} = 849 \frac{w}{m^2\mathrm{K}}$$

I. NUSSELT NUMBER

$$Nu = \frac{(849)\left(2.40 \times 10^{-3}\right)}{(0.597)} = 3.41$$

LIST OF REFERENCES

1. Oktay, S., Hannemann, R., and Bar-Cohen, A., "High Heat from a Small Package," *Mechanical Engineering*, vol. 108, no. 3, pp. 36-42, March 1986.

2. Kraus, A. D., and Bar-Cohen, A., *Thermal Analysis and Control of Electronic Equipment*, p. 7, 1983.

3. Hazard, S. J., *Single Phase Liquid Immersion Cooling of Discrete Heat Sources in a Vertical Channel*, M.S.M.E. Thesis, Naval Postgraduate School, Monterey, CA, December 1987.

4. Moffat, R. J., and Ortega, A., "Buoyancy Induced Forced Convection," *Heat Transfer in Electronic Equipment-1986*, ASME HTD-Vol. 57, pp. 135–144.

5. Ortega, A., and Moffat, R. J., "Heat Transfer From An Array of Simulated Electronic Components: Experimental Results for Free Convection With and Without a Shrouding Wall," *Heat Transfer in Electronic Equipment-1986*, ASME HTD-Vol. 48, pp. 5–15.

6. __________, "Buoyancy Induced Convection in a Non-Uniformly Heated Array of Cubical Elements on a Vertical Channel Wall," *Heat Transfer in Electronic Equipment-1986*, ASME HTD-Vol. 57, pp. 123–134, 1986.

7. Jaluria, Y., "Buoyancy-Induced Flow Due to Isolated Thermal Sources on a Vertical Surface," *ASME Journal of Heat Transfer*, vol. 104, 1982, pp. 223–227.

8. Rajakumar, C., and Johnson, D., *Finite Element Predictions of Free Convection Heat Transfer Coefficients of Simulated Electronic Circuit Boards*, presented at the ASME Winter Annual Meeting, Boston, MA, December 1987.

9. Incropera, F. P., and DeWitt, D. P., *Fundamentals of Heat and Mass Transfer*, p. 774, John Wiley and Sons, 1981.

INITIAL DISTRIBUTION LIST

		No. Copies
1.	Defense Technical Information Center Cameron Station Alexandria, VA 22304-6145	2
2.	Library, Code 0142 Naval Postgraduate School Monterey, CA 93943-5002	2
3.	Professor A. J. Healey, Code 69Hy Chairman, Department of Mechanical Engineering Naval Postgraduate School Monterey, CA 93943-5000	1
4.	Mr. Howard Stevens Head, Electrical Research Center David Taylor Research Center Annapolis, MD 21402	1
5.	Professor Y. Joshi, Code 69Ji Department of Mechanical Engineering Naval Postgraduate School Monterey, CA 93943-5000	3
6.	Professor M. D. Kelleher, Code 69Kk Department of Mechanical Engineering Naval Postgraduate School Monterey, CA 93943-5000	1
7.	Professor A. D. Kraus, Code 62Ks Department of Electrical and Computer Engineering Naval Postgraduate School Monterey, CA 93943-5000	1
8.	Mr. Duane Embree Naval Weapons Support Center Code 6042 Crane, IN 47522	1

9. LT Dan Knight, USN 1
SMC #2681
Naval Postgraduate School
Monterey, CA 93943-5000

10. Mr. Joseph Cipriano 1
Executive Director
Weapons and Combat Systems Directorate
Naval Sea Systems Command
Washington, DC 20362-5101

11. LCDR Thomas D. Willson 4
405 Paris Avenue
Brooklawn, NJ 08030